SYNTHESIS AND CHARACTERIZATION OF THIENO[3,4-*B*]PYRAZINE-BASED NEAR-INFRARED MATERIALS

A Dissertation
Submitted to the Graduate Faculty
of the
North Dakota State University
of Agriculture and Applied Science

By

Spencer John Gilman

In Partial Fulfillment of the Requirements
for the Degree of
DOCTOR OF PHILOSOPHY

Major Department:
Chemistry and Biochemistry

November 2023

Fargo, North Dakota

North Dakota State University
Graduate School

Title

Synthesis and Characterization of Thieno[3,4-*b*]pyrazine-Based Near-Infrared Materials

By

Spencer John Gilman

The Supervisory Committee certifies that this ***disquisition*** complies with North Dakota State University's regulations and meets the accepted standards for the degree of

DOCTOR OF PHILOSOPHY

SUPERVISORY COMMITTEE:

Dr. Seth Rasmussen
Chair

Dr. Gregory Cook

Dr. Pinjing Zhao

Dr. Andriy Voronov

Approved:

12/11/2023 — Date

Dr. Gregory Cook — Department Chair

ABSTRACT

Since their first report in the 1800s, conjugated polymers have gained significant attention for their ability to exhibit the optical and electronic properties of inorganic semiconductors and the physical traits of organic plastics. This has led to the development of organic electronics with notable commercial applications, such as organic photovoltaics and organic light-emitting diodes. The tunability of these materials has also allowed for the production of materials that absorb and emit near-infrared (NIR) light, making them useful for NIR photodetection and bioimaging.

NIR photodetection is important for several applications, including optical communication, artificial vision, and health monitoring. Commercially available NIR photodetectors use inorganic materials such as InGaAs and HgCdTe, which are toxic, inflexible, and have limited tunability of their spectral response range. Conjugated polymers offer an alternative to these materials as they are considerably less toxic, flexible, and their spectral response range is tunable through molecular design. Thieno[3,4-*b*]pyrazine (TP) homopolymers show potential for NIR photodetectors due to their ability to absorb NIR light. However, TP homopolymers generally exhibit low solubility, which limits their application to devices. To improve solubility, TP homopolymers were functionalized with branched side chains, resulting in soluble materials with bandgaps as low as 0.64 eV. In addition, NIR photodetectors made from these materials exhibit specific detectivity values that are competitive with some of the top-performing polymers currently used in NIR photodetectors. Moreover, TP homopolymers are of relatively low synthetic complexity compared to current state-of-the-art conjugated polymers. The overall design, synthesis, characterization, and device data for these materials will be presented.

Both absorption and emission are crucial for bioimaging, unlike NIR photodetection which only requires absorption. Fluorescence imaging allows for fast feedback and high sensitivity while being relatively inexpensive compared to traditional imaging methods. The NIR-I and NIR-II windows (700–900 and 1000–1700 nm, respectively) are ideal for fluorescence imaging due to the reduced absorption, autofluorescence, and scattering in these regions. Organic small molecule fluorophores have gained interest due to their low toxicity, fast excretion rates, tunability, and good biocompatibility. The overall design, synthesis, and characterization of several small molecule emitters will be presented.

ACKNOWLEDGMENTS

I would like to express my gratitude to Dr. Rasmussen for his help and guidance throughout my graduate career. Your open-door policy and prompt response to my questions have been helpful. I am grateful for your assistance in advancing my career in academia. Thank you for giving me unforgettable experiences, such as the trip to the University of Newcastle and various conferences. I also appreciate being included in the ACS in Focus book, which was a great learning opportunity.

I would like to thank my committee members, Dr. Gregory Cook, Dr. Pinjing Zhao, and Dr. Andriy Voronov, for their constructive feedback during my committee meetings. Your input has been helpful in enhancing my knowledge, completing my research, and assembling my dissertation. It has been a pleasure working with you.

I would also like to thank our collaborators from the University of Newcastle, Dr. Paul Dastoor, Dr. Nic Nicolaidis, and Tomas Marsh, for their assistance in providing me with valuable data for my dissertation. My time at the University of Newcastle was a fantastic learning opportunity, and I am thankful for the knowledge I have gained from you.

I am also grateful to the Rasmussen group members I overlapped with, Dr. Evan Culver, Wyatt Wilcox, Max Bultman, undergraduate students, and high school students. Our chemistry discussions have been very helpful, and I have learned a lot from you. I have enjoyed the time we spent together in and out of the lab.

Lastly, I would like to thank Norah Almowanas. Your feedback on my work and our chemistry discussions have been very helpful. You are a great friend.

DEDICATION

Dedicated to my family:

Your support has been very important to me in my graduate studies. In addition, the values you passed on to me have helped me tremendously.

TABLE OF CONTENTS

LIST OF TABLES

LIST OF FIGURES

LIST OF ABBREVIATIONS

ATP-*alt*-ODTP.....poly(acenaphtho[1,2-*b*]thieno[3,4-*e*]pyrazine-*alt*-2,3-bis(2-octyldodecyl)thieno[3,4-*b*]pyrazine)

ATP-*ran*-ODTP .....poly(acenaphtho[1,2-*b*]thieno[3,4-*e*]pyrazine-*ran*-2,3-bis(2-octyldodecyl)thieno[3,4-*b*]pyrazine)

BBTD.....benzo[1,2-*c*:4,5-*c'*]bis[1,2,5]thiadiazole

BHJ .....bulk heterojunction

BTD.....2,1,3-benzothiadiazole

CPDT .....4*H*-cyclopenta[2,1-*b*:3,4-*b'*]dithiophene

CV .....cyclic voltammetry

DArP .....direct arylation polymerization

DCM .....dichloromethane

DPV.....differential pulse voltammetry

DSC.....differential scanning calorimetry

DTP .....dithieno[3,2-*b*:2′,3′-*d*]pyrrole

DTP_2-TTZ.....2,5-bis(*N*-octyl-2-phenyldithieno[3,2-*b*:2',3'-*d*]pyrrol-6-yl)thiazolo[5,4-*d*]thiazole

DTT.....dithieno[3,2-*b*:2',3'-*d*]thiophene

D–A.....donor-acceptor

D-A-D .....donor-acceptor-donor

D*.....specific detectivity

E_B .....electron–hole pair binding energy

EDOT.....3,4-ethylenedioxythiophene

E_g.....bandgap

E_g^{elec} .....electrochemical bandgap

E_g^{opt} .....optical bandgap

EQE.....external quantum efficiency

F_2BTD.....5,6-difluorobenzo[*c*][1,2,5]thiadiazole

Fc^+/Fc.....ferrocenium/ferrocene

GPC.....gel permeation chromatography

GRIM .....Grignard metathesis

HOMO .....highest occupied molecular orbital

ICG.....indocyanine green

InDT.....indolo[3,2-*b*:4,5-*b'*]dithiophene

IPES .....inverse photoelectron spectroscopy

ITN.....isothianaphthene

ITO.....indium tin oxide

J_{SC}.....short circuit current density

LDA .....lithium diisopropylamide

LUMO.....lowest unoccupied molecular orbital

Mamx .....2,4-di-*tert*-butyl-6-[(dimethylamino)methyl]phenyl

MB .....methylene blue

MeCN.....acetonitrile

M_n.....number average molecular weight

MRI.....magnetic resonance imaging

M_w.....weight average molecular weight

NBS.....*N*-bromosuccinimide

NCC .....number of column chromatography steps

NEP.....noise equivalent power

NHC.....number of hazardous chemicals

NIR.....near-infrared

NIR-I ..... first near-infrared window

NIR-II ..... second near-infrared window

$Ni(dppp)Cl_2$ ..... [1,3-bis(diphenylphosphino)propane]dichloronickel(II)

$Ni(dppe)Cl_2$ ..... [1,2-bis(diphenylphosphino)ethane]dichloronickel(II)

NMR ..... nuclear magnetic resonance

NSS ..... number of synthetic steps

NUO ..... number of unit operations

OFETs ..... organic field-effect transistors

OLEDs ..... organic light-emitting diodes

OPVs ..... organic photovoltaics

P3AT ..... poly(3-alkylthiophene)

P3HT ..... poly(3-hexylthiophene)

PATP ..... poly(acenaphtho[1,2-*b*]thieno[3,4-*e*]pyrazine)

PC_6TP ..... poly(2,3-dihexylthieno[3,4-*b*]pyrazine)

PCBM ..... [6,6]-phenyl-C_{61}-butyric acid methyl ester

PCE ..... power conversion efficiency

PDI ..... polydispersity index

PEDOT-TP ..... poly(3,4-ethylenedioxythiophene-*alt*-thieno[3,4-*b*]pyrazine)

PEG ..... polyethylene glycol

PEHTP ..... poly(2,3-bis(2-ethylhexyl)thieno[3,4-*b*]pyrazine)

PET ..... positron emission tomography

PhInDT ..... 4-phenylindolo[3,2-*b*:4,5-*b'*]dithiophene

PHTP ..... poly(2,3-dihexylthieno[3,4-*b*]pyrazine)

PITN.....polyisothianaphthene

PPV .....poly(*p*-phenylene vinylene)

PTP.....poly(thieno[3,4-*b*]pyrazine)

Qx.....quinoxaline

RY .....reciprocal yield

S-D-A-D-S .....shielding unit-donor-acceptor-donor-shielding unit

$TBAPF_6$.....tetrabutylammonium hexafluorophosphate

TDPP.....thiophene-flanked diketopyrrolopyrrole

T_g.....glass transition temperatures

THF .....tetrahydrofuran

TII .....thiophene-based analogue of isoindigo

TMEDA .....tetramethylethylenediamine

TOMPP .....tris(2-methoxyphenyl)phosphine

TP.....thieno[3,4-*b*]pyrazine

TTz.....thiazolo[5,4-*d*]thiazole

TzQI .....thiadiazoloquinoxalinimide

UPS .....UV photoelectron spectroscopy

V_{OC}.....open circuit voltage

CHAPTER 1. INTRODUCTION

1.1. Conjugated Organic Materials

Conjugated organic materials have gained attention due to their ability to exhibit both the optical and electronic characteristics of inorganic semiconductors and the physical traits of organic plastics, such as being lightweight and flexible.[1] In addition, conjugated organic materials offer simple tunability through molecular design. These properties make them ideal for use in organic photovoltaics (OPVs), organic light-emitting diodes (OLEDs), and organic field-effect transistors (OFETs).[1]

When discussing conjugated materials, the term *conjugation* describes the connection between the π-systems present in a molecule.[2] Essentially, conjugation refers to the delocalization of π-electrons along a compound's backbone or adequate co-linear overlap between adjacent *p*-orbitals (Fig 1.1).[2] A common misconception in the literature is that conjugation comes from the alternation of single and double bonds.[2] While this may be true for systems such as polyacetylene and pentacene, this definition does not apply to systems like polyaniline, which display n-π-conjugation (i.e., when the *p*-orbital of a heteroatom accommodating an unshared electron pair contributes to the π-system (Figure 1.1)).[2,3] Another type of conjugation observed in conjugated organic materials is cross conjugation, in which three unsaturated groups are connected through an unsaturated center (e.g., 3-methylene-1,4-pentadiene (Figure 1.1)).[2–4]

Conjugated organic materials can be divided into two categories, namely those comprised of small molecules (e.g., rubrene and pentacene) and those from polymers (e.g., polythiophene and polypyrrole) (Figure 1.2). In the context of this text a small molecule will refer to a species with a specific molecular weight, whereas a polymer (in accordance with the IUPAC definition)

will refer to a substance that is made up of macromolecules (i.e., a molecule that is made up of many repeat units, which has a relatively high molecular weight).[5] Conjugated polymer samples are often polydisperse, meaning they are composed of macromolecules of varying molecular weights.

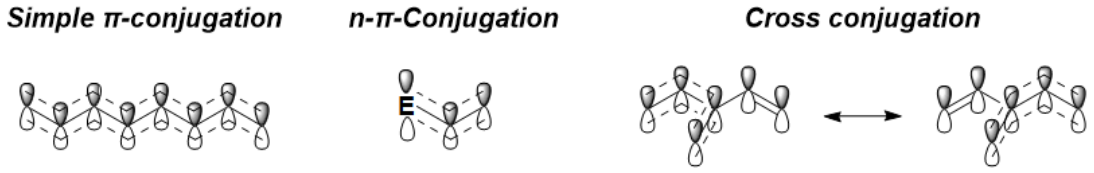

Figure 1.1. Types of conjugation observed in organic compounds.

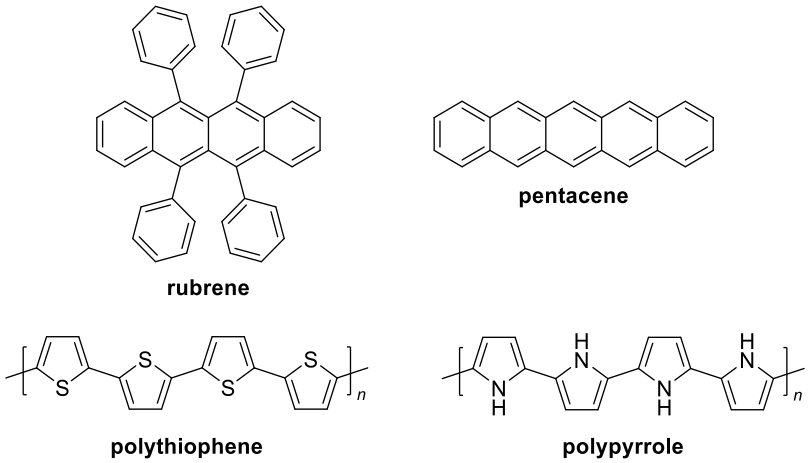

Figure 1.2. Examples of conjugated organic small molecules (rubrene and pentacene) and polymers (polythiophene and polypyrrole).

1.1.1. Conjugated Polymer History

In 1834, F. Ferdinand Runge (1794–1897) synthesized polyaniline from aniline by oxidative polymerization, which is thought to be the first report of a conjugated polymer.[6] However, the name polyaniline was not commonly used until the 1960s, and the material was initially referred to by color-based names such as emeraldine and aniline black.[6] In 1915, Italian chemist Angelo Angeli (1864–1931) synthesized polypyrrole by adding a 50% hydrogen

peroxide solution to pyrrole in acetic acid to give a black precipitate, which he named *nero di pirrolo*.[6]

Then, in the early 1960s, Donald Weiss (1924–2008) and coworkers modified a previous method used to make cross-linked polypyrroles, by heating tetraiodopyrrole under nitrogen atmosphere at elevated temperatures in a rotating flask. They prepared pressed pellets of these polypyrroles and measured resistivities of 11–200 Ω cm at 25 °C, which corresponds to conductivities of 0.005–0.09 S cm^{-1}.[6] Further analysis of these materials led them to conclude that that the polymer contained "adsorbed molecular iodine" and that removal of this iodine led to an increase in resistance. They later reported that "*The presence of the oxidant iodine, and in its absence oxygen, facilitates oxidation of the polymer*", a process now understood as p-doping and this is most likely the first report of p-doping of a conjugated polymer.[6] A few years later in 1969, Marcel Jozefowicz (b. 1934) who was working for Rene Buvet (1930–1992) found that an oxidized polyaniline material exhibited conductivities of 100 S cm^{-1}.[6]

In the 1970s, Alan J. Heeger (b. 1936), Alan G. MacDiarmid (1927–2007), and Hideki Shirakawa (b. 1936) reported metallic conductivities for a doped conjugated polymer. By doping *trans*-polyacetylene films through treatment with I_2,[7,8] they achieved conductivities of up to 160 S cm^{-1}. Later they found that using AsF_5 as a dopant led to a further increase in conductivity, with AsF_5 doped *cis*-polyacetylene films exhibiting conductivities larger than 500 S cm^{-1}.[6] Their work led to them being awarded the Nobel Prize in Chemistry in the year 2000 for their contributions to the field of conjugated and conducting polymers.[6,9]

In 1980, several reports of polythiophene were published. Although an earlier patent of the electropolymerization of thiophene was reported in 1971, this patent included little to no characterization details.[6] The first report to contain meaningful characterization was published in

January of 1980, by Takakazu Yamamoto (b. 1944) who synthesized polythiophene by polycondensation of 2,5-dibromothiophene via Kumada cross coupling. Upon doping the polymer with I_2, a conductivity of 3.4 x 10^{-4} S cm^{-1} was measured.[6] Later in that same decade, the first examples of photovoltaic devices based on polythiophenes were published.[10,11] Since then, thiophene-based materials have proven to be very effective in organic photovoltaic applications.[6]

1.2. Band Gap and Frontier Molecular Orbitals

One of the key advantages of conjugated materials is that their properties can be tuned by altering their molecular design.[1,12–14] Tunable properties include solubility,[15–18] frontier molecular orbital energies, and bandgap energy (E_g).[1,12–14,19] Among these properties, researchers have focused extensively on adjusting the bandgap of conjugated organic materials.

To explain the bandgap of a conjugated organic material, we must first discuss band structure, which involves the π molecular orbitals of a conjugated species. The molecular orbital diagrams for ethylene, butadiene, and octatetraene are shown in Figure 1.3. Ethylene has one π bonding orbital (π) and one π antibonding orbital (π*). The π bonding orbital is the highest occupied molecular orbital (HOMO), while the π antibonding orbital is the lowest unoccupied molecular orbital (LUMO). As the size of the conjugated system increases from ethylene to butadiene and then to octatetraene, the number of non-degenerate π bonding and π antibonding orbitals increases. This causes the gap between the HOMO and LUMO energy levels to decrease. Additionally, the distance between the bonding orbitals decreases and the distance between the antibonding orbitals decreases. As we increase the conjugation length even further and transition from individual molecules to the bulk, solid-state material (i.e., polyacetylene films), the number of molecular orbitals further increases, and the distance between them continue to decrease. In

addition, intermolecular interactions between individual polymer chains cause mixing and blurring of the molecular orbital energy levels, leading to a band structure, similar to what is commonly used for bulk inorganic materials.[2,20,21] In the case of bulk conjugated organic materials the π bonding orbitals make up the valence band, and the π antibonding orbitals make up the conduction band. The top of the valence band is still referred to as the HOMO, and the bottom of the conduction band is referred to as the LUMO.

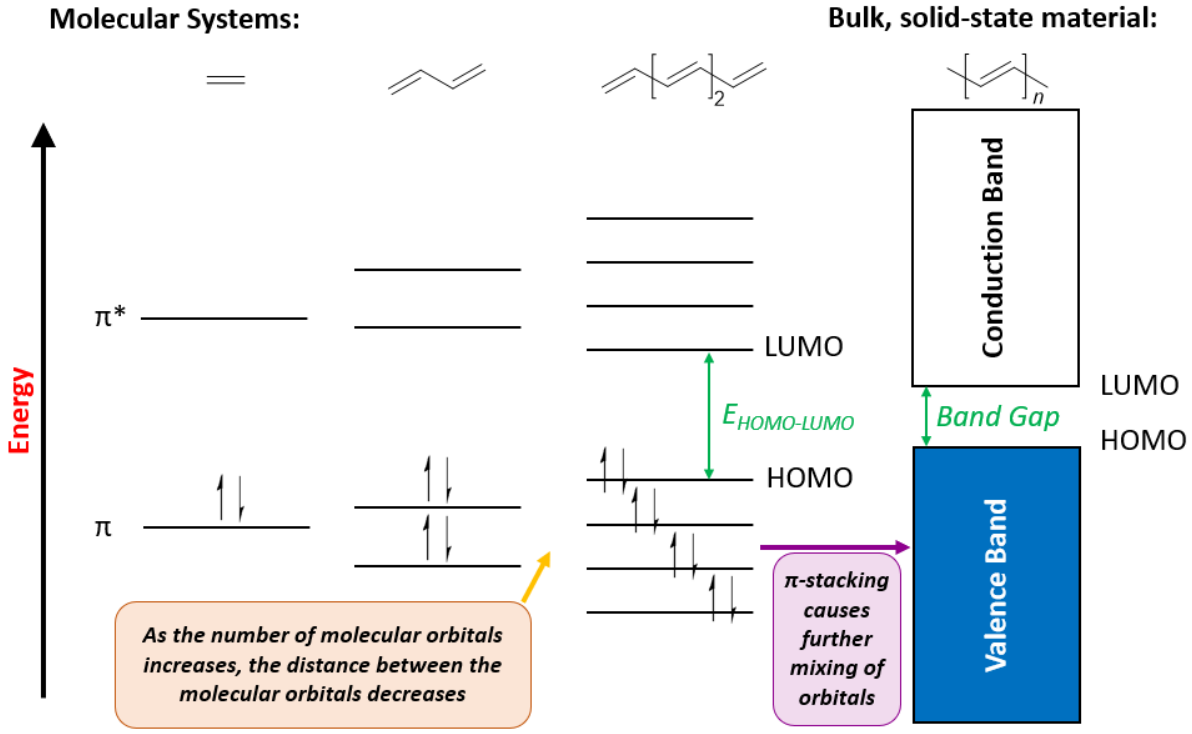

Figure 1.3. Molecular orbital diagram of ethylene, butadiene, and octatetraene and band structure of bulk, solid-state polyacetylene.

An essential property of conjugated organic materials is the band gap,[1,2,12–14,20] which is the energetic gap between the valence and conduction band of the bulk, solid-state material.[1,2,21] The bandgap is generally reported in units of electron volts (eV), with an absorption onset of 1240 nm corresponding to a bandgap of 1 eV.[1] The bandgap influences the wavelengths of light absorbed, as well as any light emitted.[1,2] Furthermore, a reduced bandgap results in a lower

thermal energy required to populate the conduction band, potentially leading to improved conductivity.[1,22] Thus, many studies have focused on adjusting the bandgap of conjugated organic materials to suit various applications.[1,2,12–14,20,22]

Another crucial property of conjugated organic materials is the frontier molecular orbital energy levels. When fabricating OFET devices, it is critical to use an organic semiconductor with a HOMO (or LUMO) similar in energy to the electrode materials Fermi level (i.e., the highest energy level an electron can occupy when there is zero thermal energy). This similarity allows for the injection of holes (i.e., the absence of an electron) (or electrons) into the HOMO (or LUMO) of the organic semiconductor. A semiconductor that transports holes (or electrons) is referred to as a p-type (or n-type) semiconductor. Some semiconducting materials are ambipolar, meaning they can transport both holes and electrons, but this is not as common.[23]

Frontier molecular orbital energy levels are also important when fabricating OPV devices. For instance, the open circuit voltage (V_{OC}) of an OPV device is thought to depend on the energetic difference between the HOMO energy level of the donor material and the LUMO energy level of the acceptor material.[24] In addition, the difference in energy between the LUMO of the donor and the LUMO of the acceptor determines whether the transfer of an electron from the donor to the acceptor is favorable.[24] This is illustrated in Figure 1.4, which shows the basic OPV operating principles when following a channel-I mechanism (i.e., the photon is absorbed by the donor material), in which upon absorption of a photon, an electron is promoted from the HOMO of the donor to the LUMO of the donor, forming a bound electron-hole pair (or exciton). The exciton can then diffuse to the interface between the donor and the acceptor, where the electron transfers from the donor LUMO to the acceptor LUMO. The electron then moves toward the cathode while the hole moves toward the anode.[24,25]

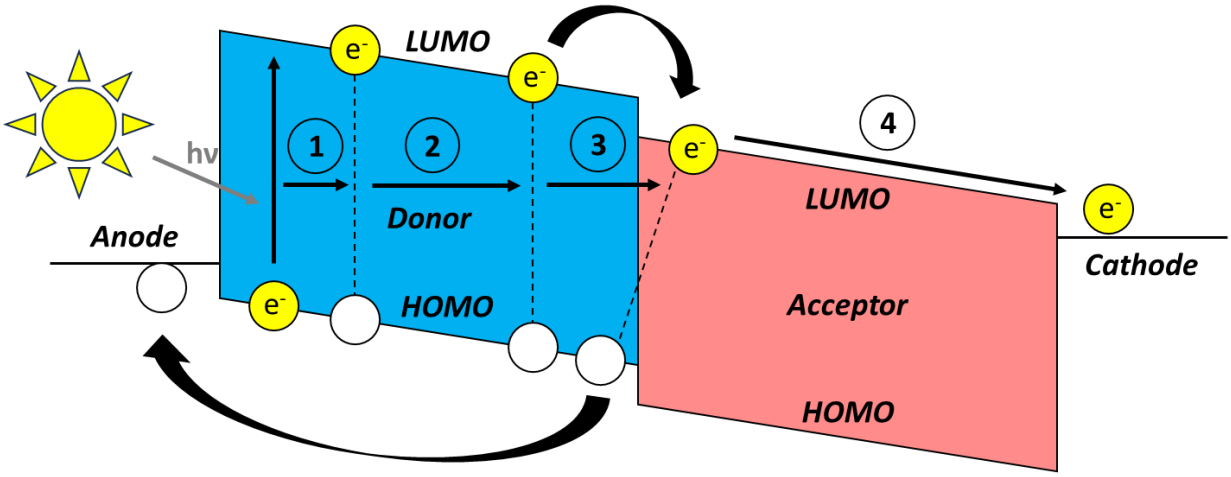

Figure 1.4. Illustration of the basic OPV operating principles by a channel-I mechanism. Step 1: the donor material absorbs a photon, which generates an exciton. Step 2: the exciton diffuses towards the donor/acceptor interface. Step 3: the electron transfers from the donor LUMO to the acceptor LUMO. Step 4: the electron moves towards the cathode and the hole moves towards the anode.

In 1984, Wudl and coworkers synthesized polyisothianaphthene (PITN) with a bandgap of 1.0 eV.[1,26] A year later, they referred to PITN as having a "*small band-gap*".[27] Following these publications, "*small bandgap*," "*narrow bandgap*," and "*low bandgap*" were used ambiguously throughout the literature. However, in 1998, Pomerantz proposed that a low bandgap material should be anything with a bandgap below 1.5 eV.[1] This was based on the fact that the parent conjugated polymers like polyacetylene, polythiophene, and polyphenylene have bandgaps greater than or equal to 1.5 eV (Figure 1.5).[1] Rasmussen and coworkers later introduced the term "*reduced bandgap*" to refer to materials with a bandgap between 1.5 and 2.0 eV.[28] However, other bandgap classifications have also been proposed. For example, Scharber and Sariciftci proposed grouping bandgap energies by their respective spectroscopic energy range with the following bandgap classifications given, visible = 3.1–1.5 eV, near-infrared (NIR) = 1.59–0.4 eV, and mid-infrared = 0.4–0.025 eV.[12] However, as the reported visible and NIR ranges overlap it would make more sense for the visible range to be 3.1–1.6 eV. Nevertheless, this proposed

grouping of bandgap energies has not gained any support. There has been a lot of effort put into designing and synthesizing reduced and low bandgap materials as they are useful for OPV and NIR photodetector applications.[1,29,30]

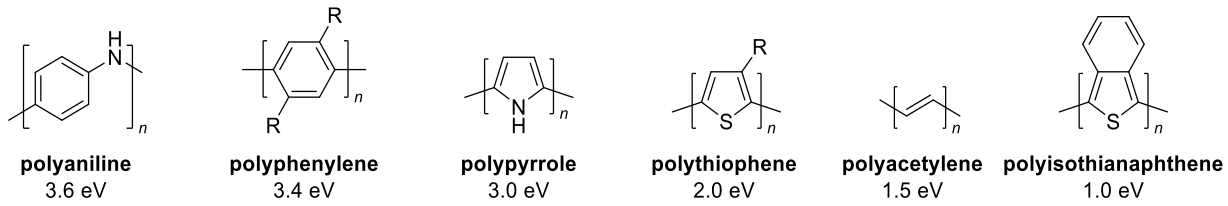

Figure 1.5. Bandgaps of various conjugated polymers.[1,2]

1.2.1. Bandgap Determination

Electrochemistry or absorption spectroscopy can be used to determine the bandgap of a solid-state material.[1] It should be noted that bandgap measurements from solution are reported in the literature. However, a bandgap determined from solution is a meaningless value as there is minimal interchain coupling while dissolved in solution. It thus does not reflect the true bandgap of the material.[1,2]

Electrochemical methods for determining bandgap include cyclic voltammetry (CV) or differential pulse voltammetry (DPV).[1,12] By these methods, the first oxidation and reduction potentials are measured, and the difference between these values corresponds to the bandgap.[1] The onset of the oxidation and reduction peaks are usually used to determine the bandgap as these values best represent the band edges of the defect-free polymer structure.[1]

Once the onset potentials are determined, the frontier molecular orbital energy levels of the material can be estimated by referencing to the ferrocenium/ferrocene (Fc^+/Fc) redox couple and converting to the units of eV. However, there is a lack of consistency on the formal potential of the Fc^+/Fc redox couple relative to vacuum, with potential values of –4.4, –4.8, and –5.1 eV

being used. Bazan and coworkers suggest a formal potential of –5.1 eV.[31] They also recommend that researchers provide details on the parameters and assumptions used in calculating the frontier molecular orbital energy levels.[2,31] Based on the recommendations of Bazan and coworkers, the frontier molecular orbitals can be determined from the following equations:[2,31]

$$E_{\text{HOMO}} = -(E_{[\text{onset,ox vs. Fc+/Fc}]} + 5.1)(\text{eV}) \qquad \text{(Equation 1.1)}$$

$$E_{\text{LUMO}} = -(E_{[\text{onset,red vs. Fc+/Fc}]} + 5.1)(\text{eV}) \qquad \text{(Equation 1.2)}$$

Due to the limited potential window of electrolyte solutions used in cyclic voltammetry, the oxidation or reduction of the species may fall outside that window. To overcome this limitation, the optical bandgap can be measured by absorption spectroscopy, where the bandgap of the solid-state material is derived from the absorption onset.[1,32] There are several ways to determine the onset value. However, a common method is to plot the long-wavelength side of the spectrum as photon energy ($h\nu$) versus the square of absorbance multiplied by photon energy ($(A*h\nu)^2$), extending the linear segment of this plot to the y-intercept gives the optical bandgap (Figure 1.6).[1]

The plot of photon energy versus absorbance multiplied by photon energy squared is derived from the following equations, which are commonly used for traditional amorphous semiconductors:

$$\alpha h\nu = B(h\nu - E_g^{opt})^n \qquad \text{(Equation 1.3)}$$

where α is the absorption coefficient, B is a constant, n is set equal to ½ for conjugated polymers, and E_g^{opt} is the optical bandgap.[1] Using the fact that $\alpha \approx A$, Equation 1.3 can be rewritten to give Equation 1.4.[1]

$$h\nu \approx \left[(A \times h\nu)^2 + E_g^{opt}\right] \qquad \text{(Equation 1.4)}$$

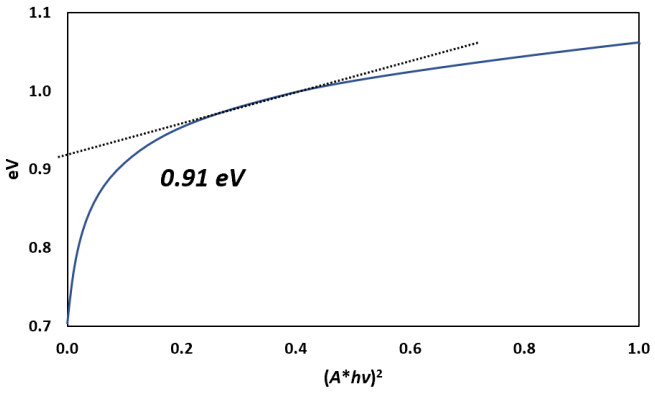

Figure 1.6. Plot of photon energy versus absorbance multiplied by photon energy squared ($(A*hv)^2$), a method used to determine optical bandgap by absorption spectroscopy.

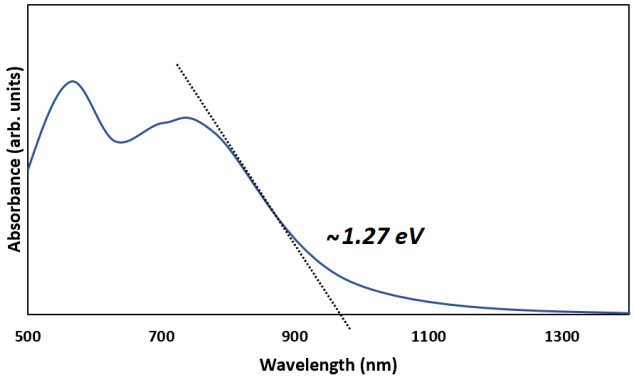

Figure 1.7. Example of how to determine the bandgap of a solid-state material by extending the steepest part of the long-wavelength side of the absorption band to the baseline.[1]

A simpler method for estimating the bandgap through absorption spectroscopy is to extend the steepest part of the long-wavelength side of the absorption band to the baseline. Once the absorption onset is determined, the following equation can be used to convert wavelength to energy:

$$E = h\nu = \frac{hc}{\lambda} \qquad \text{(Equation 1.5)}$$

where h is Planck's constant, ν is the frequency of light, c is the speed of light, and λ is the wavelength of light. Since bandgap is generally reported in units of electron volts, Planck's

constant should be in units of electron volt-seconds for this conversion. Considering the absorption spectrum shown in Figure 1.7 with an absorption onset of ~975 nm, the optical bandgap can be determined as follows:

$$\frac{(4.136\times10^{-15}\ eV\cdot s)(3.00\times10^{8}\ m\cdot s^{-1})}{975\times10^{-9}\ m} = 1.27\ eV \qquad \text{(Equation 1.6)}$$

However, this method is less accurate than other methods.[1] It should be noted that the bandgap determined through electrochemistry (E_g^{elec}) is usually larger than E_g^{opt}. This is because upon absorption of a photon, an electron is excited to the lowest excited state, and the electron and hole stay bound to each other. Therefore, the difference between E_g^{elec} and E_g^{opt} equals the electron-hole pair binding energy (E_B).[1,21] Moreover, there are alternative ways to measure the bandgap, such as UV photoelectron spectroscopy (UPS) or inverse photoelectron spectroscopy (IPES).[12,33] Optical bandgap can also be determined from the point where the absorption and emission spectra intersect.[12,34]

1.3. Bandgap Tuning

As previously stated, the bandgap of a material is an important property that dictates optical and electronic properties. Therefore, tuning the bandgap is of interest. Several factors that impact the bandgap of a material are effective conjugation length, planarity, monomer aromaticity, heteroatom effects, bond length alternation, substituents, and intermolecular interactions.[1,2,12–14,20,22]

1.3.1. Effective Conjugation Length

Extending the conjugation length of a conjugated species generally decreases the material's bandgap.[35] However, this relationship between conjugation length and bandgap only applies up to a certain conjugation length. For example, computational studies suggest that when

a polythiophene chain reaches ~22 units, electronic properties converge, and increasing conjugation past this point has little impact on the bandgap.[36] Thus, it is vital to recognize the difference between *conjugation length* and *effective conjugation length*, with the latter being dictated by the topology of the frontier molecular orbitals.[2,37] When the conjugation length becomes longer than the effective conjugation length, physical properties are still impacted, however, optical and electronic properties see little to no change.[2] Optical spectroscopy is commonly used to determine effective conjugation length.[2]

In 2003, Izumi et al. synthesized and characterized a series of soluble oligothiophenes.[38] They observed a red shift in the π–π* absorption band up to the oligomer with 96 repeat units. The shorter oligomers exhibited a linear relationship between the transition energy and the inverse number of repeat units. However, the longer oligomers (36 repeat units and above) exhibited a deviation from linearity, likely due to reaching the effective conjugation length. However, not all conjugated polymers exhibit the same effective conjugation length, as polyphenylene derivatives have been found to have an effective conjugation length of ~20 benzene rings.[39]

1.3.2. Planarity

Another factor that impacts bandgap is the mean dihedral angle between monomeric units,[13,14] with enhanced coplanarity between units generally leading to a decrease in bandgap.[12,22] As conjugation is the link between π-systems, delocalization of π-electrons occurs when there is good overlap between the *p*-orbitals of neighboring monomeric units.[2] A well-known example of planarity's impact on optical and electronic properties is regioregular and regiorandom poly(3-hexylthiophene) (P3HT).[40–43] The 3-hexylthiophene monomer is asymmetric, and thus there are several regioisomers possible for a 3-hexylthiophene trimer,

shown in Figure 1.8. Unfavorable chain-chain interactions occur in the HT-HH trimer, which can cause an increase in the dihedral angle between thiophene units and thus negatively impact π-electron delocalization (Figure 1.9). Thus, regioregular P3HT consisting of HT couplings experiences better π-electron delocalization than regiorandom P3HT, which is observed in the difference in bandgap (~1.8 eV vs. ~2.1 eV).[42] In addition, it has been found that regioregular P3HT exhibits higher electrical conductivity[40] and higher charge transport than regiorandom P3HT.[43] Beyond chain-chain interactions, a second interaction brought upon by side chains is present in poly(3-alkylthiophene)s (P3AT) between the side chain and the sulfur lone pair (Figure 1.10). However, this interaction is present in both regioregular and regiorandom P3AT.[2,44]

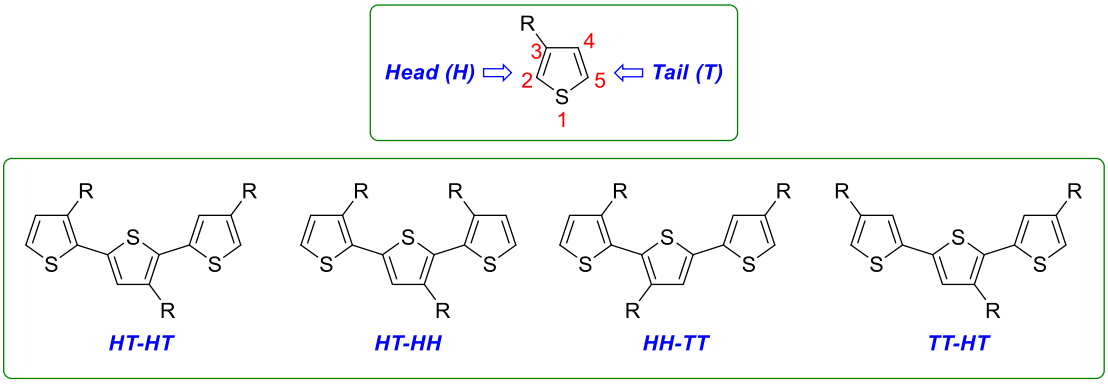

Figure 1.8. Regiochemistry of 3-hexylthiophene trimers.

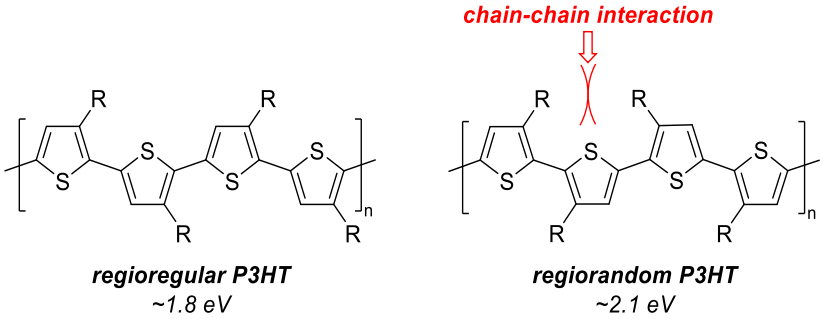

Figure 1.9. Regioregular P3HT and regiorandom P3HT and their respective bandgaps.[42]

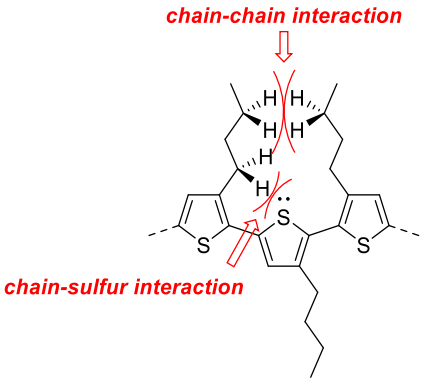

Figure 1.10. Chain-chain and chain-sulfur interactions in P3AT.[2,40]

1.3.3. Monomer Aromaticity

Another factor that impacts bandgap is the aromaticity of the monomeric units. Monomer aromaticity is related to the confinement of π-electrons to an aromatic unit.[2] A decrease in monomer aromaticity results in greater delocalization of π-electrons along the polymer backbone, resulting in a decrease in bandgap. For example, thiophene has a lower resonance energy than benzene (20.3 kJ mol^{-1} vs. 25.0 kJ mol^{-1}),[45] and thus polythiophene has a lower bandgap than polyphenylene (~2.0 eV vs. ~3.4 eV)[45,46] (Figure 1.11).[1] However, monomer resonance energy is not the only factor that impacts the bandgap. This is apparent for the polymers composed of five-membered heterocycles shown in Figure 1.11, as furan has the lowest resonance energy, but polyfuran does not have the lowest bandgap. Thus, other factors that impact the bandgap need to be considered.

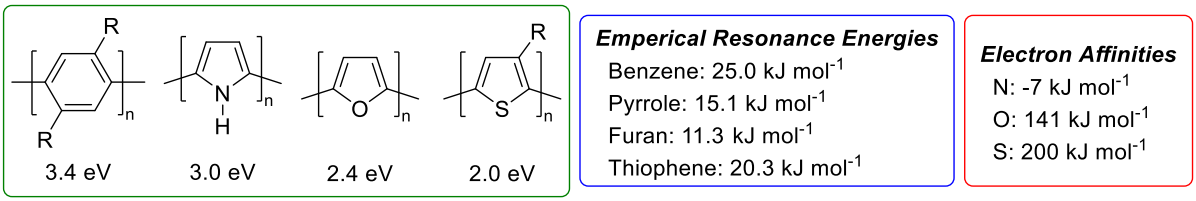

Figure 1.11. Monomer empirical resonance energies, heteroatom electron affinities, and polymer bandgaps.[1,2,45,48]

1.3.4. Heteroatom Effects

Another factor that impacts the bandgap of conjugated polymers composed of heterocyclic monomers (i.e., polythiophene and polypyrrole) is the heteroatom of the monomeric units.[1,2,22] It is believed that heteroatoms with higher electron affinities result in materials with lower bandgaps,[1,2] which explains the bandgap trend for polymers composed of five-membered heterocycles shown in Figure 1.11. For example, sulfur has a higher electron affinity than nitrogen (200 kJ mol^{-1} vs. –7 kJ mol^{-1}), and polythiophene has a smaller bandgap than polypyrrole (~2.0 eV vs. ~3.0 eV).[1,2]

1.3.5. Bond Length Alternation

Another factor that impacts bandgap is bond length alternation (Δr) – the difference in bond length between the longest and shortest carbon-carbon bond in the polymer backbone (Figure 1.12).[1,2,12,14,20] A decrease in bond length alternation generally leads to a decrease in bandgap.[1,2,12,14,20] For example, it is thought that *trans*-polyacetylene with complete delocalization of π-electrons along the polymer backbone (i.e., zero bond length alternation) would exhibit a bandgap of 0 eV.[2] However, studies suggest that complete delocalization of π-electrons in a 1D conjugated system is unstable, and thus the π-electrons are localized.[12,14] The localization of π-electrons results in the experimentally observed *trans*-polyacetylene bandgap of 1.5 eV.[2] Bond length alternation is thought to have a relatively large impact on the bandgap energy.[1,14]

For polyaromatic systems the bandgap is not directly related to bond length alternation. Instead, the bandgap is related to the quinoidal character of the backbone, which will be discussed in greater detail in section 1.5.[2,49] Nevertheless, bond length alternation has been used to estimate the degree of quinoidal character of some conjugated species, with the aromatic form

often being represented by positive Δr values and the quinoid form often being represented by negative Δr values.[2] In addition, the absolute value of Δr is generally slightly larger for the aromatic form compared to the quinoid form.[2]

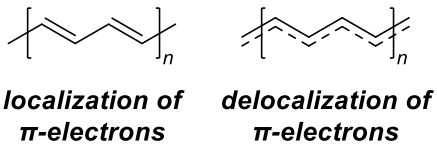

Figure 1.12. Polyacetylene with nonzero bond length alternation (left) and zero bond length alternation (right).

1.3.6. Substituents

Another factor that impacts bandgap is the nature of substituents attached to the monomeric units.[2,12–14,22] It has been found that functionalization with electron-donating [withdrawing] substituents destabilizes [stabilizes] the HOMO and LUMO energy levels (Figure 1.13).[12,13] The addition of substituents can decrease the bandgap if the impact on the HOMO and LUMO energy levels is asymmetric (Figure 1.13).[2] For example, if adding an electron-donating group leads to a greater destabilization of the HOMO relative to the LUMO, the result is a decrease in bandgap. In addition, stabilization of a material's HOMO by functionalizing with electron-withdrawing groups is a straightforward way to increase the stability of a material toward overoxidation.[50]

It has been found that the functionality should be attached directly to the conjugated backbone to maximize the substituent's electronic effect.[2] To minimize the substituent's electronic effect while retaining its physical properties, it has been found that two methylene units between the conjugated backbone and the functionality are sufficient. However, the substituent can still impact the resulting electronic properties due to steric effects.[2]

In a 1994 computational study by Brédas and Heeger,[51] they found that functionalization of poly(*p*-phenylene vinylene) (PPV) with electron-donating methoxy groups led to a greater HOMO destabilization than LUMO destabilization and thus a decreased bandgap relative to PPV, which they claim matches well with experimental results. In addition, they found that functionalization of PPV with electron-withdrawing cyano groups led to a greater LUMO stabilization than HOMO stabilization and thus a decreased bandgap relative to PPV.

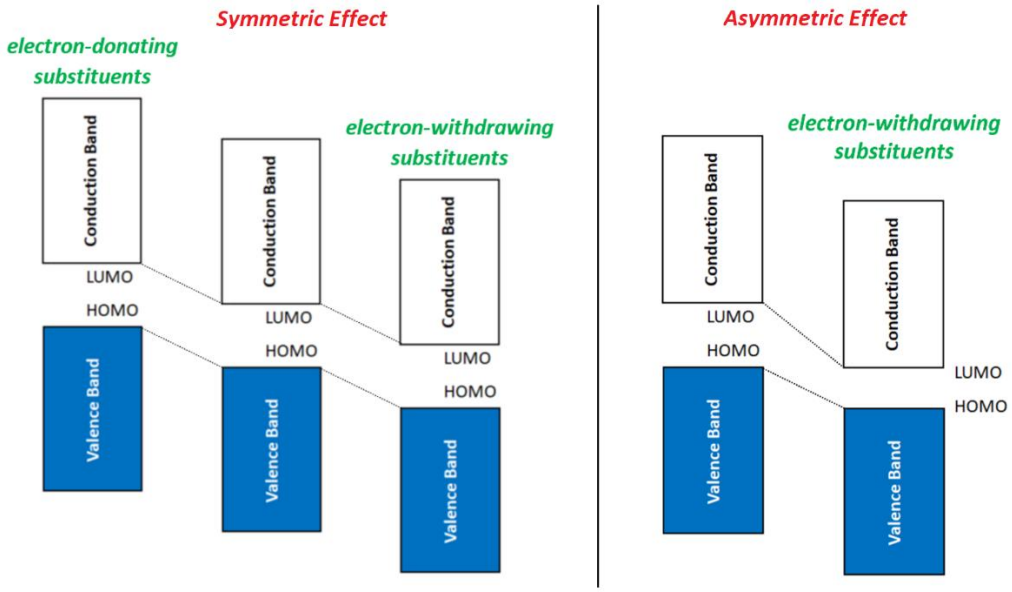

Figure 1.13. Impact of substituents with symmetric and asymmetric effects on frontier molecular orbital energy levels.

Rasmussen and coworkers have shown that the position and nature of the substituents can result in asymmetric tuning of the frontier molecular orbital energy levels and consequently tune the bandgap of the resulting material. When thieno[3,4-*b*]pyrazine (TP) was functionalized at the 2- and 3-positions with electron-donating groups, they observed that the resulting polymer exhibited an increase in bandgap relative to the alkyl functionalized analog. They suggest the increase in bandgap is due to the HOMO of TP being thiophene localized and the LUMO of TP

being pyrazine localized. Thus attaching the electron-donating group to the pyrazine ring has a greater impact on the LUMO than the HOMO, causing an increase in bandgap (Figure 1.14).[52,53]

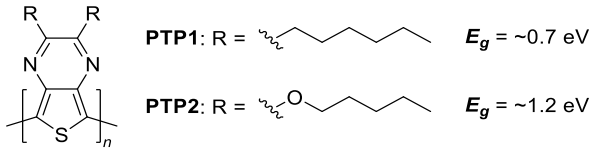

Figure 1.14. TP homopolymers functionalized with alkyl and alkoxy side chains studied by Rasmussen and coworkers.

In addition to electronic effects, there can also be intramolecular interactions brought on by substituents. For example, poly(3,4-ethylenedioxythiophene) has been found to exhibit sulfur-oxygen interactions between neighboring units, which increases the planarity of this polymer (Figure 1.15).[54] In addition, the crystal structure of a TP-3,4-ethylenedioxythiophene (EDOT) trimer has been found to be planar, potentially due to sulfur-nitrogen interactions.[54]

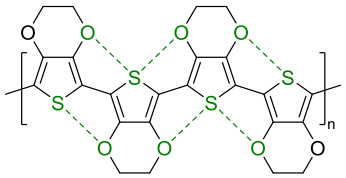

Figure 1.15. Sulfur-oxygen interactions present in poly(3,4-ethylenedioxythiophene).

Another example of functionalization causing an increase in bandgap was observed by Rasmussen in coworkers in 2023.[55] It was found that a TP-benzothiadiazole (TP-BTD) alternating copolymer exhibited a bandgap of 1.02 eV and that this polymer exhibited strong hydrogen bonding between the aromatic hydrogen of the BTD unit and the nitrogen of the TP unit, which led to increased planarity in this polymer. However, a similar fluorinated polymer (TP-F_2BTD) exhibited a bandgap of 1.60 eV, which is potentially due to repulsive interactions

between the fluorine of the F_2BTD unit and the nitrogen of the TP unit, which causes an increase in the dihedral angle between monomeric units (Figure 1.16).

1.3.7. Intermolecular Interactions and π-Stacking

Intermolecular interaction and π-stacking are other factors that impact bandgap.[1,2,12,14,22] Intermolecular interactions are mainly accountable for the blending of molecular orbitals upon creating the valence and conduction bands in the bulk solid-state material.[1,56] An increase in intermolecular interactions causes a decrease in the bandgap by improving the electron delocalization between adjacent polymer chains.[1] In addition, π-stacking can result in planarization of the conjugated backbone, which further decreases bandgap.[2]

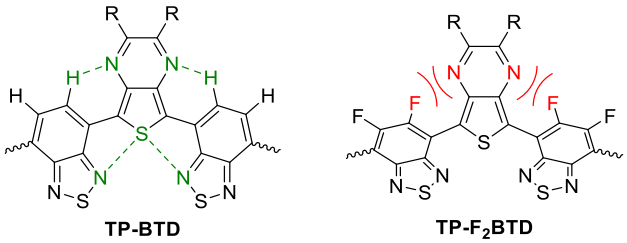

Figure 1.16. Hydrogen bonding in TP-BTD and repulsive nitrogen–fluorine interactions in TP-F_2BTD alternating copolymers synthesized by Rasmussen and coworkers.

The term π-stacking or π-π interactions are used to describe favorable interactions between aromatic systems. However, it is crucial to understand that these terms do not suggest favorable interactions between the π-electrons of both aromatic systems.[57,58] If this were the case, an eclipsed interaction (Figure 1.17) between aromatic species would be common, however, this is not the case.[58] Alternatively, slipped-stack and edge-to-face interactions are observed (Figure 1.17), which are favorable due to the uneven charge distribution in aromatic species where the π-electron cloud above and below the aromatic ring possess a partial negative charge, and the edges of the aromatic ring possess a partial positive charge. Thus favorable interactions occur between the partial positive and negative portions of each species.[2,57,58]

In the case of overlap between electron-rich and electron-poor aromatic species, an eclipsed orientation can be adopted due to the difference in polarization between the two systems.[2,58] However, it has also been suggested that these "*aromatic donor–acceptor interactions*" could be due to favorable interactions between the substituents attached to the aromatic rings instead of the interaction between aromatic rings with different polarization.[58]

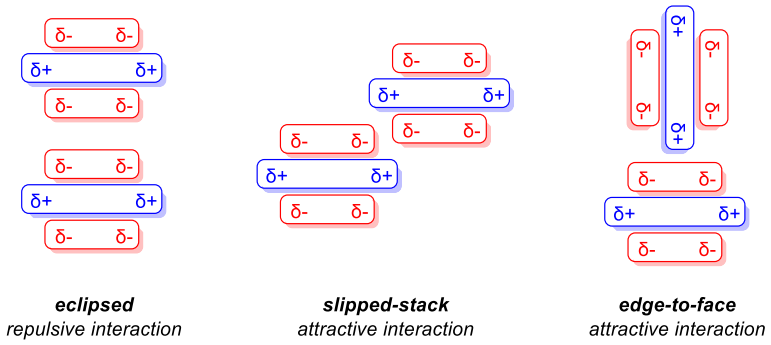

Figure 1.17. Possible repulsive and attractive interactions between two aromatic species.

1.4. Side Chains and Solubility

Solution-processable conjugated polymers often have rigid π-conjugated backbones and flexible side chains attached to some portion of the monomeric units (Figure 1.18). The flexible side chains are often employed to improve the solubility and processability of the resulting material.[15–18,59,60] In addition, side chains can be used to avoid low solubility-induced precipitation of the growing polymer chain during synthesis, thus yielding higher molecular weight polymers.[61]

Alkyl chains can enhance the solubility of conjugated polymers in common organic solvents.[15–18,59,60] Reid et al. proposed that the side chains impact the interactions between the polymer and solvent and interactions between solvent molecules, and these interactions overcome the free energy of aggregation and lead to enhanced solubility.[62] They also suggest

that side chains led to increased disorder, which is entropically favored. However, these entropic effects are considered minor compared to enthalpic effects.

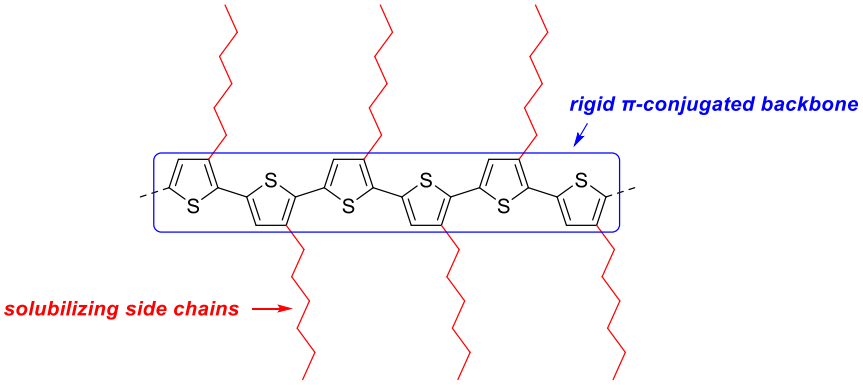

Figure 1.18. Conjugated polymer with a rigid π-conjugated backbone and solubilizing side chains.

The length of linear alkyl side chains has been used to tune polymer solubility. It has been found that polythiophenes require alkyl side chains longer than butyl chains to give materials with adequate solubility.[17] However, alkyl side chains that are too long can negatively impact interchain interactions and the solid-state material's absorption.[2] In addition, long side chains can lead to side chain crystallization, which decreases the polymer's solubility.[61]

An alternative option to linear alkyl side chains are branched alkyl side chains (Figure 1.19), which tend to give polymers with enhanced solubility due to steric and thermodynamic effects.[15–18,59,60,62] Branched alkyl side chains discourage side chain crystallization, sometimes seen with linear alkyl side chains.[2] However, commonly employed branched side chains are branched at the 2-position (e.g., 2-ethylhexyl and 2-octyldodecyl),[15,16,18] which is close to the polymer backbone, and thus can lead to enhanced steric hindrance.

Discussed above are side chains that only entail carbon and hydrogen atoms. However, other possible side chains include heteroatoms such as Si, O, and F. The difference in

electronegativity, bond lengths, and bond angles brought on by these heteroatoms can allow tuning of the resulting polymer properties.[2]

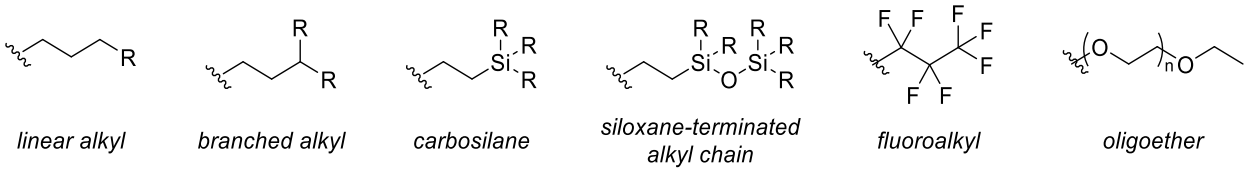

Figure 1.19. Common side chains applied to conjugated polymers.

Side chains that include silicon atoms (i.e., carbosilane and siloxane-terminated chains) (Figure 1.19) have been found to increase the resulting materials' solubility and flexibility. It is thought that polymers functionalized with siloxane-terminated side chains exhibit enhanced solubility due to the differences in bond lengths between Si–O and C–C bonds and bond angles between Si–O–Si and C–C–C.[59] Another class of side chains that have gained interest are fluoroalkyl side chains (Figure 1.19). It has been found that fluoroalkyl side chains can discourage water and oxygen diffusion, increasing the stability of the resulting material.[60] The enhanced stability can be attributed to the larger van der Waals radii of fluoroalkyl chains compared to traditional alkyl chains.[15] However, fluoroalkyl side chains often exhibit poor solubility in common organic solvents, and they can bioaccumulate.[16] Oligoether side chains (Figure 1.19) have gained interest due to their hydrophilicity.[63] Oligoether side chains exhibit enhanced polarity due to the large electronegativity difference between carbon and oxygen.[63] This can enhance the solubility of conjugated polymers in polar solvents, which can be useful for biological applications and green processing.[63] Oligoether side chains exhibit enhanced flexibility compared to traditional alkyl side chains, which is attributed to the decreased steric interactions between the neighboring methylene carbons and oxygen atom in oligoether side

chains (–CH_2–O–CH_2–) compared to the steric interactions between neighboring methylene carbons in traditional alkyl side chains (–CH_2–CH_2–).[63]

1.5. Quinoid Character

The quinoid character is another factor that impacts the bandgap of polymers with repeating aromatic units (i.e., polythiophene).[1,2,12,14,20,22,32,49,64] Polymers that consist of repeating aromatic units have two resonance forms – aromatic and quinoid (Figure 1.20). An increase in the quinoid character of a polymer backbone generally leads to a decrease in bandgap. However, the quinoid form is usually higher in energy than the aromatic form (Figure 1.20). Thus it has been found that increasing stability of the quinoid form causes a decrease in bandgap.[1,35,49,65]

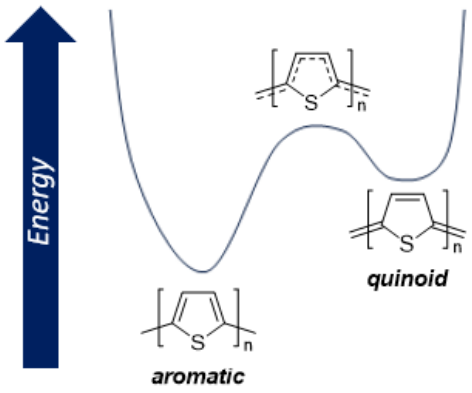

Figure 1.20. Aromatic and quinoid form of polythiophene.

A well-known example of the impact that quinoid character has on bandgap is polyisothianaphthene (PITN), which was first synthesized by Wudl and coworkers in 1984.[26] In the monomeric unit of PITN, a benzene ring is fused with a thiophene ring. Thus, only one of these rings is allowed to have an aromatic sextet. Since benzene has a higher resonance energy than thiophene, benzene is more likely to be in the aromatic form, thus increasing the quinoid character of the polymer backbone, leading PITN to exhibit a smaller bandgap than polythiophene (~1.0 eV vs. ~2.0 eV) (Figure 1.21).[1,14,22] However, the decrease in bandgap of

PITN is accompanied by a significant destabilization of the HOMO energy level (Figure 1.21), which increases PITN's susceptibility to oxidation. It has been found that PITN is not stable under ambient conditions, limiting its application to devices.[35]

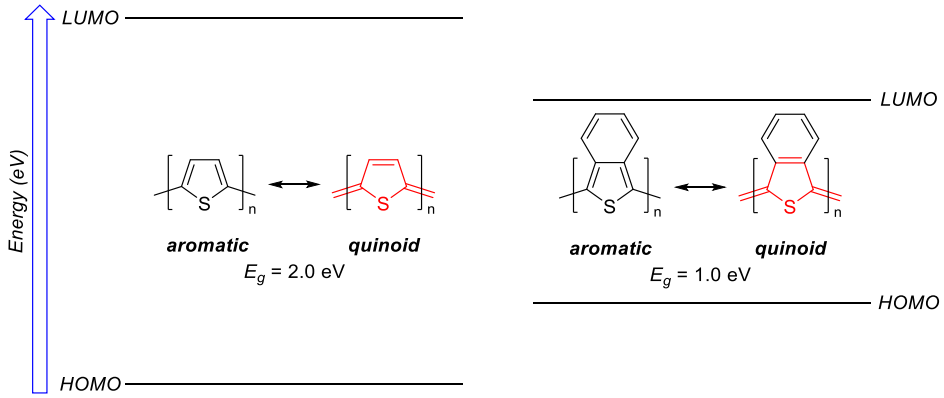

Figure 1.21. Illustration of polythiophenes and PITNs frontier molecular orbital energy levels.

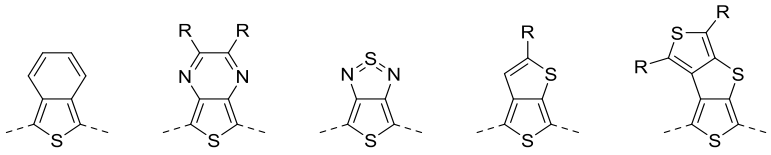

Figure 1.22. Proquinoidal monomeric units.

Monomeric units which are not quinoidal in the monomeric form but, when applied to a polymer, can increase the quinoidal nature of that polymer (i.e., isothianaphthene) are sometimes referred to as *proquinoidal* units (Figure 1.22).[19,65] A common characteristic of proquinoidal units is the fusing of aromatic rings to the main-chain ring, which causes an increase in the quinoidal character of the polymer backbone due to competition for aromaticity between the fused aromatic rings, as discussed above.[65] Monomeric units that adopt a true quinoidal constitution have been introduced recently and applied to produce low bandgap polymers.[19,35,65] One example is pyrrole-based quinoid monomers, which have been used to produce low bandgap

materials (Figure 1.23).[19,35] Their quinoidal and electron-deficient nature leads to low bandgaps and stabilized frontier molecular orbital energy levels.[19,35] In addition, the ability to functionalize at the *N*-positions with alkyl chains allows the synthesis of processable materials.[19,35]

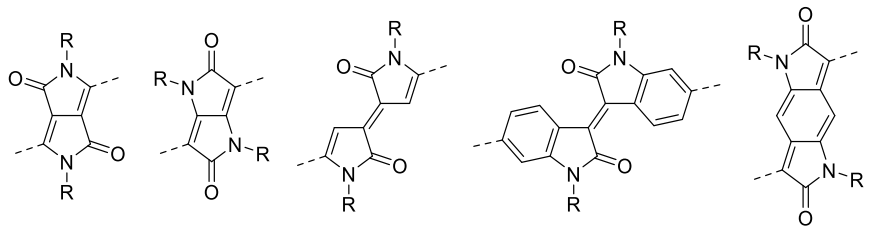

Figure 1.23. Pyrrole-based quinoidal units.

1.6. Donor-Acceptor Framework

The most common approach to generating low bandgap materials is through donor-acceptor (D–A) frameworks.[1,2,12,19,66] This approach was first utilized by Havinga and coworkers in 1992[67,68] when they synthesized copolymers in which the monomeric units alternated between donor (electron rich) and acceptor (electron poor) units. A donor unit is a monomer with a high-lying HOMO, and an acceptor unit is a monomer with a low-lying LUMO. Some common examples of donor and acceptor units used to synthesize D–A polymers are shown in Figure 1.24.

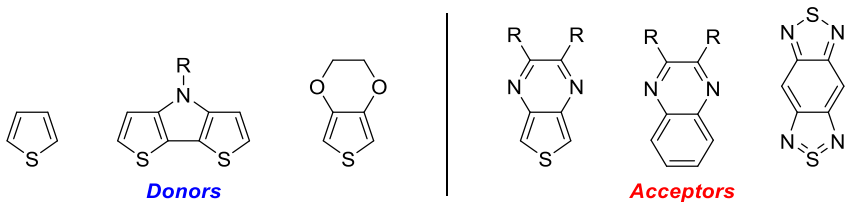

Figure 1.24. Common units applied to D–A systems.

Several explanations for the low bandgaps observed in donor-acceptor polymers have been given. However, the most widely accepted explanation is that hybridization of the frontier

molecular orbital energy levels of the donor and acceptor unit leads to a decrease in bandgap.[1,2,20,69] Shown in Figure 1.25 is an illustration of frontier orbital mixing in donor-donor, acceptor-acceptor, and donor-acceptor dimers. Both homodimers exhibit a destabilized HOMO and a stabilized LUMO relative to their respective monomers, and thus a decrease in the HOMO–LUMO energy. The decrease in the HOMO–LUMO energy of the homodimers is consistent with the idea that increasing conjugation length leads to a decrease in HOMO-LUMO energy. Due to the energetic mismatch between the frontier orbitals of the donor and acceptor, hybridization in the asymmetric dimer leads to a HOMO, which is characteristic of the donor unit, and a LUMO, which is characteristic of the acceptor unit.[1,2,19] Thus, the donor-acceptor dimer exhibits a smaller HOMO–LUMO energy than both homodimers.[1]

It has been found that there is generally mixing between the HOMOs of the donor and acceptor units in D–A frameworks. However, the destabilization of the D–A dimer HOMO is less than that of the symmetric dimer HOMO due to a mismatch in energy between the HOMO energy levels of the donor and acceptor units. In contrast, no mixing is generally observed for the LUMOs as the energetic difference between the LUMO energy levels is generally too large to allow for adequate mixing.[1,2,19] A common misconception is that the HOMO is localized on the donor unit, and the LUMO is localized on the acceptor unit in D–A systems.[2] However, theoretical calculations have suggested that the HOMO is delocalized along the polymer backbone.[2]

An alternate explanation to why D–A frameworks give low bandgaps has been proposed to be due to the contribution of a second resonance structure, which is shown in Figure 1.26. A mixture of these resonance forms would give a polymer with a decreased bond length alternation, and thus a smaller bandgap.[1,64,70] However, there is no experimental evidence in

support of this explanation.[2] Also, a recently reported crystal structure of a donor-acceptor dimer exhibited no shortening of the bond between the donor and acceptor units.[71]

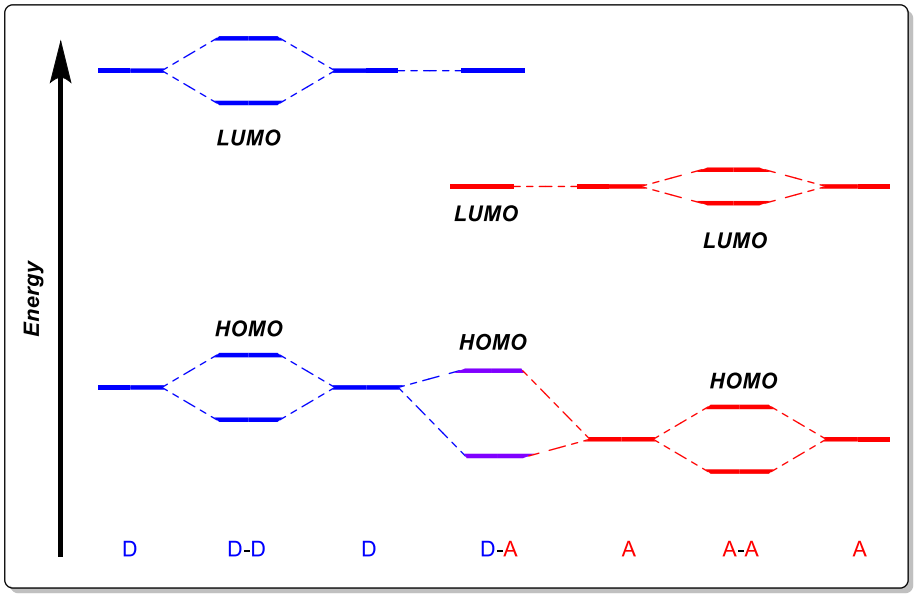

Figure 1.25. Hybridization of frontier molecular orbitals of donor-donor, donor-acceptor, and acceptor-acceptor dimers.

Figure 1.26. Proposed resonance structures of D–A polymers.

Some question whether D–A interactions exist. Some suggest that instead of D–A interactions, the low bandgaps stem from the alternation of aromatic and quinoid units.[1,2] This is because almost all donor units are aromatic, and most acceptor units are proquinoidal. Thus the aromatic and quinoidal contributions decrease the bond length alternation, which gives a lower bandgap.[1,2] An example of a low bandgap D–A polymer is shown in Figure 1.27. Some D–A–D small molecules with long-wavelength absorption and emission are shown in Figure 1.28.

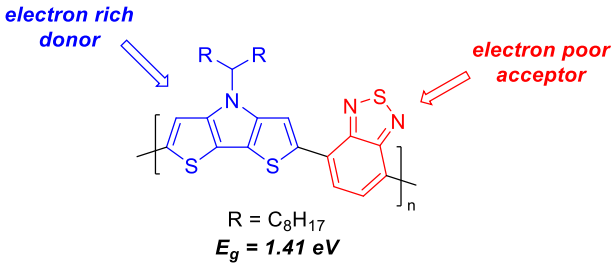

Figure 1.27. Example of a low bandgap D–A alternating copolymer.[72]

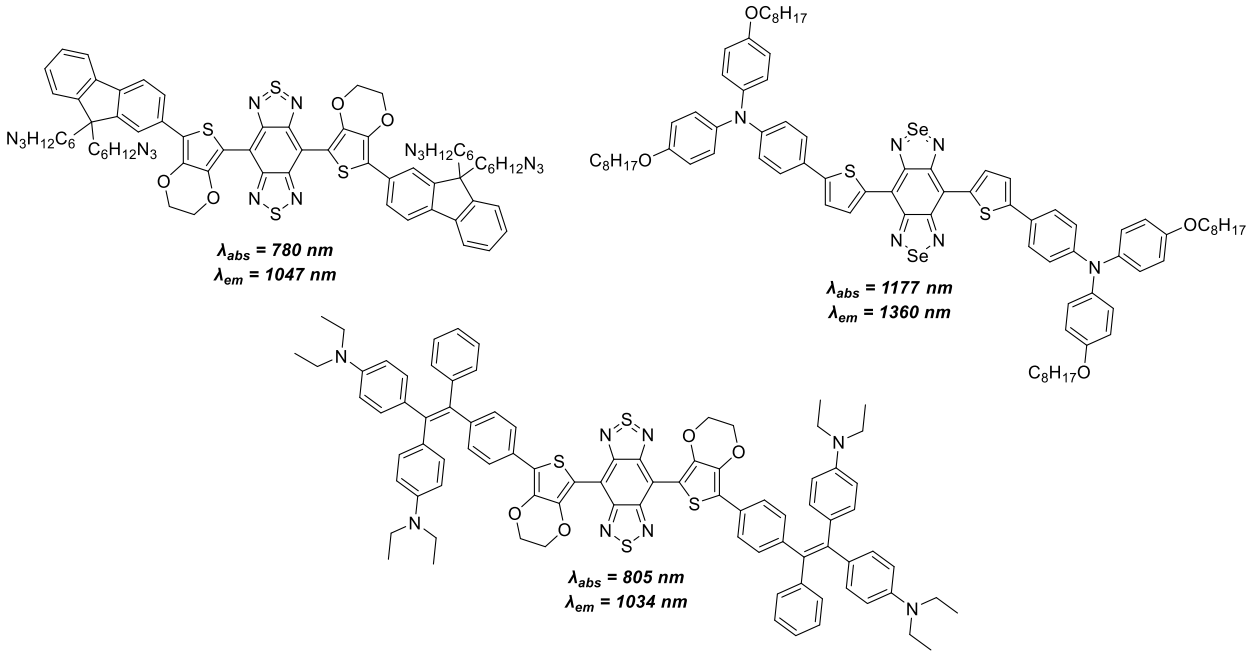

Figure 1.28. Examples of D–A–D small molecules and their respective absorption and emission wavelengths.[73–75]

1.7. Thieno[3,4-*b*]pyrazine as an Ambipolar Unit

The donor-acceptor framework was initially proposed for polysquaraines and polycroconaines,[67,68] and this model has since been applied to virtually all D–A systems.[76] A common misconception that is repeated throughout the literature is that monomeric units are classified as either a donor, acceptor, or neutral spacer – a unit used to introduce space between the donor and acceptor units to reduce steric interactions.[2,19,77] However, in 2009, Janssen and

coworkers suggested that one reason that thiophene-TP copolymers exhibit low bandgaps is due to the donor and acceptor character of the TP unit.[78] A more detailed 2014 study of TP-based oligomers found that TP has similar donor strength to the strong donor EDOT (Figure 1.29).[79] Thus, Rasmussen and coworkers have proposed classifying TP as an *ambipolar unit*, as it exhibits characteristics of a strong donor and a strong acceptor.[19,79] The ambipolar nature of TP can be attributed to the fusion of the electron-rich thiophene ring with the electron-poor pyrazine ring (Figure 1.29).[19] The ambipolar nature of TP is also shown in Figure 1.29 in which the acceptor strength of TP falls between the common acceptors quinoxaline (Qx) and BTD, and the donor strength of TP is almost as great as the common donor EDOT.[19]

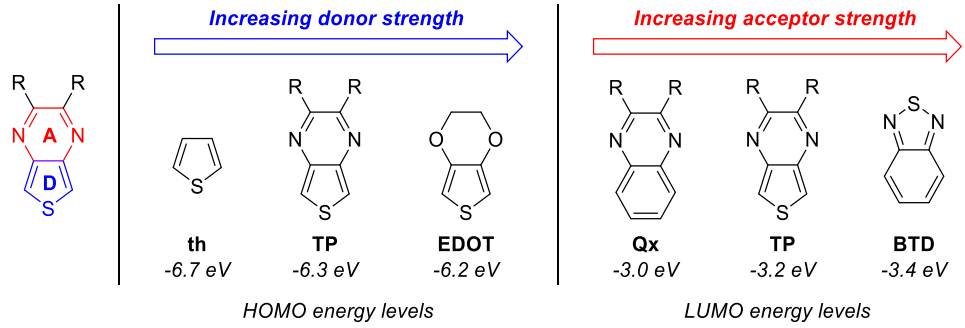

Figure 1.29. Illustration of the ambipolar nature of TP with the electron-rich thiophene ring and electron-poor pyrazine ring highlighted (left). Comparison of the HOMO energy levels of TP and common donors (middle). Comparison of the LUMO energy levels of TP and common acceptors (right).[19,55]

With the understanding that TP acts as a strong donor and a strong acceptor, some trends observed in TP-based polymers can be explained. First, the bithiophene-TP "donor-acceptor" copolymer exhibits a higher bandgap and lower HOMO energy level than the TP homopolymer (Figure 1.30).[19] This is because bithiophene is a weaker donor than TP. Thus hybridization of HOMO energy levels gives a stabilized HOMO energy level relative to the TP homopolymer, thus increasing the bandgap by ~0.8 eV.[19] However, pairing TP with a strong donor such as

dithieno[3,2-*b*:2',3'-*d*]pyrrole leads to enough destabilization of the HOMO energy level to match that of the TP homopolymer, thus giving a similar bandgap.[19,80]

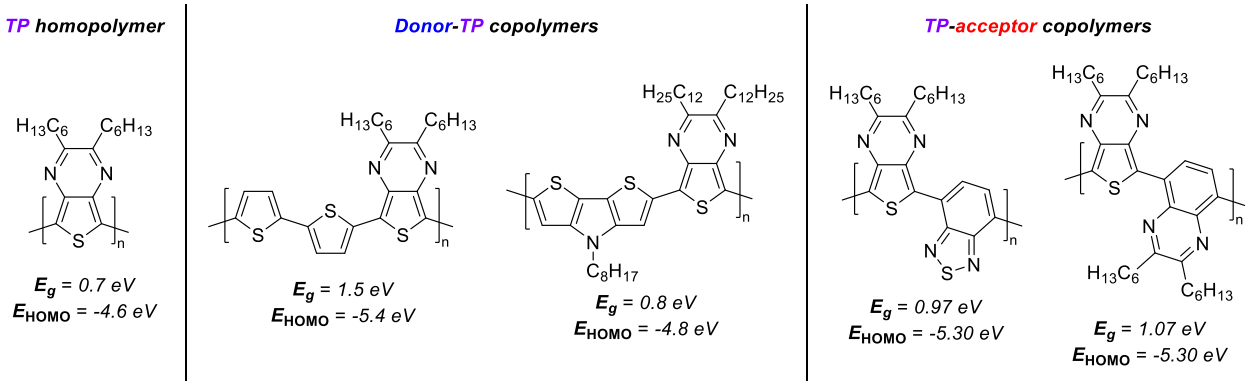

Figure 1.30. TP-based polymers and their corresponding bandgap and HOMO energy level.[19]

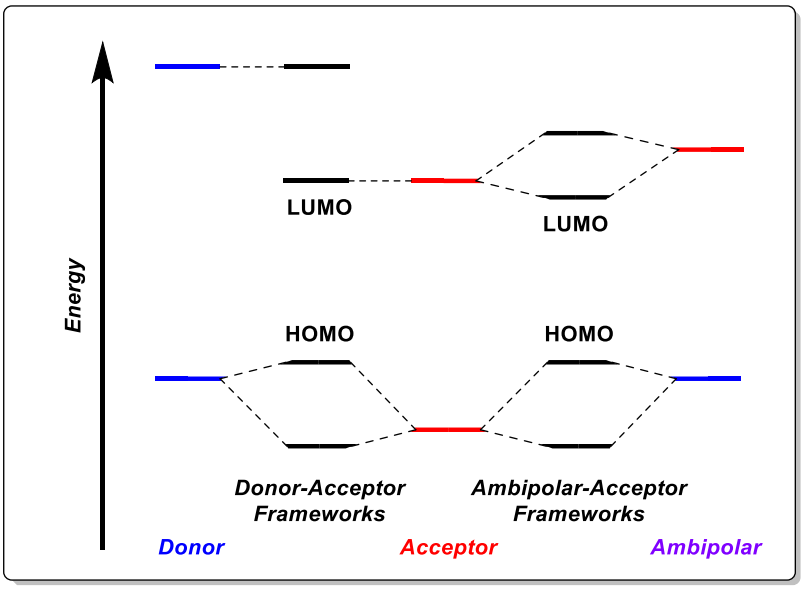

Figure 1.31. Hybridization of frontier molecular orbitals in donor-acceptor and ambipolar-acceptor frameworks.

In recent years it has been found that TP can also be paired with acceptors to produce low bandgap polymers (Figure 1.30).[19,55,76,81] This paring of TP with an acceptor leads to polymers with stabilized HOMO energy levels relative to the TP homopolymer and low-lying LUMOs due to stabilization brought on by LUMO orbital mixing between TP and the acceptor unit (Figure

1.31).[19] These TP-acceptor alternating copolymers exhibit low-lying LUMO energy levels and low bandgaps, allowing them to act as non-fullerene acceptors in OPVs.[55]

1.8. References

(1) Rasmussen, S. C. Low Bandgap Polymers. In *Encyclopedia of Polymeric Nanomaterials*; Kobayashi, S., Müllen, K., Eds.; Springer: Berlin, 2013; pp 1–13.

(2) Rasmussen, S. C.; Gilman, S. J.; Wilcox, W. D. *Conjugated Polymers – Synthesis and Design*; ACS In Focus, American Chemical Society: Washington, D.C., 2023, *Submitted*.

(3) Muller, P. *Pure Appl. Chem.* **1994**, *66* (5), 1077–1184.

(4) Phelan, N. F.; Orchin, M. *J. Chem. Educ.* **1968**, *45* (10), 633–637.

(5) Hodge, P.; Hellwich, K.-H.; Hiorns, R. C.; Jones, R. G.; Kahovec, J.; Luscombe, C. K.; Purbrick, M. D.; Wilks, E. S. *Pure Appl. Chem.* **2020**, *92* (5), 797–813.

(6) Rasmussen, S. C. *ChemPlusChem* **2020**, *85* (7), 1412–1429.

(7) Shirakawa, H.; Louis, E. J.; MacDiarmid, A. G.; Chiang, C. K.; Heeger, A. J. *Chem. Commun.* **1977**, 578–580.

(8) Chiang, C. K.; Fincher Jr., C. R.; Park, Y. W.; Heeger, A. J.; Shirakawa, H.; Louis, E. J.; Gau, S. C.; MacDiarmid, A. G. *Phys. Rev. Lett.* **1977**, *39*, 1098–1101.

(9) Rasmussen, S. C. *Conductive Polymers: Electrical Interactions in Cell Biology and Medicine*; Zhang, Z., Rouabhia, M., Moulton, s., Eds,; CRC Press: Boca Raton, FL, USA, 2017; pp 1–21.

(10) Glenis, S.; Horowitz, G.; Tourillon, G.; Garnier, F. *Thin Solid Films* **1984**, *111* (2), 93–103.

(11) Glenis, S.; Tourillon, G.; Garnier, F. *Thin Solid Films* **1984**, *122*, 9–17.

(12) Scharber, M. C.; Sariciftci, N. S. *Adv. Mater. Technol.* **2021**, *6* (4), 2000857.

(13) Liu, C.; Wang, K.; Gong, X.; Heeger, A. J. *Chem. Soc. Rev.* **2016**, *45* (17), 4825–4846.

(14) Roncali, J. *Macromol. Rapid Commun.* **2007**, *28* (17), 1761–1775.

(15) Lei, T.; Wang, J.-Y.; Pei, J. *Chem. Mater.* **2014**, *26* (1), 594–603.

(16) Mei, J.; Bao, Z. *Chem. Mater.* **2014**, *26* (1), 604–615.

(17) Zhang, Z.-G.; Li, Y. *Sci. China Chem.* **2015**, *58* (2), 192–209.

(18) Luo, N.; Ren, P.; Feng, Y.; Shao, X.; Zhang, H.-L.; Liu, Z. *J. Phys. Chem. Lett.* **2022**, *13* (4), 1131–1146.

(19) Rasmussen, S. C.; Gilman, S. J.; Wilcox, W. D. The Eternal Quest for Practical Low Bandgap Polymers. *Gen. Chem.* **2023**, *9*, 220010.

(20) Van Mullekom, H. *Mater. Sci. Eng. R Rep.* **2001**, *32* (1), 1–40.

(21) Bredas, J.-L. *Mater. Horiz.* **2014**, *1* (1), 17–19.

(22) Roncali, J. *Chem. Rev.* **1997**, *97* (1), 173–206.

(23) Tang, M. L.; Reichardt, A. D.; Wei, P.; Bao, Z. *J. Am. Chem. Soc.* **2009**, *131* (14), 5264–5273.

(24) Mazzio, K. A.; Luscombe, C. K. *Chem. Soc. Rev.* **2015**, *44* (1), 78–90.

(25) Darling, S. B.; You, F. *RSC Adv.* **2013**, *3*, 17633–17648.

(26) Wudl, F.; Kobayashi, M.; Heeger, A. J. *J. Org. Chem.* **1984**, *49* (18), 3382–3384.

(27) Bredas, J. L.; Themans, B.; Andre, J. M.; Heeger, A. J.; Wudl, F. *Synth. Met.* **1985**, *11* (6), 343–352.

(28) Rasmussen, S. C.; Schwiderski, R. L.; Mulholland, M. E. *Chem. Commun.* **2011**, *47* (41), 11394–11410.

(29) Dou, L.; Liu, Y.; Hong, Z.; Li, G.; Yang, Y. *Chem. Rev.* **2015**, *115* (23), 12633–12665.

(30) Rasmussen, S. C.; Gilman, S. J.; Culver, E. W.; Wilcox, W. D.; *Gen. Chem.* **2021**, *7* (2), 200019.

(31) Cardona, C. M.; Li, W.; Kaifer, A. E.; Stockdale, D.; Bazan, G. C. *Adv. Mater.* **2011**, *23* (20), 2367–2371.

(32) Chochos, C. L.; Choulis, S. A. *Prog. Polym. Sci.* **2011**, *36* (10), 1326–1414.

(33) Krause, S.; Casu, M. B.; Schöll, A.; Umbach, E. *New J. Phys.* **2008**, *10* (8), 085001.

(34) Vandewal, K.; Benduhn, J.; Nikolis, V. C. *Sustain. Energy Fuels* **2018**, *2* (3), 538–544.

(35) Mikie, T.; Osaka, I. *J. Mater. Chem. C* **2020**, *8* (41), 14262–14288.

(36) Ma, J.; Li, S.; Jiang, Y. *Macromolecules* **2002**, *35* (3), 1109–1115.

(37) Milián-Medina, B.; Gierschner, J. *Wiley Interdiscip. Rev. Comput. Mol. Sci.* **2012**, *2* (4), 513–524.

(38) Izumi, T.; Kobashi, S.; Takimiya, K.; Aso, Y.; Otsubo, T. *J. Am. Chem. Soc.* **2003**, *125* (18), 5286–5287.

(39) Klaerner, G.; Miller, R. D. *Macromolecules* **1998**, *31* (6), 2007–2009.

(40) McCullough, R. D.; Lowe, R. D. *J. Chem. Soc., Chem. Commun.* **1992**, *1*, 70–72.

(41) McCullough, R. D.; Lowe, R. D.; Jayaraman, M.; Anderson, D. L. *J. Org. Chem.* **1993**, *58* (4), 904–912.

(42) McCullough, R. D. *Adv. Mater.* **1998**, *10* (2), 93–116.

(43) Sirringhaus, H.; Brown, P. J.; Friend, R. H.; Nielsen, M. M.; Bechgaard, K.; Langeveld-Voss, B. M. W.; Spiering, A. J. H.; Janssen, R. A. J.; Meijer, E. W.; Herwig, P.; De Leeuw, D. M. *Nature* **1999**, *401* (6754), 685–688.

(44) Rasmussen, S. C.; Pickens, J. C.; Hutchison, J. E. *Chem. Mater.* **1998**, *10* (7), 1990–1999.

(45) Katritzky, A. R.; Pozharskii, A. F. *Handbook of Heterocyclic Chemistry*, 2nd ed.; Pergamon: Amsterdam, 2000; pp 80.

(46) Chung, T.-C.; Kaufman, J. H.; Heeger, A. J.; Wudl, F. *Phys. Rev. B* **1984**, *30* (2), 702–710.

(47) Lee, C. H.; Kang, G. W.; Jeon, J. W.; Song, W. J.; Kim, S. Y.; Seoul, C. *Synth. Met.* **2001**, *117*, 75–79.

(48) Glenis, S.; Benz, M.; LeGoff, E.; Schindler, J. L.; Kannewurf, C. R.; Kanatzidis, M. G. *J. Am. Chem. Soc.* **1993**, *115* (26), 12519–12525.

(49) Brédas, J. L. *J. Chem. Phys.* **1985**, *82* (8), 3808–3811.

(50) Ho, H. A.; Brisset, H.; Frère, P.; Roncali, J. *J. Chem. Soc., Chem. Commun.* **1995**, *22*, 2309–2310.

(51) Brédas, J. L.; Heeger, A. J. *Chem. Phys. Lett.* **1994**, *217*, 507–512.

(52) Wen, L.; Nietfeld, J. P.; Amb, C. M.; Rasmussen, S. C. *Synth. Met.* **2009**, *159* (21–22), 2299–2301.

(53) Kenning, D. D.; Rasmussen, S. C. *Macromolecules* **2003**, *36* (17), 6298–6299.

(54) Roncali, J.; Blanchard, P.; Frère, P. *J. Mater. Chem.* **2005**, *15* (16), 1589–1610.

(55) Wilcox, W. D.; Culver, E. W.; Nicolaidis, N. C.; Gilman, S. J.; Marsh, T. J.; Dastoor, P. C.; Rasmussen, S. C. **2023**, *In Prep*.

(56) Cornil, J.; Beljonne, D.; Calbert, J.-P.; Brédas, J.-L. *Adv. Mater.* **2001**, *13* (14), 1053–1067.

(57) Hunter, C. A.; Sanders, J. K. M. *J. Am. Chem. Soc.* **1990**, *112* (14), 5525–5534.

(58) Martinez, C. R.; Iverson, B. L. *Chem. Sci.* **2012**, *3* (7), 2191.

(59) Yang, Y.; Liu, Z.; Zhang, G.; Zhang, X.; Zhang, D. *Adv. Mater.* **2019**, *31* (46), 1903104.

(60) Lv, S.; Li, L.; Mu, Y.; Wan, X. *Polym. Rev.* **2021**, *61* (3), 520–552.

(61) Mulholland, M. E.; Wen, L.; Rasmussen, S. C. *Topol. Supramol. Polym. Sci.* **2015**, *2* (1), 18–29.

(62) Reid, D. R.; Jackson, N. E.; Bourque, A. J.; Snyder, C. R.; Jones, R. L.; de Pablo, J. J. *J. Phys. Chem. Lett.* **2018**, *9* (16), 4802–4807.

(63) Meng, B.; Liu, J.; Wang, L. *Polym. Chem.* **2020**, *11* (7), 1261–1270.

(64) Bundgaard, E.; Krebs, F. C. *Sol. Energy Mater. Sol. Cells* **2007**, *91* (11), 954–985.

(65) Ji, X.; Fang, L. *Polym. Chem.* **2021**, *12* (10), 1347–1361.

(66) Holliday, S.; Li, Y.; Luscombe, C. K. *Prog. Polym. Sci.* **2017**, *70*, 34–51.

(67) Havinga, E.; Hoeve, W.; Wynberg, H. *Polym. Bull.* **1992**, *29*, 119–126.

(68) Havinga, E. E.; Ten Hoeve, W.; Wynberg, H. *Synth. Met.* **1993**, *55* (1), 299–306.

(69) Brocks, G.; Tol, A. *J. Phys. Chem.* **1996**, *100* (5), 1838–1846.

(70) Chen, M.; Perzon, E.; Andersson, M. R.; Marcinkevicius, S.; Jönsson, S. K. M.; Fahlman, M.; Berggren, M. *Appl. Phys. Lett.* **2004**, *84* (18), 3570–3572.

(71) Anderson, T. E.; Culver, E. W.; Badía-Domínguez, I.; Wilcox, W. D.; Buysse, C. E.; Ruiz Delgado, M. C.; Rasmussen, S. C. *Phys. Chem. Chem. Phys.* **2021**, *23* (46), 26534–26546.

(72) Yue, W.; Zhao, Y.; Shao, S.; Tian, H.; Xie, Z.; Geng, Y.; Wang, F. *J. Mater. Chem.* **2009**, *19* (15), 2199.

(73) Yang, Q.; Ma, Z.; Wang, H.; Zhou, B.; Zhu, S.; Zhong, Y.; Wang, J.; Wan, H.; Antaris, A.; Ma, R.; Zhang, X.; Yang, J.; Zhang, X.; Sun, H.; Liu, W.; Liang, Y.; Dai, H. *Adv. Mater.* **2017**, *29* (12), 1605497.

(74) Qian, G.; Dai, B.; Luo, M.; Yu, D.; Zhan, J.; Zhang, Z.; Ma, D.; Wang, Z. Y. *Chem. Mater.* **2008**, *20* (19), 6208–6216.

(75) Lin, J.; Zeng, X.; Xiao, Y.; Tang, L.; Nong, J.; Liu, Y.; Zhou, H.; Ding, B.; Xu, F.; Tong, H.; Deng, Z.; Hong, X. *Chem. Sci.* **2019**, *10* (4), 1219–1226.

(76) Culver, E. W.; Anderson, T. E.; López Navarrete, J. T.; Ruiz Delgado, M. C.; Rasmussen, S. C. *ACS Macro Lett.* **2018**, *7* (10), 1215–1219.

(77) Mulholland, M. E.; Konkol, K. L.; Anderson, T. E.; Schwiderski, R. L.; Rasmussen, S. C. *Aust. J. Chem.* **2015**, *68* (11), 1759.

(78) Karsten, B. P.; Viani, L.; Gierschner, J.; Cornil, J.; Janssen, R. A. J. *J. Phys. Chem. A* **2009**, *113* (38), 10343–10350.

(79) Wen, L.; Heth, C. L.; Rasmussen, S. C. *Phys. Chem. Chem. Phys.* **2014**, *16* (16), 7231–7240.

(80) Evenson, S. J.; Mulholland, M. E.; Anderson, T. E.; Rasmussen, S. C. *Asian J. Org. Chem.* **2020**, *9* (9), 1333–1339.

(81) Anderson, T. E.; Culver, E. W.; Almyahi, F.; Dastoor, P. C.; Rasmussen, S. C. *Synlett* **2018**, *29* (19), 2542–2546.

CHAPTER 2. SYNTHESIS AND CHARACTERIZATION OF POLY(THIENO[3,4-*b*]-PYRAZINE)S FUNCTIONALIZED WITH BRANCHED ALKYL SIDE CHAINS

2.1. Introduction

As discussed in chapter 1, the properties of conjugated organic polymers can be tuned through molecular design, with a significant focus on bandgap tuning. Low bandgap (E_g < 1.5 eV) polymers are often targeted as they are suitable for use in photonic devices. Organic photovoltaic (OPV) devices made from low bandgap polymers can absorb light of longer wavelengths, resulting in a better overlap with the solar spectrum.[1–5] For example, a polymer with a bandgap of 2.0 eV can absorb around 30% of the solar radiation, while a polymer with a bandgap of approximately 1.1 eV can absorb approximately 77%.[1] Additionally, low bandgap polymers can be used to complement wider bandgap materials, like poly(3-hexylthiophene), in tandem solar cells.[6] However, due to the Shockley-Queisser limit, a solar cell's theoretical maximum power conversion efficiency with a single p-n junction is thought to be achieved with a material with a bandgap of 1.34 eV.[7,8]

Another application of low bandgap conjugated polymers is in near-infrared (NIR) photodetectors. NIR photodetectors are used for optical communication, nighttime surveillance, and remote control.[9–11] However, commercially available NIR photodetectors are made from inorganic materials such as InGaAs, which have disadvantages such as expensive manufacturing, rigidity, and limited spectral response tuning.[9] In contrast, conjugated polymers allow for inexpensive manufacturing, good flexibility, and simple tunability of their spectral response range.[9] However, less than 20 polymers exhibit photoresponse below 1000 nm, the majority of which are of high synthetic complexity.[9]

Thieno[3,4-*b*]pyrazine (TP) homopolymers show promise as candidates for OPVs and NIR photodetectors. These homopolymers have been found to absorb throughout the visible and well into the NIR portion of the spectrum.[12] They also exhibit good stability, and their properties can be adjusted by functionalization at the 2- and 3-positions.[13–15] Moreover, TP can be produced from thiophene in five steps with an overall yield of up to 75%.[15,16]

2.1.1. Thieno[3,4-b]pyrazine Homopolymers

In 1984, Wudl and coworkers synthesized the first low bandgap polymer, polyisothianaphthene (PITN), with a bandgap of 1.0 eV.[17] However, a computational study conducted by Nayak and Marynick in 1990 suggested that PITN is not planar in its aromatic form due to steric interactions between the sulfur and hydrogen atoms of neighboring isothianaphthene units.[18] To address this, they turned to poly(thieno[3,4-*b*]pyrazine) (PTP), which was expected to exhibit enhanced planarity and, therefore, a lower bandgap. Their calculations agreed, with the quinoid form of PTP having a calculated bandgap of 0.70 eV, whereas PITNs was 0.80 eV.

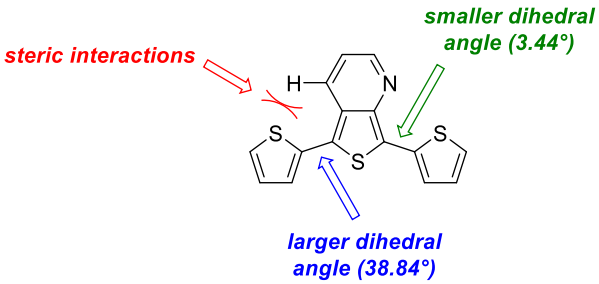

Figure 2.1. 2,4-bis(2-thienyl)thieno[3,4-*b*]pyridine with sulfur-hydrogen steric interactions shown.

Experimental data presented in 1994 by Ferraris et al.[19] provided evidence of the nonplanarity in PITN. Their study focused on the crystal structure of 2,4-bis(2-thienyl)thieno[3,4-*b*]pyridine and found that the thiophene ring at the 4-position (the side that

resembled PITN) exhibited a larger dihedral angle than the thiophene ring at the 2-position (the side that resembled PTP) (Figure 2.1).

In 1992, Pomerantz and coworkers made the first PTP by oxidative polymerization using $FeCl_3$ in chloroform under dry air (Figure 2.2).[20] They reported that the polymer had a weight average molecular weight of 3500 and exhibited a bandgap of ca. 0.95 eV, which was one of the lowest reported bandgaps at this time. However, they reported that the material was paramagnetic, but gave no explanation to why this was.

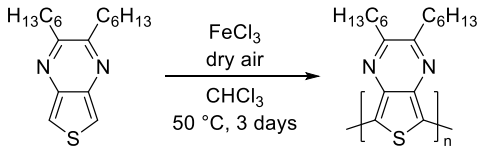

2.1a **2.2a**

Figure 2.2. Oxidative polymerization of TP in 1992 carried out by Pomerantz and coworkers.

In 1995, Vanderzande and coworkers synthesized unfunctionalized PTP by adding phosphorus pentasulfide to furo[3,4-*b*]pyrazine-5,7-dione while refluxing in xylenes (Figure 2.3).[21,22] The polymer was analyzed by elemental analysis and found to have a higher sulfur content than would be expected and some phosphorous contamination. This polymerization was revisited by Hagan et al. in 2001, where they reported the polymer to have a bandgap of 1.0 eV.[23]

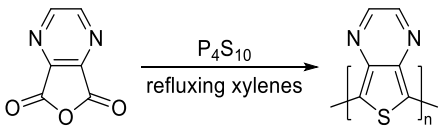

2.3 **2.2b**

Figure 2.3. Synthesis of PTP from furo[3,4-*b*]pyrazine-5,7-dione and phosphorus pentasulfide.

In 1998, Tamura et al. made eight TP homopolymers with alkyl chains and phenyl groups, as shown in Figure 2.4.[24] They made polymers by the lithiation of TP followed by

oxidation with copper(II) chloride. The polymers number average molecular weight ranged from 1200 to 6500, with the highest weight coming from polymer **2.2i**. In addition, they found that polymers **2.2e** and **2.2i** had bandgaps of less than 0.5 eV.

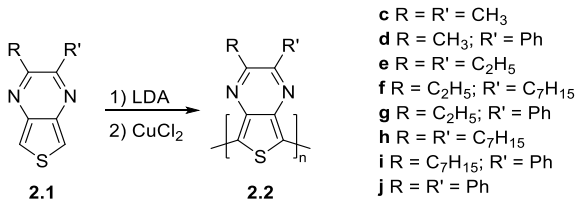

Figure 2.4. Polymerization of TPs reported by Tamura et al.

In 2003, Kenning and Rasmussen reported the electropolymerization of several PTPs (Figure 2.5).[12] They hypothesized that the paramagnetic properties of the PTP samples produced by Pomerantz and colleagues in 1992 could be due to Fe^{3+} chelation (Figure 2.5). To avoid iron contamination, they opted to create the polymers through electropolymerization. Initially, they reported that their electrochemically produced polymer films were relatively soluble in chloroform and tetrahydrofuran, however, they later reported that after further analysis, the materials were less soluble than they originally reported.[13] They reported bandgaps of 0.66 to 0.79 eV, with the lowest bandgap reported for polymer **2.2c**. They suggest that the higher bandgap of the polymer made through chemical oxidation could be attributed to Fe^{3+} chelation and overoxidation.

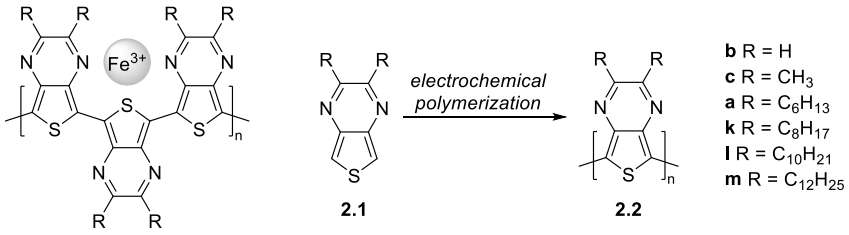

Figure 2.5. Fe^{3+} chelation in PTP (left) and the electrochemical polymerization of TPs (right) by Kenning and Rasmussen.

In 2008, Rasmussen and coworkers compared two methods of polymerization for creating polymer **2.2a**: GRIM polymerization and chemical oxidative polymerization with $FeCl_3$.[13] To synthesize **2.2a** with GRIM polymerization, they added one equivalent of a MeMgCl to **2.4a** resulting in Grignard metathesis to yield intermediate **2.5a**. They then added [1,3-bis(diphenylphosphino)propane]dichloronickel(II) (Ni(dppp)Cl_2) to produce polymers via Kumada Coupling (Figure 2.6). The GRIM polymerized material had a number average molecular weight of 4800–4900 and a polydispersity of 1.45–1.48, while the $FeCl_3$ polymerized material had a number average molecular weight of 4300 and polydispersity of 2.14. Furthermore, the GRIM polymerized material had a broader spectral profile, improved solution and film stability, increased solubility, better film formation, and a slightly lower bandgap than the $FeCl_3$ polymerized material. Nevertheless, because both polymerization methods produced materials with low molecular weight, they suspected that this was due to the poor solubility of **2.2a**.

In 2014, Koeckelberghs and coworkers reported their optimization of the GRIM polymerization of **2.1m** (Figure 2.7).[25] They initially used the precatalyst Ni(dppp)Cl_2, and they obtained completely soluble material with a number average molecular weight of 9100, but that was described as having a "high polydispersity" (no PDI value was reported), suggesting that the polymerization was not controlled. To improve the polymerization, they tried the precatalyst [1,2-bis(diphenylphosphino)ethane]dichloronickel(II) (Ni(dppe)Cl_2), which resulted in material with a higher number average molecular weight (12800), which was again described as having a high polydispersity, although no value was reported. They attributed the high polydispersities to the low solubility of the nickel precatalysts. They then switched to more soluble precatalysts (*o*-tolyl-Ni(dppp)Br and *o*-tolyl-Ni(dppe)Br), resulting in polymers with lower molecular weights of

5100 and 5800 and polydispersities of 1.3 and 1.6, respectively. They then went on to report that these polydispersities were "significantly lower" than that of the polymers made without the *o*-tolyl-Ni precatalyst. Their results led them to conclude that the GRIM polymerization of **2.2** is limited by catalyst dissociation from the growing polymer chain. They suggest that the dissociation is due to the electron-deficient nature of the polymer, which leads to a weak association between the active catalyst and the growing polymer chain.

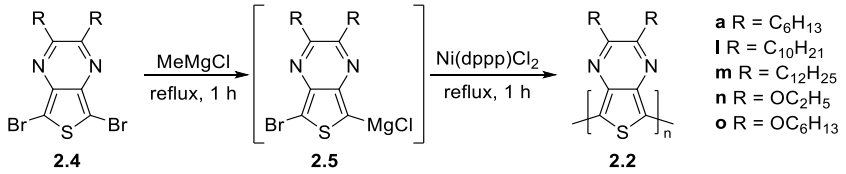

Figure 2.6. TP homopolymers prepared by Rasmussen and coworkers in 2008 and 2015.

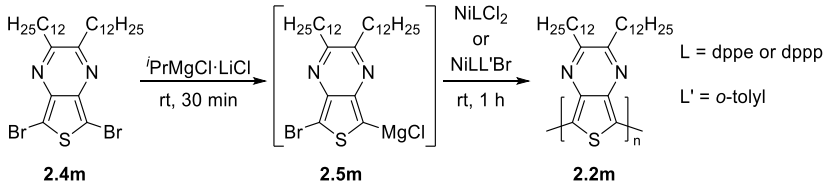

Figure 2.7. TP homopolymers reported by Koeckelberghs and coworkers in 2014.

In 2015, Rasmussen and colleagues conducted a follow-up study to their initial GRIM polymerization of **2.2**. Their objective was to enhance the solubility of **2.2** to produce materials with higher molecular weight (Figure 2.6).[14] They functionalized **2.2** with longer alkyl chains and alkoxy chains to achieve this. However, the polymers functionalized with longer alkyl side chains (decyl (**2.2l**) and dodecyl (**2.2m**)) were still of low molecular weight (2500 and 3300, respectively). They hypothesized that the low molecular weight was due to side chain crystallization, which reduced their solubility. Their hypothesis is reasonable as side chain crystallization has been observed for polythiophenes with side chains longer than decyl chains.[26]

Additionally, they found that the ethoxy functionalized polymer (**2.2n**) had a very low molecular weight (920) due to the short side chains that resulted in poor solubility. Side chains of butyl or longer are required to provide polythiophenes with adequate solubility.[27] The hexyloxy functionalized polymer (**2.2o**) had a higher molecular weight (4100), similar to that of the **2.2a**. They found that the bandgaps of polymers **2.2l**, **2.2m**, and **2.2o** were larger than that of **2.2a**. The larger bandgaps of polymers **2.2l** and **2.2m** were likely due to their low molecular weights. These polymers had a degree of polymerization of about six and seven, respectively, which is far below the effective conjugation length of polythiophenes (ca. 20 to 30 thiophene rings).[28,29] Polymer **2.2o** exhibited a larger bandgap than the alkyl functionalized polymers due to the electron-donating nature of the alkoxy side chains, which causes appreciable LUMO destabilization and, thus, an increase in bandgap.

2.1.2. Catalyst Transfer Polymerization

Targeting a catalyst transfer polymerization (CTP) mechanism for the preparation of PTPs is desirable as CTP has been used to produce materials with controlled molecular weight and low polydispersity due to its quasi-living nature.[30,31] The proposed CTP mechanism can be found in Figure 2.8 and is described as follows:[32–34] First, two activated monomers undergo transmetalation with one precatalyst molecule. Reductive elimination gives a dimer, which the catalyst stays associated with. The catalyst moves along the aromatic ring and undergoes oxidative addition to the arene C–X bond. Further chain growth is achieved through transmetalation with an activated monomer followed by reductive elimination. Throughout the polymerization, the catalyst remains associated with the growing polymer chain.

The relationship between the catalyst and the propagating polymer chain is crucial for the quasi-living nature in CTP.[33,35,36] If the catalyst and aromatic unit are too strongly associated, it

is unlikely that the oxidative addition step will occur. Conversely, if the association is too weak, the catalyst may dissociate from the growing chain, resulting in a step growth polymerization, which are somewhat uncontrolled and often result in high polydispersities.[37–39]

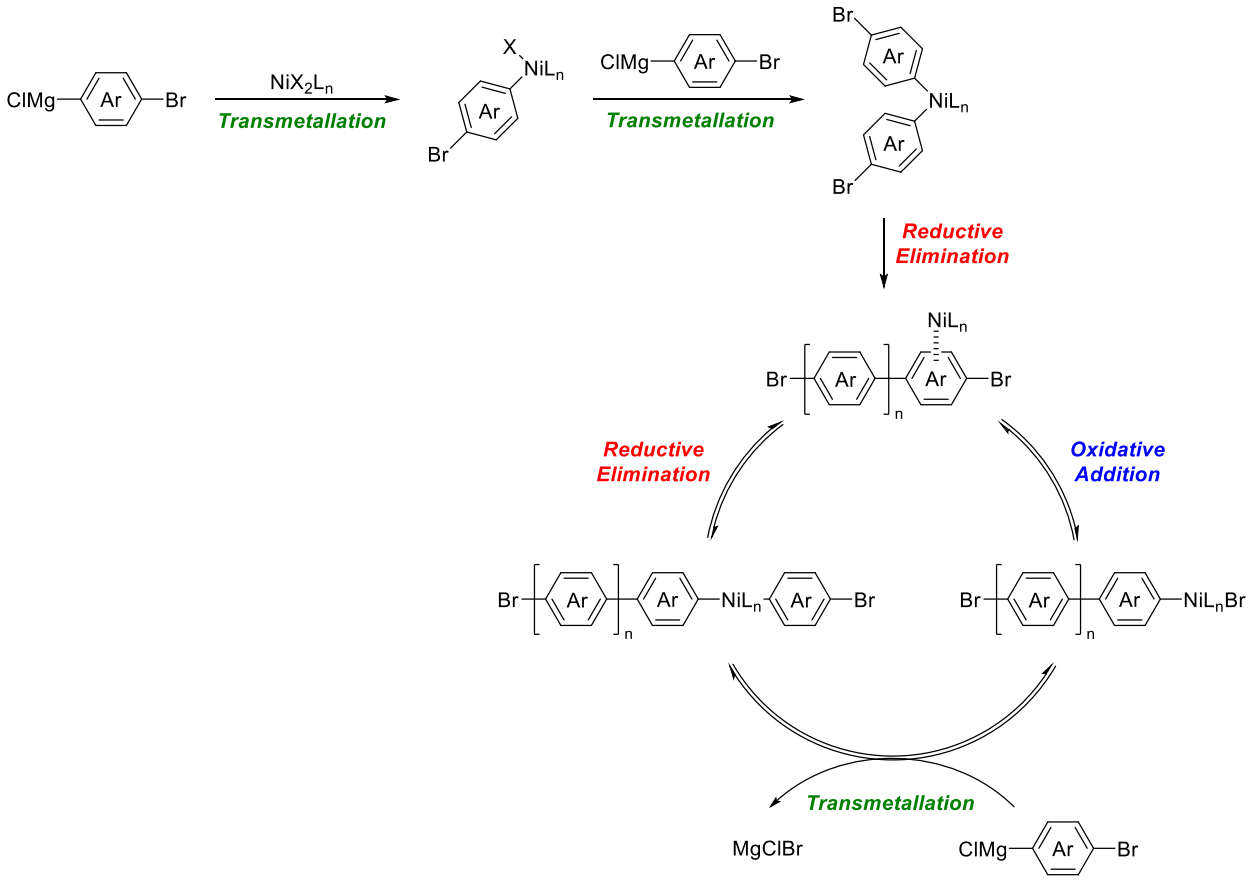

Figure 2.8. Catalyst transfer polymerization via Kumada cross coupling mechanism.

2.1.3. Motivation for This Work

Rasmussen and Koeckelberghs have separately reported that polymer **2.2** produced by GRIM polymerization has a low molecular weight, but they have different theories to explain why. Koeckelberghs and coworkers suggest that the low molecular weight is due to catalyst dissociation is due to the electron-deficient nature of the polymer, which leads to a weak association between the active catalyst and the growing polymer chain. However, this seems

unlikely as discussed in chapter 1, TP exhibits properties of both a strong donor and a strong acceptor with the thiophene ring being of electron rich character, and with the polymerization occurring at the thiophene ring it is unlikely that dissociation due to the electron-deficient nature of the polymer is occurring. Nevertheless, this low molecular weight is problematic as it is unlikely that these polymers are reaching their effective conjugation length. To address this issue, this work focused on increasing the molecular weight of **2.2**, which could potentially result in a decrease in bandgap and improve the film-forming properties.[14] This research aimed to achieve this by addressing the low solubility issue Rasmussen and coworkers proposed. In chapter 1, it was mentioned that branched alkyl side chains lead to improved solubility compared to linear alkyl side chains due to a combination of steric and thermodynamic effects.[40–46] Therefore, this work focused on functionalizing **2.2** with branched side chains to increase their solubility.

2.2. Results and Discussion

2.2.1. Design and Synthesis

This work aimed to enhance the solubility of **2.2** by functionalization with branched alkyl side chains. Three common branched side chains were chosen: 2-ethylhexyl, 3,7-dimethyloctyl, and 2-octyldodecyl. While 2,3-bis(2-ethylhexyl)thieno[3,4-*b*]pyrazine (**2.1r**) had been reported in 2018,[47] and 2,3-bis(2-octyldodecyl)thieno[3,4-*b*]pyrazine (**2.1q**) was prepared by Wyatt Wilcox, 2,3-bis(3,7-dimethyloctyl)thieno[3,4-*b*]pyrazine (**2.1p**) was an unknown species. In addition, the corresponding α-dione needed to make **2.1p** had not been previously reported. As a result, **2.1p** was synthesized from 3,7-dimethyl-1-octanol (**2.6**) (Figure 2.9).

Following an established procedure 1-bromo-3,7-dimethyloctane (**2.7**) was synthesized from **2.6** via S_N2 reaction using triphenylphosphine and *N*-bromosuccinimide (NBS).[48]

Following this, 2,6,13,17-tetramethyloctadecane-9,10-dione (**2.9p**) was synthesized from **2.7** through a modified version of a reaction previously reported by Rasmussen and coworkers.[16] To convert **2.7** to the corresponding Grignard reagent (**2.8**), slight deviation from the reported procedure was taken by heating the reaction at 50 °C for two hours after **2.7** was added to magnesium. Other researchers have also reported using heat for the formation of **2.8**.[49] Reaction of the Grignard reagent with oxalyl chloride in the presence of lithium chloride and copper(I) bromide gave the α-dione as a yellow oil in 46% yield. Following a previously reported procedure,[16] a double condensation reaction between **2.9p** and 3,4-diaminothiophene gave **2.1p** in 21% yield.

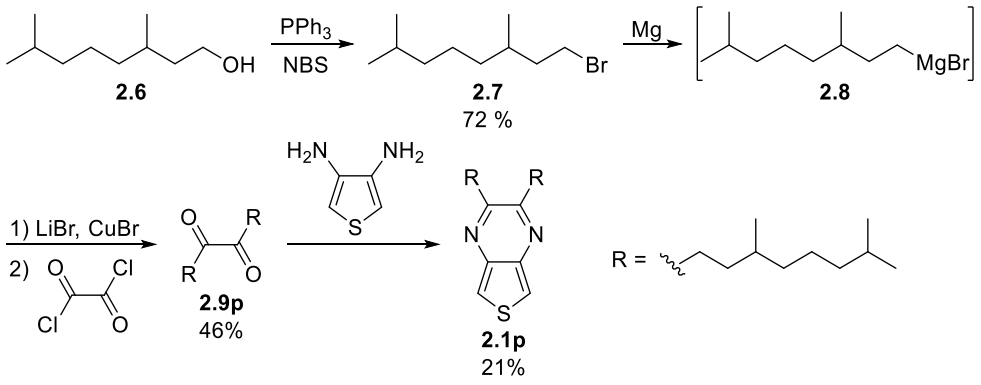

Figure 2.9. Synthesis of 2,3-bis(3,7-dimethyloctyl)thieno[3,4-*b*]pyrazine.

Previous attempts to synthesize TP **2.1q** resulted in low yields; thus, this reaction was further investigated (Figure 2.10 and Table 2.1). Initially, the low yields were thought to be due to the low solubility of dione **2.9q** in the reaction solvent, ethanol. Efforts were made to increase the solubility of dione **2.9q** by heating the reaction at reflux for three hours, which did increase the solubility of the dione, but the reaction yield was still low. There was concern for product decomposition at high temperatures, and thus, the reaction time was decreased to 30 minutes, but a similar yield was obtained. Finally, alternative measures were taken to solubilize the dione

using a mixed solvent system. The reaction was carried out in a 1:1 mixture of ethanol and ethyl acetate. As this increased the dione's solubility, the yield was still low. Future work should investigate the low yields of this reaction with a focus on the purity of dione **2.9q**.

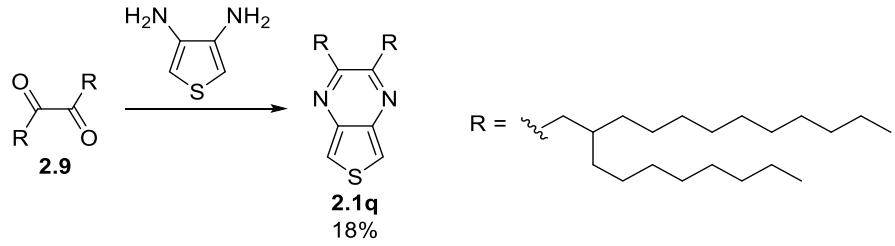

Figure 2.10. Synthesis of 2,3-bis(2-octyldodecyl)thieno[3,4-*b*]pyrazine.

Table 2.1. Attempts to optimize 2,3-bis(2-octyldodecyl)thieno[3,4-*b*]pyrazine synthesis.

Entry	Temperature	Time	Solvent	Yield (%)
1	rt	3 h	EtOH	18
2	reflux	3 h	EtOH	18
3	reflux	0.5 h	EtOH	16
4	rt	3 h	EtOH: EtOAc (1:1)	16

To brominate the branched TPs (**2.1p**, **2.1q**, and **2.1r**), a modified procedure from a previously reported method also used for other TPs was followed (Figure 2.11).[13,14] The procedure involved treating **2.1** with NBS in dimethylformamide at low temperatures. Previously reported TPs had linear side chains; thus, pouring the reaction over ice caused precipitation of **2.4** allowing for the simple collection of **2.4** by filtration. In contrast, the brominated branched TPs did not precipitate when pouring the reaction over ice. Therefore, the reaction mixture was extracted with ethyl acetate and concentrated to yield the crude product, which was purified using a short silica plug. The brominated monomers **2.4p**, **2.4q**, and **2.4r** were collected in 45%, 82%, and 67% yield, respectively.

GRIM polymerization of **2.4p**, **2.4q**, and **2.4r** was carried out following a previously reported procedure by Rasmussen and coworkers (Figure 2.11).[13] Homopolymers of **2.2** were made by adding 1.05 equivalents of methylmagnesium bromide to **2.4** in tetrahydrofuran, then heating the reaction at reflux for one hour to cause Grignard metathesis. In the case of **2.4q**, the reaction was heated at reflux for two hours to further encourage Grignard metathesis, as one hour proved to be too short potentially due to the bulky branched side chains. Adding 0.5 mol% $Ni(dppp)Cl_2$ and another hour of heating at reflux yielded the dark-purple polymer. Polymer **2.2ar** was made by adding 0.5 equiv of each monomer (**2.4a** and **2.4r**) to the reaction. Polymers **2.2a**, **2.2p**, **2.2r**, and **2.2ar** were produced in good yields (65–79%). Additionally, it was found that these polymerizations were reproducible. Polymer **2.2q** was produced in relatively low yields (33%), which is likely due to polymer **2.2q** being a gel, making purification difficult. Another factor that could cause the low yield of polymer **2.2q** could be due to the bulky side chains inhibiting polymerization.

Molecular weight data was obtained using gel permeation chromatography (GPC) with 1,2,4-trichlorobenzene at 100 °C and compared to polystyrene standards. Molecular weight data can be found in Table 2.2. Polymer **2.2a** had a higher molecular weight than previously reported,[13] potentially due to different GPC analysis conditions. Polymer **2.2r** exhibited a lower molecular weight than was expected based on the concentrations of monomer and initiator/catalyst used. However, polymer **2.2r** was found to be completely soluble in the reaction vessel and chloroform, suggesting that the low molecular weight of this polymer is not due to low solubility. Polymer **2.2q** had a relatively low average degree of polymerization, potentially due to the large side chains inhibiting polymerization. Polymers **2.2q** and **2.2r** exhibited complete solubility in chloroform, whereas the other polymers only had partial solubility. The

improved solubility of **2.2q** and **2.2r** may be attributed to the larger branch located near the conjugated backbone.

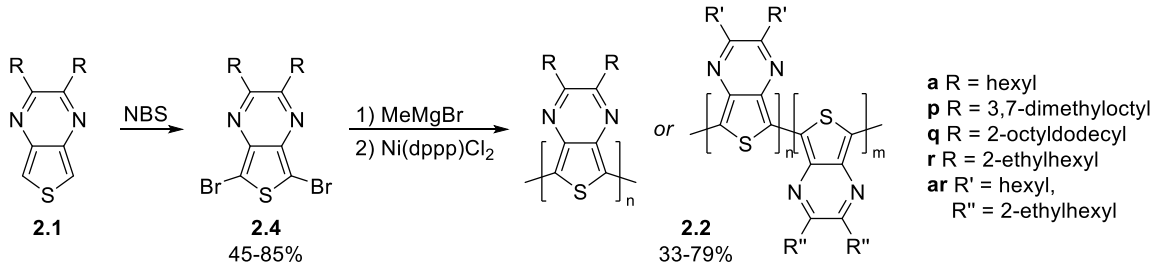

Figure 2.11. Synthesis of branched PTPs via GRIM polymerization.

In their 2008 report, Rasmussen and coworkers investigated the preparation of polymer **2.2a** by GRIM polymerization.[13] They conducted the reaction at both reflux and room temperature and found that more insoluble material was produced at room temperature. This insoluble material likely had a higher molecular weight than the soluble material. Based on this finding, it was hypothesized that using room temperature conditions to prepare polymer **2.2r** would result in a soluble fraction with a higher molecular weight as polymer **2.2r** exhibits better solubility than polymer **2.2a**. However, it was found that polymerization of **2.4r** at room temperature resulted in a significant amount of insoluble material, and a low soluble fraction yield of 13%. In addition, the soluble material from the room temperature reaction was of lower molecular weight than the material produced by the reflux reaction (Table 2.2).

Previous work has shown that introducing LiCl during GRIM polymerizations can reduce polydispersity.[50] It is thought that LiCl breaks up the Grignard aggregates, thereby increasing their reactivity.[51,52] It was found that adding 1.0 equivalent of LiCl to the polymerization of **2.4r** resulted in **2.2r** in a similar yield (67%). Additionally, the resulting polymer was still completely

soluble in chloroform. However, the addition of LiCl resulted in a lower M_n and a higher polydispersity index (PDI).

Table 2.2. Reaction yield and molecular weight data for PTPs.

Material	Yield (%)[c]	Insoluble Material	M_n[d]	PDI[d]	n (average)
2.2a	66	Yes	6700	1.56	22
2.2p	79	Yes	10900	1.44	26
2.2q	33	No	6600	1.19	9
2.2r	68	No	7400	1.39	21
2.2r[a]	13	Yes	5900	1.20	16
2.2r[b]	70	No	6800	1.46	19
2.2ar	65	Yes	7000	1.68	21

[a] Polymer made at room temperature. [b] Polymer made with the addition of LiCl. [c] Yield was determined from the theoretical yield of the polymer repeat unit. [d] Gel permeation chromatography with polystyrene standards was used to determine M_n and PDI.

2.2.2. Absorption Spectroscopy

To understand the impact that branched side chains have on the optical and electronic properties of monomeric TPs, photophysical characterization was carried out on **2.1p** and **2.2r**. The photophysical for the branched TPs **2.1p** and **2.2r** are shown in Table 2.3 along with the TPs functionalized with linear alkyl side chains for comparison. The UV-vis absorption spectra for the branched TPs **2.1p** and **2.2r** are shown in Figure 2.12. The branched TPs have similar absorption spectra to the TPs with linear side chains. The spectra consist of several bands, two of high intensity between 304 and 319 nm along with a high energy shoulder between 292 and 297 nm. As pointed out by Rasmussen and coworkers, these lower energy bands likely stem from the same electronic transition, and the different bands are likely due to the vibronic progression of that electronic transition.[53] However, the lower energy band at ~350 nm is of relatively weak intensity, and is thought to be a charge transfer band.[15] As can be seen the branched TPs exhibit a

slight red shift relative to the TPs functionalized with linear side chains, which is likely due to their spectra being measured in chloroform. This was previously reported by Rasmussen and coworkers to cause a slight red shift in the spectra due to halogen bonding between the solvent and the pyrazine nitrogens.[53]

Table 2.3. Photophysical data for 2,3-functionalized TPs.

R	λ_{max} (nm)	ε (M^{-1} cm^{-1})
hexyl[a,b]	292 (sh)	9800
	305	11200
	314	11000
	349	1900
octyl[a,b]	292 (sh)	9700
	304	11600
	315	10200
	350	1900
decyl[a,b]	292 (sh)	7700
	305	11600
	314	11200
	350	2100
3,7-dimethyloctyl[c]	295 (sh)	7500
	309	12600
	318	12700
	350	2600
2-ethylhexyl[c]	297 (sh)	6800
	310	10400
	319	10300
	350	2000

[a] Ref. 53. [b] Data obtained from CH_3CN solutions.

[c] Data obtained from $CHCl_3$ solutions.

Shown in Table 2.4 and Figures 2.13 and 2.14 are the solution and solid-state UV-vis-NIR absorption data for the branched PTPs (**2.2p**, **2.2q**, **2.2r**, and **2.2ar**) and **2.2a**. The absorption spectra of all the polymers exhibit the two absorption bands typically observed in

donor-acceptor systems.[54] The high energy band corresponds to the π-π* transition, while the low energy band corresponds to the intramolecular charge transfer from the backbone to the pendant pyrazine rings.[14,15,55] Going from solution to solid state, the low energy band is redshifted in all polymers due to the planarization of the polymer backbone and improved interchain interactions.

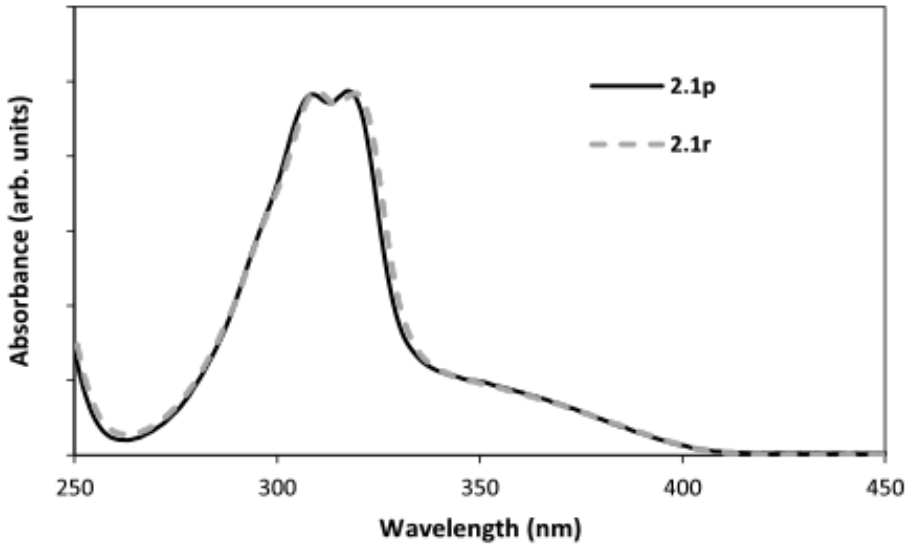

Figure 2.12. UV-vis absorption spectra of branched TPs in $CHCl_3$.

Table 2.4. UV-vis-NIR data for PTPs.

Material	λ_{max} (nm, $CHCl_3$)[b]	λ_{max} (nm, film)[b,d]	E_g (eV)
2.2a	862, (940)	886, (990)	1.07
2.2p	(900), 1011	(925), 1041	1.07
2.2q	838, (910)	867, (975)	1.10
2.2r	(910), 1040	(940, 1040), 1076	1.07
2.2r[a]	(910), 1031	929, (1040), 1062	1.07
2.2r[b]	(910), 994	910, (1004)	1.08
2.2ar	(900), 1012	(940), 1038	1.06

[a] Polymer made at room temperature. [b] Polymer made with the addition of LiCl. [c] Values in parentheses denote prominent shoulders. [d] Unannealed films.

Polymers **2.2p**, **2.2r**, and **2.2ar** exhibit a narrower spectral profile than polymers **2.2a** and **2.2q**. Polymers **2.2p**, **2.2r**, and **2.2ar** also exhibit a red-shifted λ_{max} and a steeper absorption onset than polymers **2.2a** and **2.2q**. Polymer **2.2r** exhibits the most red-shifted λ_{max} in solution and solid state. All polymers have similar bandgaps ranging from 1.06 to 1.10 eV. The blue-shifted absorption spectra of **2.2q** is likely due to low molecular weight and steric effects caused by the bulky branched side chains, which twists the polymer backbone.

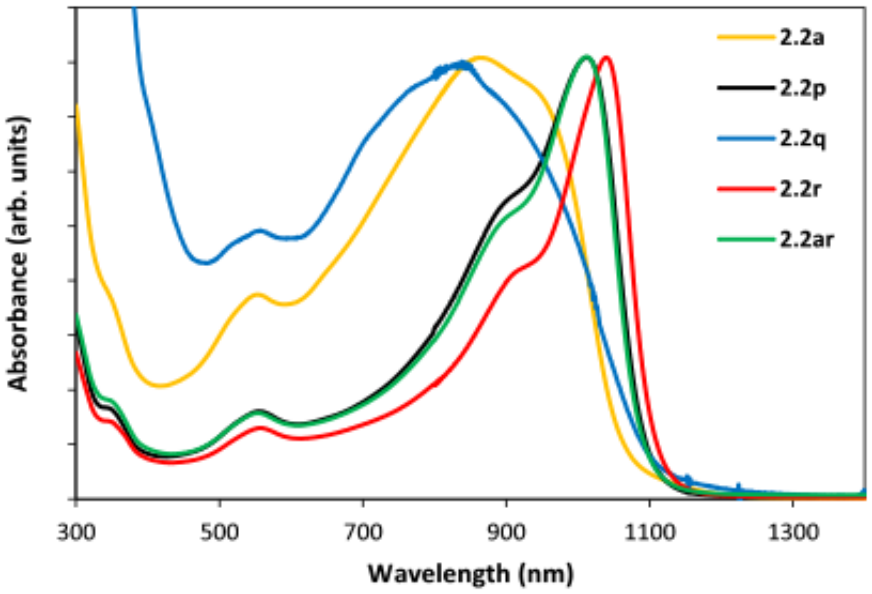

Figure 2.13. UV-vis-NIR spectra of PTPs in $CHCl_3$.

As the spectral profiles of polymers **2.2a** and **2.2r** were different, there was uncertainty about whether the low energy peak of both polymers was of similar intensity. To clarify this, a thin film of a 1:1 blend of polymers **2.2a** and **2.2r** was prepared, and the spectra of the blend was compared to those of the pristine polymers (Figure 2.15). The results showed that both polymers contributed almost equally to the polymer blend spectrum. Therefore, even though polymer **2.2r** has a red-shifted absorption spectrum compared to polymer **2.2a**, it doesn't exhibit a significant decrease in absorption intensity.

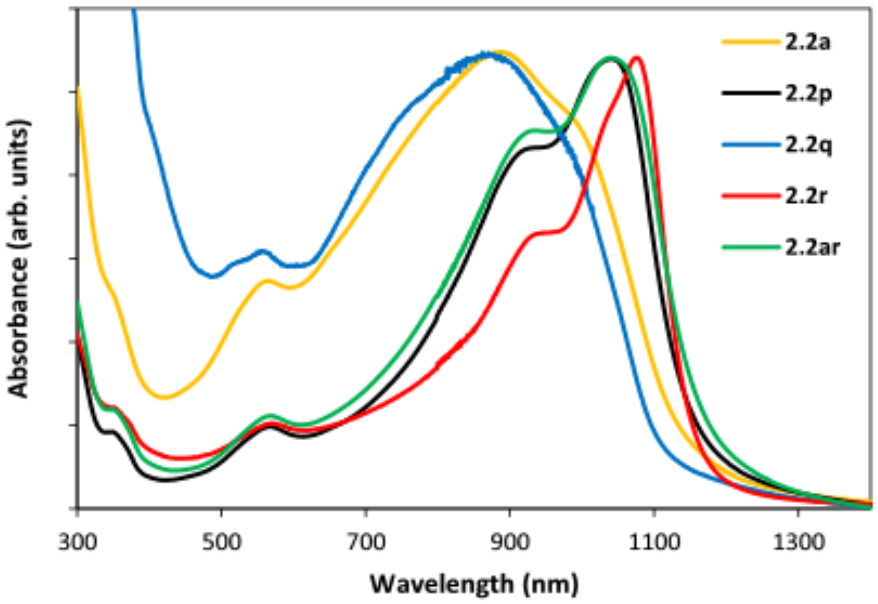

Figure 2.14. UV-vis-NIR spectra of PTP films.

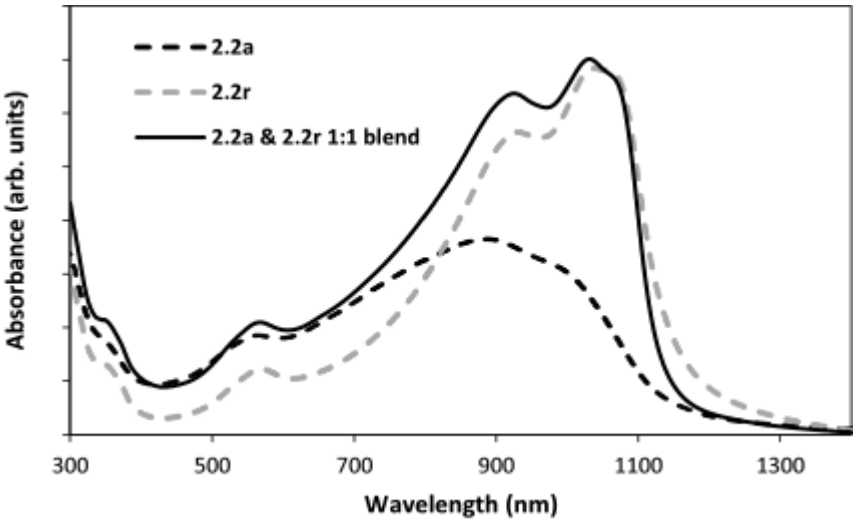

Figure 2.15. Solid-state UV-vis-NIR spectra of pristine **2.2a**, pristine **2.2r**, and a 1:1 blend of both polymers.

Figure 2.17 shows the UV-vis-NIR spectra of polymer **2.2r** prepared at room temperature and at reflux. The polymer synthesized at room temperature exhibits a broader spectral profile than the polymer synthesized at reflux. Furthermore, the solution and solid state low energy λ_{max}

values are slightly blue shifted for the polymer made at room temperature. However, the absorption onsets for both polymer samples are the same in the solid state. As a result, both samples exhibit the same bandgap of 1.07 eV.

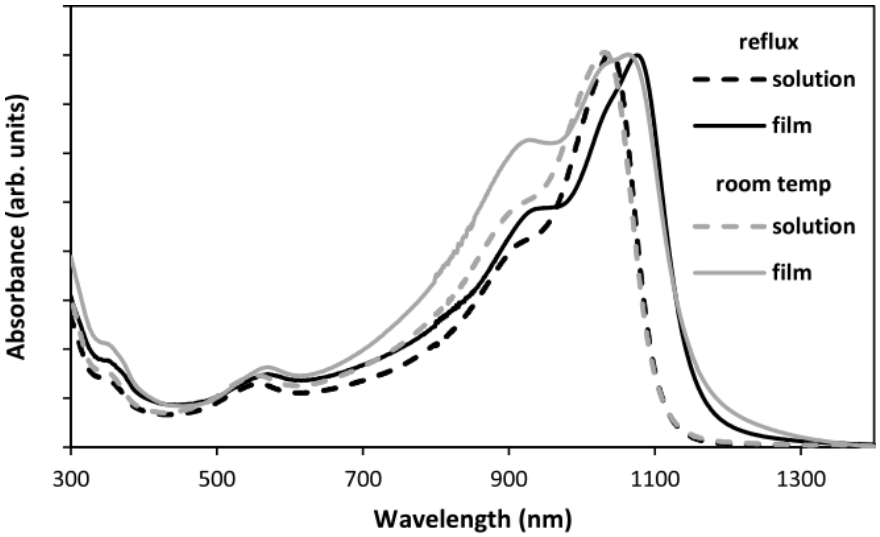

Figure 2.16. Solution and solid-state absorption spectra of **2.2r** made at reflux and room temperature.

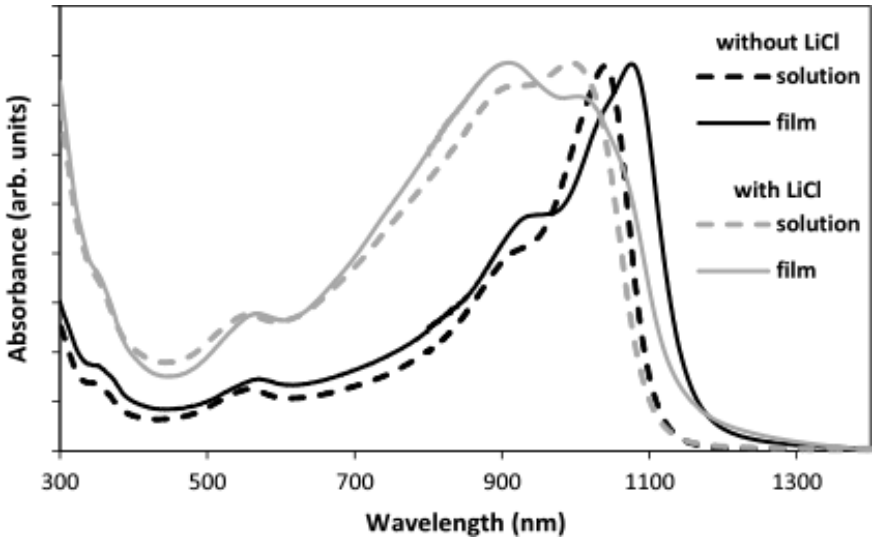

Figure 2.17. Solution and solid-state absorption spectra of **2.2r** made with and without LiCl.

Miyakoshi et al. found that the addition of LiCl to GRIM polymerizations can result in a decrease in PDI.[50] However, it was found that the addition of LiCl to the polymerization of **2.4r** resulted in higher PDI. The UV-vis-NIR spectra of polymer **2.2r** made with the addition of LiCl can be found in Figure 2.17. The material exhibited a blue-shifted λ_{max} and a less steep absorption onset compared to when LiCl was not used in the polymerization. The LiCl made polymer had a slightly larger bandgap of 1.08 eV and a wider spectral profile, which may be attributed to the higher PDI of the polymer.

2.2.2. Polymer Film Annealing and Glass Transition Temperatures

In 2008, Rasmussen and coworkers annealed **2.2a** films under air and nitrogen at 100 °C.[13] Films were annealed at 100 °C because the glass transition temperature of the polymer is 96–97 °C. Annealing under air caused a blue shift in absorption onset and a decrease in absorption intensity, which they suggest is due to oxidative damage of the film. Conversely, annealing under nitrogen caused a red shift in the absorption onset and, thus, a decrease in bandgap.

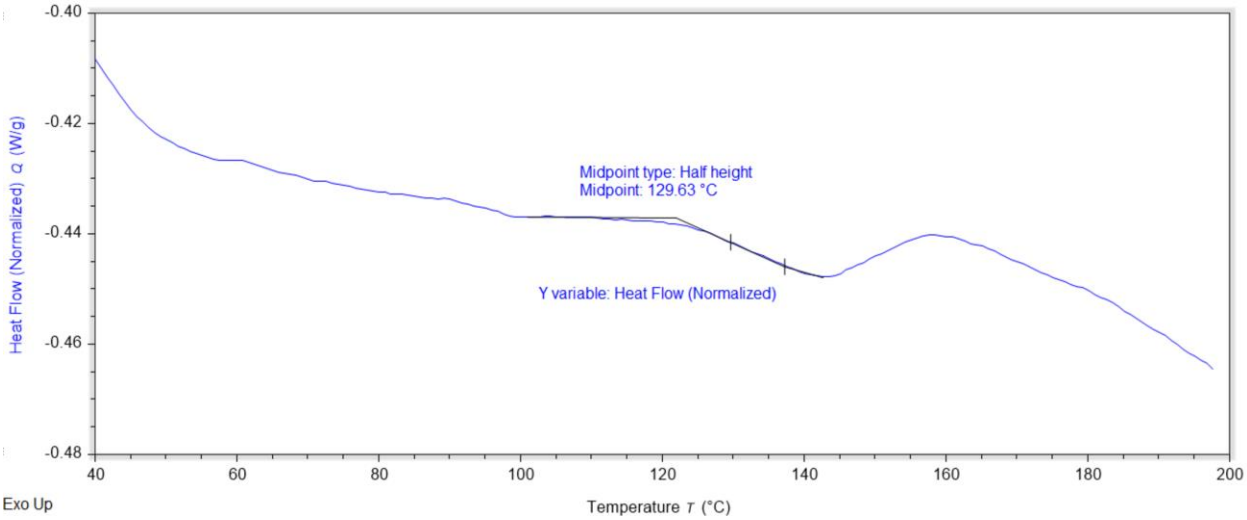

Figure 2.18. DSC curve of **2.2p** recorded at a rate of 10 °C/min.

Differential scanning calorimetry (DSC) was used to determine glass transition temperatures (T_g) for polymers **2.2p** and **2.2r** (Figures 2.18 and 2.19). The T_g of polymer **2.2p** was determined to be ca. 130 °C. The increase in T_g compared to polymer **2.2a** is likely a result of the longer side chains. Determining the T_g of polymer **2.2r** proved difficult, which is possibly a result of the bulkier side chains.

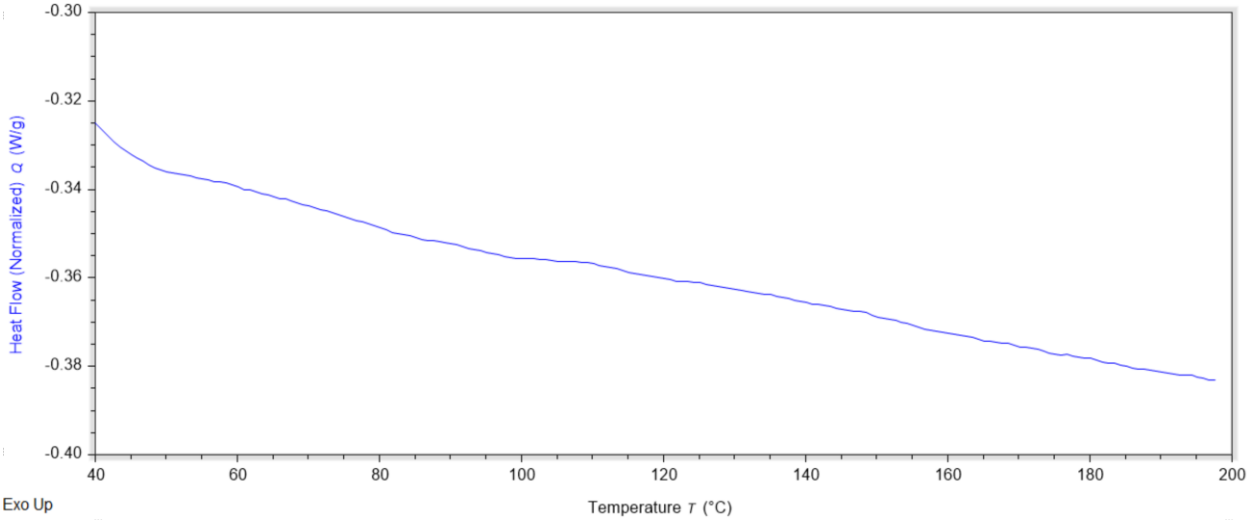

Figure 2.19. DSC curve of **2.2r** recorded at a rate of 10 °C/min.

As the T_g of polymer **2.2p** was determined to be 130 °C, it was hypothesized that annealing the polymer film slightly above this temperature would result in a red shift in the films absorption onset. Thus, thin films of polymer **2.2p** were annealed for 30 minutes under N_2 atmosphere at 150 °C. Figure 2.20 displays the UV-vis-NIR spectra of both unannealed and annealed films. Annealing resulted in a decrease in the intensity of the low-energy peak and a slight blue-shift in the λ_{max} value. However, the intensity of the high-energy shoulder increased. This change is potentially due to the branched side chains inhibiting ordering of the film packing.

2.2.3. Electrochemistry

Electrochemical data for branched TPs **2.1p** and **2.1r** can be found in Table 2.5, and the corresponding cyclic voltammograms can be found in Figure 2.21. As was previously observed for other TP analogs, branched TPs **2.1p** and **2.1r** exhibit an irreversible oxidation around 1.3 V. The irreversibility of this oxidation is likely a result of the production of thiophene-based radical cations and subsequent coupling of these species.[16,56,57] A quasireversible reduction is also observed at ca. -2.0 V, which has been shown to correspond to the reduction of the pyrazine ring.[16,58]

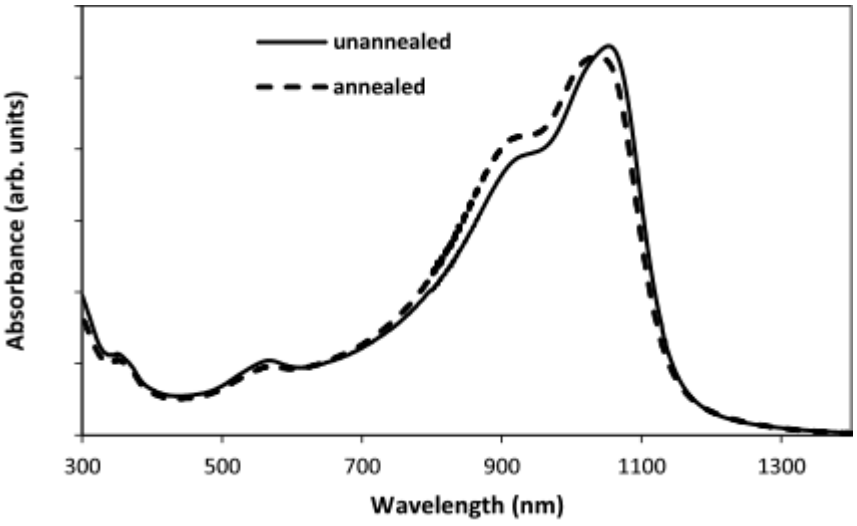

Figure 2.20. UV-vis-NIR spectra of **2.2p** thin film unannealed and annealed under N_2 for 30 minutes at 150 °C.

Cyclic voltammetry was used to estimate the frontier molecular orbital energy levels of polymers **2.2a**, **2.2p**, **2.2r**, and **2.2ar**. Electrochemical data can be found in Table 2.6, and cyclic voltammograms are shown in Figure 2.22. All polymers have similar oxidation onsets and thus similar HOMO energy levels. All polymers also have similar LUMO energy levels, with the lowest for polymer **2.2p**, which may be attributed to the higher molecular weight of this polymer. All polymers exhibit electrochemical bandgaps of 1.5 to 1.6 eV. The difference in energy

between the electrochemical bandgaps and the optical bandgaps is due to the exciton binding energy.[59] Collection of electrochemical data for thin films of **2.2q** proved difficult due to the polymers partial solubility in acetonitrile.

Table 2.5. Electrochemical data for 2,3-functionalized TPs.[a]

R	oxidation	reduction	
	E_{pa} (V)	$E_{1/2}$ (V)	ΔE (mV)
hexyl[b]	1.35	-2.01	150
octyl[b]	1.35	-1.99	130
decyl[b]	1.33	-1.99	140
3,7-dimethyloctyl	1.26	-2.06	150
2-ethylhexyl	1.35	-2.09	240

[a] All potentials are reported versus Ag/Ag^+. Measurements were made in CH_3CN with 0.10 M $TBAPF_6$. [b] Ref. 16.

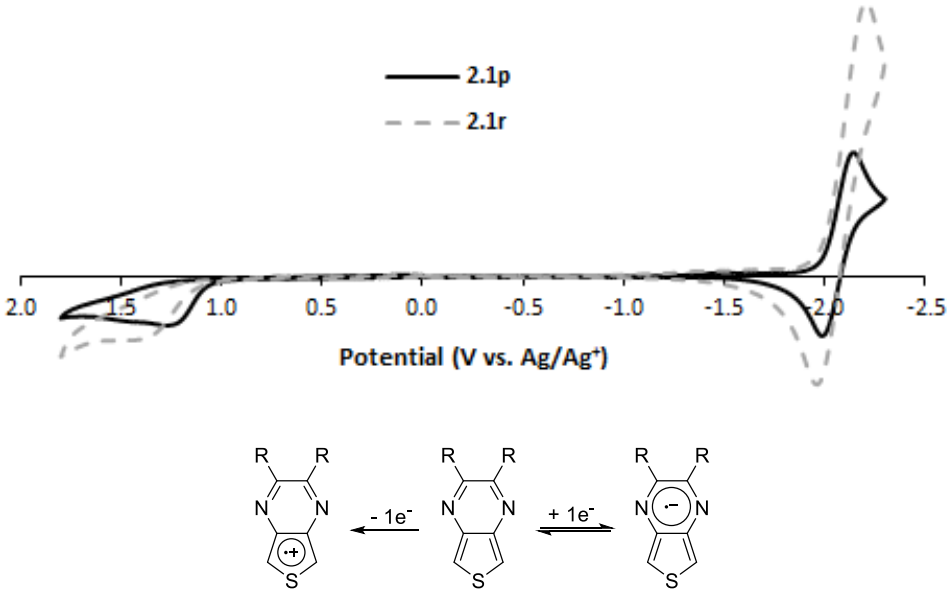

Figure 2.21. Branched TP monomer cyclic voltammograms.

Table 2.6. PTP electrochemical data.

Material	E_{HOMO} (eV)[a]	E_{LUMO} (eV)[b]	E_g^{elec} (eV)
2.2a	-5.2	-3.6	1.6
2.2p	-5.2	-3.7	1.5
2.2r	-5.2	-3.6	1.6
2.2ar	-5.2	-3.6	1.6

[a] $E_{HOMO} = -(E_{[onset,ox\ vs.\ Fc+/Fc]} + 5.1)$(eV). [b] $E_{LUMO} = -(E_{[onset,red\ vs.\ Fc+/Fc]} + 5.1)$(eV).

2.2.4. OPV and NIR Photodetector Device Data

Bulk heterojunction (BHJ) photonic devices were fabricated with **2.2r** as the donor material and [6,6]-phenyl-C_{61}-butyric acid methyl ester (PCBM) as the acceptor material. Absorption spectra of thin films of **2.2r**, PCBM, and blends of **2.2r**:PCBM (1:1 and 1:2 ratios) are shown in Figure 2.23. PCBM contributes to the high energy absorption of the blend, while **2.2r** contributes to both the high and low energy absorption, with the most significant contribution being in the low energy portion of the spectrum.

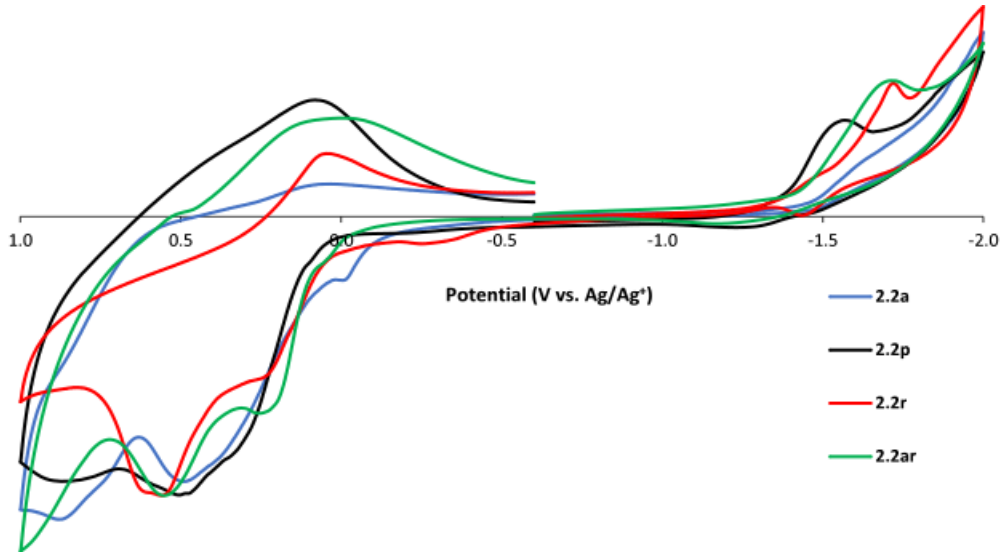

Figure 2.22. Cyclic voltammograms of PTPs made by GRIM polymerization.

In 2013, Rasmussen and coworkers fabricated BHJ OPV devices with a **2.2a**:PCBM active layer.[60] They optimized the device performance by adjusting **2.2a**:PCBM ratios, using different solvents to spin the active layer, and varying annealing times. They observed the highest photoconversion efficiency (PCE) of 0.13% from a device with a 1:2 ratio of **2.2a** to PCBM, spun from chlorobenzene, and annealed for 15 minutes. This device exhibited an open circuit voltage (V_{OC}) of 0.26 V, a short circuit current density (J_{SC}) of 1.30 mA cm^{-1}, and a fill factor of 0.37.

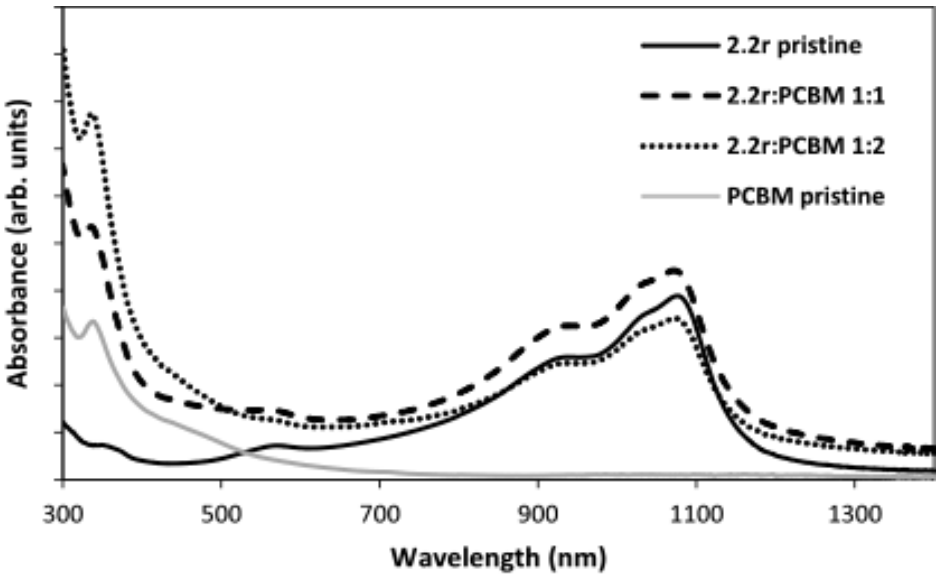

Figure 2.23. Thin film absorption spectra of pristine **2.2r**, pristine PCBM, and blends of **2.2r**:PCBM.

BHJ OPV devices were fabricated with a **2.2r**:PCBM active layer, and the results can be found in Table 2.7 and Figure 2.24. Devices were optimized by adjusting **2.2r**:PCBM ratios, using different solvents to spin the active layer, and varying annealing times. The device with the highest PCE of 0.229% was made with a 1:1 ratio of **2.2r** to PCBM, spun from chlorobenzene, and left unannealed. This device exhibited a V_{OC} of 0.25 V, a J_{SC} of 1.82 mA cm^{-1}, and a fill factor of 0.51. More recently, our collaborator, Tomas Marsh, at the Centre for Organic

Electronics, University of Newcastle made a device with a PCE of ~0.27% from a device with a 1:2 ratio of **2.2r** to PCBM, spun from dichlorobenzene, and left unannealed.

Table 2.7. OPV data for **2.2r**:PCBM devices.

2.2r:PCBM ratio	Annealed	Solvent	V_{oc} (V)	J_{sc} (mA cm^{-1})	FF	Eff (%)
1:1	5 min	CF	0.26	0.68	0.47	0.082
1:1	unannealed	CB	0.25	1.82	0.51	0.229
1:1	5 min	CB	0.24	1.03	0.53	0.131
1:1	15 min	CB	0.23	0.95	0.53	0.116
1:2	5 min	CB	0.24	1.12	0.53	0.144
1:2	15 min	CB	0.24	1.09	0.54	0.140
1:1	unannealed	DCB	0.24	1.34	0.48	0.152
1:1	5 min	DCB	0.24	1.58	0.49	0.185

CF = chloroform, CB = chlorobenzene, and DCB = 1,2-dichlorobenzene.

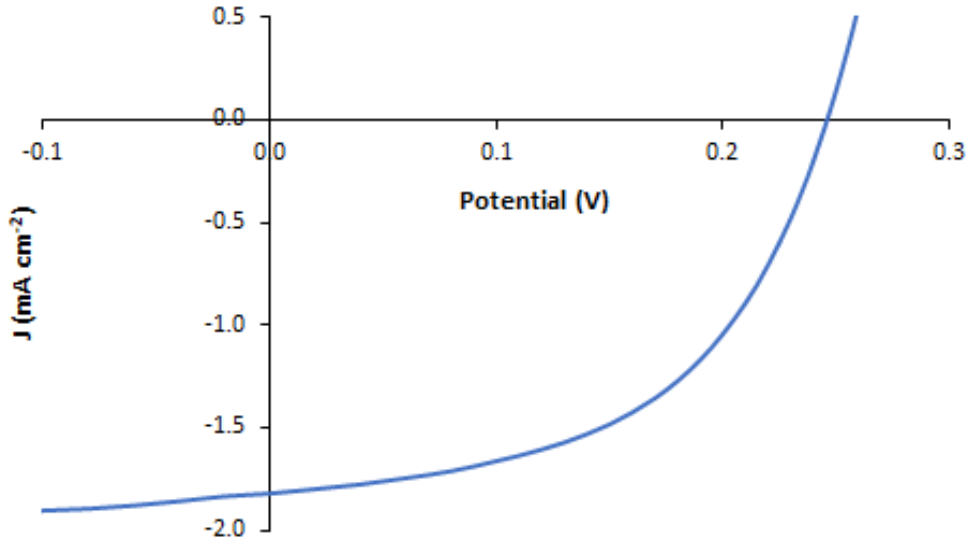

Figure 2.24. J-V curve of the highest performing **2.2r**:PCBM device (1:1 ratio of **2.2r** to PCBM, spun from chlorobenzene, and unannealed).

V_{OC} is thought to be dependent upon the energy difference between the HOMO of the donor material and the LUMO of the acceptor material.[61] OPVs were also fabricated from poly(3-hexylthiophene) (P3HT), which exhibited V_{OC} values around 0.52 V, which is interesting as the HOMO energy level of P3HT and **2.2r** is about equal (Figure 2.25), thus these devices

should have similar V_{OC} values. This was also observed for devices made from polymers **2.2a**.[62] It has been suggested that **2.2a**:PCBM devices exhibit relatively low V_{OC} values because the LUMO energy levels of **2.2a** and PCBM are similar, which does not create a large enough driving force for good charge separation to occur, resulting in recombination.[62] This could explain the low V_{OC} values for **2.2r**:PCBM devices, as **2.2r** also has a low-lying LUMO. Furthermore, **2.2r**:PCBM devices exhibited a larger J_{SC} and fill factor than **2.2a**:PCBM devices, which could be attributed to the enhanced processability of **2.2r**. This leads to improved interfaces between the donor and acceptor material, and the active layer and the hole and electron transport layers.

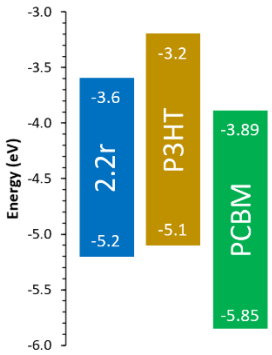

Figure 2.25. Energy level diagram of **2.2r**, P3HT, and PCBM.[63,64]

Rasmussen and coworkers showed that PCEs could be increased by annealing **2.2a**:PCBM devices when the active layer was spun from chlorobenzene.[60] However, PCEs decreased upon annealing **2.2r**:PCBM devices with an active layer spun from chlorobenzene. The decrease in PCE aligns with the change in UV-vis-NIR spectra of **2.2r**:PCBM films spun from chlorobenzene (Figure 2.26), where the intensity of the low energy peak decreases with increasing annealing time.

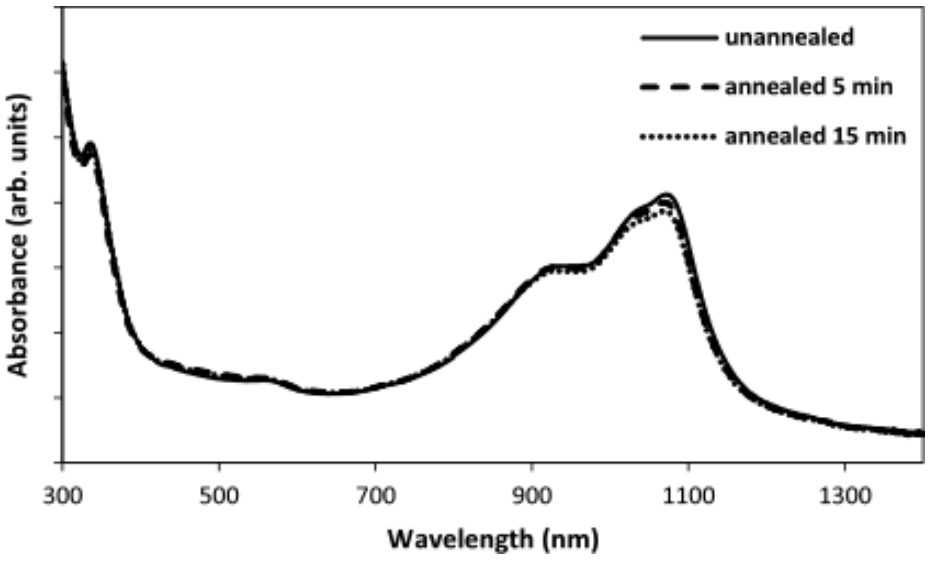

Figure 2.26. Absorption spectra of unannealed and annealed **2.2r**:PCBM 1:1 films spun from chlorobenzene.

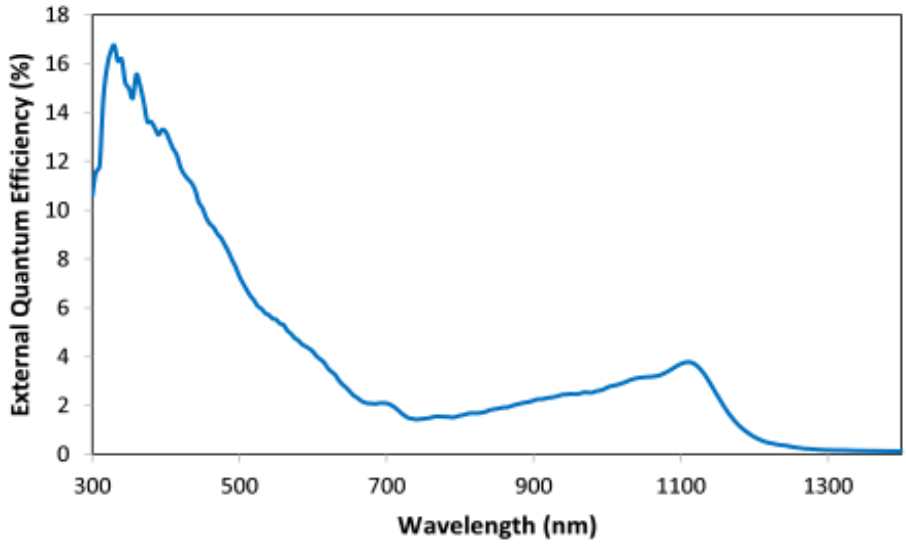

Figure 2.27. External quantum efficiency spectrum of the highest performing **2.2r**:PCBM device (1:1 ratio of **2.2r** to PCBM, spun from chlorobenzene, and unannealed).

An external quantum efficiency (EQE) spectrum was obtained for the top performing **2.2r**:PCBM device (Figure 2.27). EQE data was collected and processed by Nic Nicolaidis at the Centre for Organic Electronics, University of Newcastle. EQE is the ratio of the collected

photogenerated charge carriers to the number of photons that strike the device and is wavelength dependent.[11,61,65,66] The **2.2r**:PCBM device had a maximum response at 330 and 1110 nm, with EQEs of 16.8% and 3.78%, respectively. The **2.2r**:PCBM device exhibited a maximum EQE at a longer wavelength than the **2.2a**:PCBM device (1110 nm vs. 925 nm), and a larger EQE at that wavelength.[13] Furthermore, the **2.2r**:PCBM device exhibits a response out to ~1300 nm, which is significant given that only about 20 polymers exhibit photoresponse past 1000 nm.[9] Additionally, **2.2r** is one of the least synthetically complex polymers among those that exhibit photoresponse below 1000 nm, making it a more practical option.

A specific detectivity ($D^*(\lambda)$) spectrum was collected for the highest performing **2.2r**:PCBM BHJ device. Specific detectivity data was collected and processed by Nic Nicolaidis at the Centre for Organic Electronics, University of Newcastle. Specific detectivity is an important parameter that is used to assess the performance of photodetectors.[9,11,66–69] However, to explain specific detectivity, two other figures of merit must first be discussed. The first is responsivity, which is the ratio of photocurrent generated in the photodetector to the incident optical power at a specific wavelength and is generally given in units of A W^{-1}.[11,66–69] Responsivity is determined from the following equation:

$$R = \frac{I_{ph}}{P_{light}} \qquad \text{(Equation 2.1)}$$

where the I_{ph} is the photocurrent and P_{light} is the incident light power. The second figure of merit is the noise equivalent power (NEP).[9,11,66,69] NEP is the incident optical power used to overcome the noise and observe a signal. NEP describes the sensitivity of the device and is determined from the following equation:

$$NEP = \frac{I_n / \sqrt{\Delta f}}{R} \qquad \text{(Equation 2.2)}$$

where I_n is the noise current measured in the dark and describes the combined impact of thermal noise, shot noise, and flicker noise and Δf is the electrical bandwidth of the noise measurement. Specific detectivity considers the NEP and device area and is determined from the following equation:

$$D^* = \frac{\sqrt{A}}{NEP} \qquad \text{(Equation 2.3)}$$

where A is the device area. Specific detectivity is wavelength dependent.

*D** values are usually reported in units of cm $Hz^{1/2}$ W^{-1} (also referred to as Jones) with a *D** value of $>10^{11}$ Jones targeted.[9] It is important to note that *D** values reported in the literature are often overestimated because dark current is used instead of the total noise. Dark current does not take thermal noise into account, which is thought to be significant in organic NIR photodetectors.[11,66,67,69]

The *D** spectrum for the top performing **2.2r**:PCBM device is shown in Figure 2.28. The devices exhibit a low energy maximum *D** value at 1110 nm of 8.0 x 10^9 Jones. At first glance, this *D** value may seem low as current polymer NIR photodetectors have achieved *D** values $>10^{13}$.[70] However, as mentioned above, most *D** values reported in the literature are overestimated by over an order of magnitude, as dark current is used instead of the total noise. Thus, *D** values were determined using the dark current to determine how much this method overestimates the *D** value and to better compare the **2.2r**:PCBM device results with values reported in the literature. Using dark current the top performing **2.2r**:PCBM device exhibited a *D** value of 2.98 x 10^{12} Jones at 1110 nm. Further efforts by Tomas Marsh and Nic Nicolaidis at the Centre for Organic Electronics, University of Newcastle fabricated and tested devices with a higher dark current *D** value of 3.07 x 10^{12} Jones at 1075 nm from a device with a 1:2 ratio of **2.2r** to PCBM, spun from dichlorobenzene, and annealed for 5 minutes. Shown in Figure 2.29 is

a comparison of polymer **2.2r** with some of the top performing polymers used in NIR photodetectors. As can be seen polymer **2.2r** exhibits a competitive *D** value and is less complex than other polymers used in NIR photodetectors.[9]

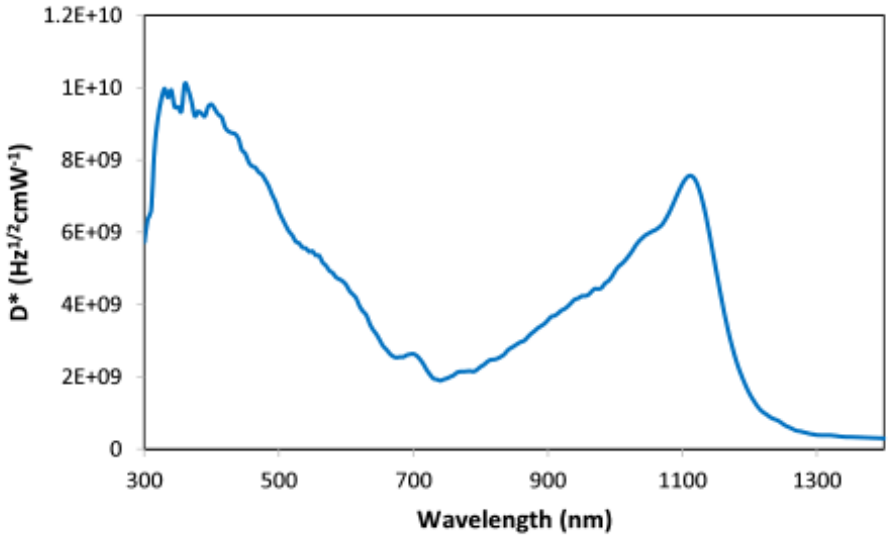

Figure 2.28. Specific detectivity spectrum of the highest performing **2.2r**:PCBM device (1:1 ratio of **2.2r** to PCBM, spun from chlorobenzene, and unannealed).

2.2.5. Synthetic Complexity

The synthetic complexity of **2.2r** was compared to some of the top performing polymers used in NIR photodetectors. Synthetic complexity has been used to compare some of the state-of-the-art donor polymers used in OPVs.[71] The equation is as follows:

$$SC = \frac{35NSS}{NSS_{max}} + \frac{25logRY}{logRY_{max}} + \frac{15NUO}{NUO_{max}} + \frac{15NCC}{NCC_{max}} + \frac{10NHC}{NHC_{max}} \qquad \text{(Equation 2.4)}$$

where NSS is the number of synthetic steps used to make the monomers plus one (to account for the polymerization step), RY is the reciprocal yield of the monomers, NUO is the number of unit operations to isolate and purify the monomers, NCC is the number of column chromatography steps, and NHC is the number of hazardous chemicals used to make the monomers (the NHC of

a given hazardous chemical equals the number H statements in its safety data sheet, with the H statements considered listed in ref. 71). Number of unit operations includes quenching/neutralization, extraction, column chromatography, recrystallization, and distillation/sublimation. The number of column chromatography steps is counted twice in the synthetic complexity calculation, as it is not ideal for large scale synthesis. Additionally, the terms are weighted differently, with the number of synthetic steps carrying the most weight. The synthetic complexity is relative, and changes based on the polymers used for comparison. The max values correspond to the highest value for the group of compared polymers. However, one short sight of this equation is that the polymerization step is not considered for in the RY, NUO, NCC, or NHC values, thus a polymer that is made with a very inefficient polymerization method could still have a good synthetic complexity value.

Nonetheless, this is a useful equation used to gauge the complexity of conjugated polymers. The synthetic complexity of **2.2r** was compared to some of the top performing polymers used in NIR photodetectors (polymers **2.10**–**2.13**, Figure 2.29). In addition, all values used for the variables in Equation 2.4 for polymers **2.2r** and **2.10**–**2.13** and an example calculation can be found in the experimental section (section 2.4.7).

2.3. Conclusion

Branched alkyl side chain functionalized PTPs (**2.2p**, **2.2q**, **2.2r**, and **2.2ar**) were synthesized by GRIM polymerization. Branched side chains were employed to increase the solubility of the polymer to avoid low solubility-induced precipitation during synthesis, resulting in higher molecular weight polymers. However, polymer **2.2r** exhibited a lower molecular weight than was expected, but was completely soluble in the reaction vessel and chloroform, suggesting that the low molecular weight of this polymer is not due to low solubility.

Interestingly, polymer **2.2p**, functionalized with 3,7-dimethyloctyl side chains, was of the highest molecular weight but did not exhibit a significant decrease in bandgap. It was found that polymers **2.2q** and **2.2r**, functionalized with 2-octyldodecyl and 2-ethylhexyl side chains, respectively, were completely soluble in chloroform and exhibited enhanced processability relative to polymer **2.2a**, functionalized with hexyl side chains.

It was found that polymers **2.2p**, **2.2r**, and **2.2ar** exhibited red-shifted absorption λ_{max} values in both solution and solid state compared to the hexyl functionalized analog (**2.2a**). However, polymer **2.2q** exhibited the most blue-shifted absorption λ_{max} values in both solution and solid state. The blue-shifted absorption spectra of **2.2q** is likely due to low molecular weight and steric effects caused by the bulky branched side chains, which twists the polymer backbone. All polymers analyzed in this chapter exhibited a similar bandgap of 1.06 to 1.10 eV.

BHJ photonic devices were fabricated with **2.2r**:PCBM active layers. The optimized **2.2r**:PCBM device exhibited a PCE of 0.229%, which was a significant increase compared to the previously reported **2.2a**:PCBM devices. The improved PCE is largely attributed to the improved processability of **2.2r**, potentially resulting in better interfaces between the donor and acceptor material and between the active layer and transport layers. EQE and *D** spectra were collected for the optimized **2.2r**:PCBM device. It was found that the device exhibited a low energy maximum response at 1110 nm, with EQE and *D** values at 1110 nm of 3.78% and 8.0×10^9 Jones, respectively. However, when using the dark current to determine *D** it was found that the devices exhibited *D** values at 1075 nm of 3.07×10^{12} Jones. Furthermore, the optimized **2.2r**:PCBM device exhibits photoresponse out to ca. 1300 nm, making **2.2r** one of only about 20 polymers that show photoresponse below 1000 nm, and of these polymers **2.2r** is one of the least structurally complex.

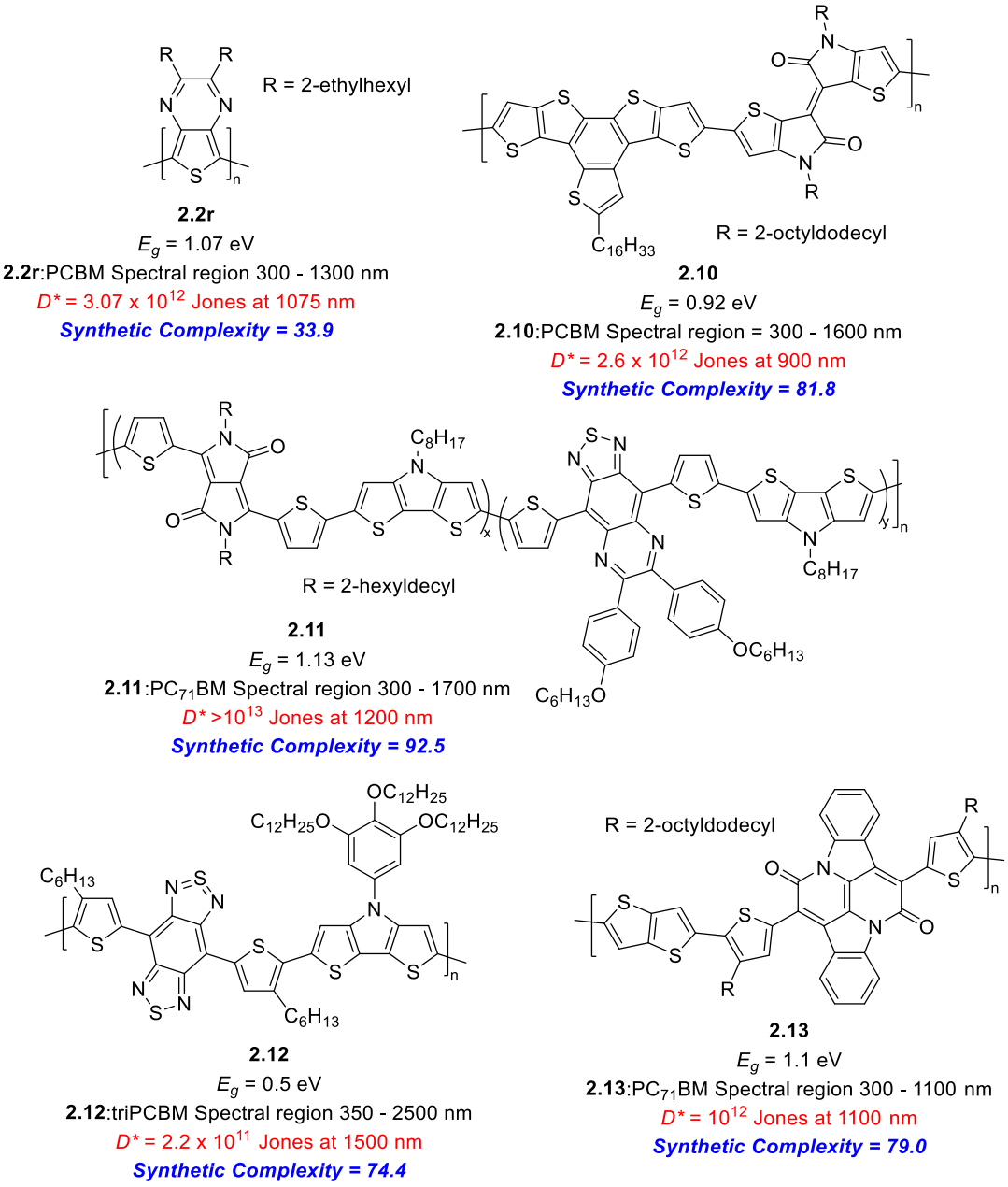

Figure 2.29. Several top performing polymers used for NIR photodetectors.

2.4. Experimental

2.4.1. General

All materials were reagent grade and used without further purification unless noted. DMF was dried by mixing with $MgSO_4$ and flushing through a silica gel plug. DCM was dried by

flushing through a silica gel plug. THF was dried by distillation over sodium/benzophenone. All dry solvents were transferred via standard syringe techniques. All reactions were carried out under a dry nitrogen stream. Reaction glassware was oven dried before use. ^{1}H and ^{13}C NMR were collected using a 400 MHz spectrometer using $CDCl_3$ as the solvent. NMR peak multiplicity is reported as follows: s = singlet, d = doublet, t = triplet, sept = septet, and m = multiplet. A digital thermal couple with a 0.1 °C resolution was used to determine melting points. Previously reported procedures were followed to synthesize 3,4-diaminothiophene,[16] 2,3-bis(2-ethylhexyl)thieno[3,4-*b*]pyrazine,[47] 5,7-dibromo-2,3-dihexylthieno[3,4-*b*]pyrazine,[13] and poly(2,3-dihexylthieno[3,4-*b*]pyrazine).[13]

1-Bromo-3,7-dimethyloctane (2.7). Compound **2.7** was prepared via a modification of a previously reported procedure.[48] To a 1000 mL three neck round bottom flask was added, dry dichloromethane (600 mL), 3,7-dimethyl-1-octanol (25.6 g, 168 mmol), and triphenylphosphine (48.3 g, 184 mmol). NBS (32.8 g, 184 mmol) was added slowly to maintain the reaction temperature below 30 °C. The reaction was let stir overnight. Solvent was removed via rotary evaporation. Purification by column chromatography using hexanes gave the product as a clear oil (26.8 g, 72%). ^{1}H NMR ($CDCl_3$, 400 MHz): δ 3.48–3.40 (m, 2H), 1.95–1.85 (m, 1H), 1.74–1.63 (m, 2H), 1.58–1.50 (m, 1H), 1.35–1.26 (m, 4H), 1.20–1.13 (m, 2H), 0.91 (d, J = 6.5 Hz, 3H), 0.90 (d, J = 6.5 Hz, 6H). ^{13}C NMR ($CDCl_3$, 400 MHz): δ 40.1, 39.2, 36.7, 32.1, 31.7, 27.9, 24.6, 22.7, 22.6, 19.0.

2,6,13,17-Tetramethyloctadecane-9,10-dione (2.9). Compound **2.9** was prepared by the modification of a previously reported procedure.[16] To a 250 mL three neck round bottom flask equipped with an addition funnel was added, magnesium (3.04 g, 125 mmol), iodine (1 grain), and dry THF (75 mL). **2.7** (25.6 g, 115.7 mmol) was added dropwise keeping the temperature

below 50 °C. After completion of the addition the reaction was stirred for 30 min. The reaction was heated to 50 °C and stirred for 2 h. The reaction was let cool to room temperature. To a separate 500 mL three neck round bottom equipped with an addition funnel and mechanical stirrer was added, CuBr (16.1 g, 112 mmol) and dry THF (85 mL). To a separate 250 mL single neck round bottom flask was added, LiBr (19.4 g, 223 mmol) and dry THF (85 mL). The LiBr solution was transferred to the flask containing CuBr, and this mixture was cooled to -100 °C using an ethanol/liquid nitrogen bath. The Grignard reagent was added dropwise to the LiBr/CuBr mixture maintaining the temperature between -100 and -90 °C. Oxalyl chloride (5.92 g, 46.6 mmol) was added dropwise maintaining the temperature between -100 and -85 °C. The reaction was stirred for 60 min maintaining the temperature between -100 and -90 °C. The reaction was warmed to room temperature, quenched with saturated aqueous NH_4Cl. The mixture was extracted with ethyl acetate, dried with Na_2SO_4, filtered, and concentrated. Column chromatography with 95:5 hexanes:ethyl acetate gave a yellow oil that was used without further purification (7.18 g, 46%). ^{1}H NMR ($CDCl_3$, 400 MHz): δ 2.78–2.73 (m, 4H), 1.58–1.07 (m, 20H), 0.89 (d, J = 6.5 Hz, 12H), 0.86 (d, J = 6.5 Hz, 6H).

2,3-Bis(3,7-dimethyloctyl)thieno[3,4-*b*]pyrazine (2.1p). Compound **2.1p** was prepared by the modification of a previously reported procedure.[47] To a 500 mL single neck round bottom flask was added, 3,4-diaminothiophene (1.94 g, 17.0 mmol), **2.9** (5.75 g, 17.0 mmol), and absolute ethanol (325 mL). The reaction was stirred at room temperature for 3 h. Water (~400 mL) was added. The mixture was extracted with DCM, dried with Na_2SO_4, filtered and concentrated. The crude product was purified by column chromatography with 95:5 hexanes:ethyl acetate to give the product as a yellow-brown oil that turned to a tan solid (1.48 g, 21%) upon pumping. Mp 27.8–28.8 °C; ^{1}H NMR ($CDCl_3$, 400 MHz): δ 7.82 (s, 2H), 3.00–2.84

(m, 4H), 1.85–1.79 (m, 2H), 1.67–1.51 (m, 6H), 1.45–1.16 (m, 12H), 1.02 (d, *J* = 6.3 Hz, 6H), 0.89 (d, *J* = 6.6 Hz, 12H). ^{13}C NMR ($CDCl_3$, 400 MHz): δ 156.7, 141.7, 115.8, 39.3, 37.1, 35.7, 33.5, 33.2, 28.0, 24.8, 22.7, 22.6, 19.7.

5,7-Dibromo-2,3-bis(2-ethylhexyl)thieno[3,4-*b*]pyrazine (2.4r). Compound **2.4r** was prepared by the modification of a previously reported procedure.[13] **2.1r** (1.57 g, 4.35 mmol) was added to a 500 mL three-neck round-bottom flask equipped with an addition funnel. Dry DMF (130 mL) was added and the solution was cooled to -78 °C in an acetone/dry ice bath. In a separate flask, NBS (1.94 g, 10.9 mmol) was dissolved in dry DMF (45 mL) and put under dry N_2. The NBS solution was added dropwise to the **2.1r** solution (ca. 30 min addition). The mixture was then warmed to -20 °C in a brine/dry ice bath and stirred for 3.5 h. The mixture was poured onto ice and stirred until the ice melted. Brine was then added, and the mixture was extracted with ethyl acetate. The organic fractions were combined, washed with water, dried with Na_2SO_4, filtered, and concentrated to give a brown oil. The crude product was purified with a short silica gel plug (80:20 hexanes:DCM) to give a yellow-orange oil (1.51 g, 67%). ^{1}H NMR ($CDCl_3$, 400 MHz): δ 2.82 (d, *J* = 7.0 Hz, 4H), 2.02 (sept, *J* = 6.1 Hz, 2H), 1.45–1.23 (m, 16H), 0.90 (t, *J* = 7.4 Hz, 6H), 0.87 (t, *J* = 7.2 Hz, 6H). ^{13}C NMR ($CDCl_3$, 400 MHz): δ 158.0, 139.2, 103.2, 39.6, 38.0, 32.8, 28.9, 26.1, 23.1, 14.2, 11.0. NMR data agree well with previously reported values.[72]

5,7-Dibromo-2,3-bis(3,7-dimethyloctyl)thieno[3,4-*b*]pyrazine (2.4p). Compound **2.4p** was prepared in a similar fashion to compound **2.4r** by exchanging **2.1p** for **2.1r**. The product was collected as a yellow-brown oil (45%). ^{1}H NMR ($CDCl_3$, 400 MHz): δ 3.01–2.86 (m, 4H), 1.87–1.80 (m, 2H), 1.67–1.51 (m, 6H), 1.45–1.16 (m, 12H), 1.01 (d, *J* = 6.3 Hz, 6H), 0.90 (d, *J* =

6.6 Hz, 12H). ^{13}C NMR ($CDCl_3$, 400 MHz): δ 158.5, 139.4, 103.1, 39.3, 37.2, 35.2, 33.1, 33.0, 28.0, 24.8, 22.7, 22.6, 19.6.

5,7-Dibromo-2,3-bis(2-octyldodecyl)thieno[3,4-*b*]pyrazine (2.4q). Compound **2.4q** was prepared in a similar fashion to compound **2.4r** by exchanging **2.1q** for **2.1r**. The crude product was purified with a short silica gel plug (50:50 hexanes:DCM) to give a yellow-brown oil (2.69 g, 82%). ^{1}H NMR ($CDCl_3$, 400 MHz): δ 2.84 (d, J = 6.9 Hz, 4H), 2.11–2.06 (m, 2H), 1.36–1.26 (m, 64H), 0.92–0.88 (m, 12H). ^{13}C NMR ($CDCl_3$, 400 MHz): δ 157.9, 139.1, 103.1, 39.9, 36.6, 33.7, 31.9, 30.0, 29.7, 29.7, 29.6, 29.4, 29.4, 26.7, 26.6, 22.7, 14.1.

Poly(2,3-bis(2-ethylhexyl)thieno[3,4-*b*]pyrazine) (2.2r). Polymer **2.2r** was prepared by the modification of a previously reported procedure.[13] To a 50 mL three neck round bottom flask equipped with a condenser was added, **2.4r** (1.04 g, 2.0 mmol) and dry THF (10 mL). Methylmagnesium bromide (0.7 mL, 3.0 M solution in diethyl ether) was added via syringe dropwise. The reaction was heated at reflux for 1 h. Ni(dppp)Cl_2 (0.0054 g, 0.010 mmol) was added and the reaction was heated at reflux for another 1 h. The reaction was let cool to room temperature and precipitated by adding dropwise via Pasteur pipette to MeOH (~100 mL) at 0 °C. The mixture was stirred at 0 °C for 2 h. The precipitate was loaded onto a glass frit and washed with methanol via Soxhlet apparatus for 24 h. The soluble fraction was extracted with $CHCl_3$ and concentrated to give a purple-black solid. The solid was pumped for 4 h to yield the desired product (0.49 g, 68%). ^{1}H NMR ($CDCl_3$, 400 MHz): δ 3.14, 2.03, 1.47, 1.24, 0.95, 0.83. GPC: Mw = 10300, Mn = 7400, PDI = 1.39.

Poly(2,3-bis(3,7-dimethyloctyl)thieno[3,4-*b*]pyrazine) (2.2p). Polymer **2.2p** was prepared in a similar fashion to polymer **2.2r** by exchanging **2.4p** for **2.4r**. The product was

collected as a purple-black solid (79%). ^{1}H NMR ($CDCl_3$, 400 MHz): δ 3.25, 2.12, 1.85, 1.58, 1.28, 1.11, 1.07, 0.91, 0.79. GPC: Mw = 15800, Mn = 10900, PDI = 1.44.

Poly(2,3-dihexylthieno[3,4-*b*]pyrazine-*ran*-2,3-bis(2-ethylhexyl)thieno[3,4-*b*]pyrazine) (2.2ar). Polymer **2.2ar** was prepared in a similar fashion to polymer **2.2r** by adding 0.5 equiv. of **2.4a** and 0.5 equiv of **2.4r** instead of 1 equiv. of **2.4r**. The product was collected as a purple-black solid (65%). ^{1}H NMR ($CDCl_3$, 400 MHz): δ 3.23, 2.08, 1.62, 1.52, 1.38, 1.28, 0.99, 0.89. GPC: Mw = 11700, Mn = 7000, PDI = 1.68.

Poly(2,3-bis(2-octyldodecyl)thieno[3,4-*b*]pyrazine) (2.2q). Polymer **2.2q** was prepared by the modification of a previously reported procedure.[13] To a 50 mL three neck round bottom flask equipped with a condenser was added, **2.4q** (1.71 g, 2.00 mmol) and dry THF (10 mL). Methylmagnesium bromide (0.7 mL, 3.0 M solution in diethyl ether) was added via syringe dropwise. The reaction was heated at reflux for 2 h. Ni(dppp)Cl_2 (0.0054 g, 0.010 mmol) was added and the reaction was heated at reflux for another 1 h. The reaction was let cool to room temperature and concentrated via rotary evaporation. The crude product was dissolved in $CHCl_3$, washed with water, dried with Na_2SO_4, filtered, and concentrated. The resulting black gel was washed several times with MeOH, then with acetone until the washes were colorless. The black gel was pumped for 3 h to yield the desired product (0.46 g, 33%). ^{1}H NMR ($CDCl_3$, 400 MHz): δ 3.19, 2.82, 2.10, 2.02, 1.68, 1.49, 1.27, 0.90, 0.78. GPC: Mw = 7800, Mn = 6600, PDI = 1.19.

Poly(2,3-bis(2-ethylhexyl)thieno[3,4-*b*]pyrazine) (2.2r) – room temperature conditions. The room temperature polymerization was carried out by the modification of a previously reported procedure.[13] To a 100 mL three neck round bottom flask was added, **2.4r** (1.04 g, 2.0 mmol) and dry THF (10 mL). Methylmagnesium bromide (0.7 mL, 3.0 M solution in diethyl ether) was added via syringe dropwise. The reaction was stirred for 5 min. Another 50

mL of dry THF was added. Then Ni(dppp)Cl_2 (0.0054 g, 0.010 mmol) was added, and the reaction was let stir for another 15 min. The reaction was poured over MeOH (~100 mL) at 0 °C. The mixture was stirred at 0 °C for 2 h. The precipitate was loaded onto a glass frit and washed with methanol via Soxhlet apparatus for 24 h. The soluble fraction was extracted with $CHCl_3$ and concentrated to give a purple-black solid. The solid was pumped for 4 h to yield the desired product (0.09 g, 13%). GPC: Mw = 7100, Mn = 5900, PDI = 1.20.

Poly(2,3-bis(2-ethylhexyl)thieno[3,4-*b*]pyrazine) (2.2r) – with LiCl. To a 25 mL three neck round bottom flask equipped with a condenser was added, **2.4r** (0.49 g, 0.95 mmol), LiCl (0.044 g, 1.04 mmol) and dry THF (5 mL). Methylmagnesium bromide (0.35 mL, 3.0 M solution in diethyl ether) was added via syringe dropwise. The reaction was heated at reflux for 1 h. Ni(dppp)Cl_2 (0.0026 g, 0.0048 mmol) was added and the reaction was heated at reflux for another 1 h. The reaction was let cool to room temperature and precipitated by adding dropwise via Pasteur pipette to MeOH (~100 mL) at 0 °C. The mixture was stirred at 0 °C for 2 h. The precipitate was loaded onto a glass frit and washed with methanol via Soxhlet apparatus for 24 h. The soluble fraction was extracted with $CHCl_3$ and concentrated to give a purple-black solid. The solid was pumped for 4 h to yield the desired polymer (0.24 g, 70%). GPC: Mw = 10000, Mn = 6800, PDI = 1.46.

2.4.2. Electrochemistry

Electrochemical analysis was performed using a three-electrode cell with a platinum disc working electrode and a platinum wire auxiliary electrode. The Ag/Ag^+ reference electrode was prepared with a 0.01 M $AgNO_3$ and 0.1 M tetrabutylammonium hexafluorophosphate ($TBAPF_6$) solution in dry MeCN. MeCN used for electrochemistry was dried by distillation over CaH_2 under dry N_2. Polymer films were prepared by drop casting a polymer solution in $CHCl_3$ onto the

working electrode. Electrochemical cells were oven dried. Solutions of 0.10 M $TBAPF_6$ in dry MeCN were deoxygenated by sparging with argon before each scan and blanked with argon during the scan. Measurements were taken with a sweep rate of 100 mV s^{-1}. E_{HOMO} and E_{LUMO} values were estimated by taking the onsets of first oxidation and reduction and referencing to ferrocene (5.1 V vs. vacuum).[73]

2.4.3. Absorption Spectroscopy

Absorption spectroscopy measurements were collected using a Carry 500 dual-beam UV-vis-NIR spectrophotometer. Solution-state spectra were collected with the analyte dissolved in $CHCl_3$. Spin coated polymer films on glass plates were used for solid-state analysis. Optical bandgaps were determined from the solid-state spectra by extending the steepest part of the low energy absorption onset to the baseline.

2.4.4. Differential Scanning Calorimetry

DSC analysis was carried out using a TA Instrument model DSC 2500. The scans were from 25°C to 200°C. The heating rate was 10 °C/min. The sample sizes were 2–3 mg.

2.4.5. Photonic Device Fabrication

Patterned ITO glass slides were cleaned via sonication in detergent, acetone, and isopropyl alcohol. The slides were then cured with ozone treatment. PEDOT:PSS layers were spin coated onto the ITO slide and annealed at 140 °C for 30 minutes. Solutions of **2.2r**:PCBM in chloroform, chlorobenzene, or 1,2-dichlorobenzene were prepared and spin coated under nitrogen atmosphere (active layer with a thickness was 85–140 nm). If annealed the active layer was annealed under nitrogen atmosphere at 140 °C. A layer of ZnO was spin coated and annealed at 90 °C for 5 minutes under nitrogen atmosphere. The aluminum cathode was thermally deposited in a vacuum deposition chamber to give a thickness of ~100 nm.

2.4.6. Device Characterization

External quantum efficiency (EQE) measurements were made using a chopped halogen lamp source coupled through an Oriel Cornerstone scanning monochromator. The output light (2 nm bandwidth monochromatic light) was then coupled via a quartz fiber bundle into a glovebox where it was focused to illuminate the cell area with no overfilling. Order sorting filters were used at higher wavelengths to remove lower wavelengths from the broadband input light. The illuminated device output electrodes were connected to a Stanford Research Systems SR830 lock-in amplifier. Source intensity fluctuations were monitored using a reference diode that measured a reflection off a glass wedge. The monitor data was acquired by a separate Stanford Research Systems SR830 lock-in amplifier that allows absolute spectral corrections via a look-up table, which was generated from a reference scan performed prior to the measurement of the EQE. Output signals from both phase-locked loop measurements were recorded on a PC as is the illumination wavelength.

The noise floor measurements were performed using a B1500A Semiconductor Device Analyser with a medium power source measure unit (SMU) B1511B. The dark current obtained was fast Fourier transformed via Matlab.

2.4.7. Synthetic Complexity

Synthetic complexity was calculated following the guidelines in reference 71. Values used for the calculation are given in Table 2.8 and an example calculation for polymer **2.2r** is given in Figure 2.30.

Table 2.8. Values used for synthetic complexity calculations for polymers used for NIR photodetectors with the values in red used as the max values.

			Number of Purification Steps							
Polymer	Synthetic Steps	Reciprocal yield (100/yield of the comonomers)	Quenching/neutralization	Extraction	Column Chromatography	Recrystallization	Distillation/sublimaiton	Number of hazardous chemicals	Synthetic Complexity (relative)	References used for calculation
2.2r	7	1.96	1	5	2	1	1	32	33.9	16, this work
2.10	15	14.83	1	5	7	0	1	65	81.8	74
2.11	18	7.07	2	7	10	1	0	86	92.5	70, 75-86
2.12	14	12.99	3	6	3	5	0	60	74.4	75, 78-80, 87-93
2.13	12	16.36	3	8	7	0	1	51	79.0	94-96

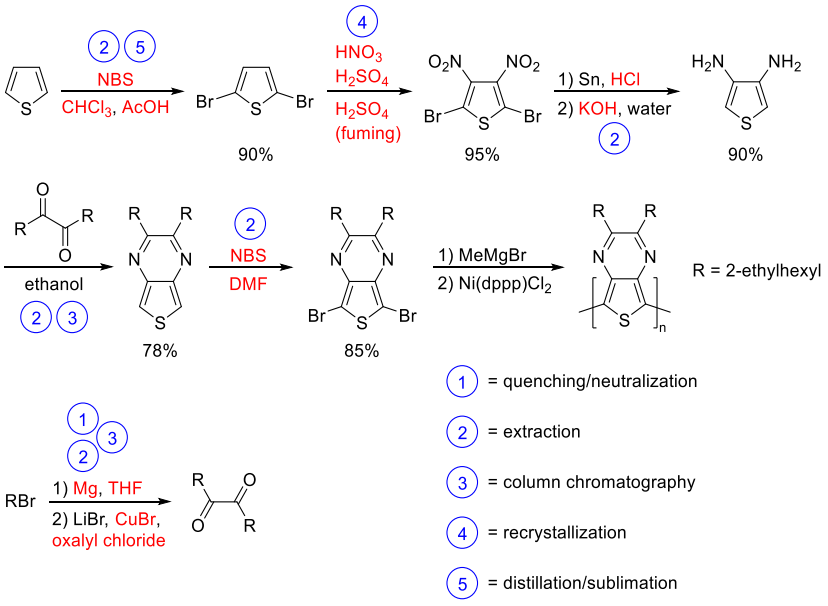

Figure 2.30. Example synthetic complexity calculation for **2.2r** with unit operations represented by the blue numbers and hazardous chemicals in red. The polymerization step is not included in this calculation.

2.5. References

(1) Nunzi, J.-M. *C. R. Phys.* **2002**, *3* (4), 523–542.

(2) Jung, J. W.; Jo, J. W.; Jung, E. H.; Jo, W. H. *Org. Electron.* **2016**, *31*, 149–170.

(3) Xu, T.; Yu, L. *Mater. Today* **2014**, *17* (1), 11–15.

(4) Kroon, R.; Lenes, M.; Hummelen, J. C.; Blom, P. W. M.; De Boer, B. *Polym. Rev.* **2008**, *48* (3), 531–582.

(5) Rasmussen, S. C.; Gilman, S. J.; Wilcox, W. D. *Gen. Chem.* **2023**, *9*, 220010.

(6) Li, G.; Chang, W.-H.; Yang, Y. *Nat. Rev. Mater.* **2017**, *2* (8), 17043.

(7) Shockley, W.; Queisser, H. J. *J. Appl. Phys.* **1961**, *32* (3), 510–519.

(8) Rühle, S. *Sol. Energy* **2016**, *130*, 139–147.

(9) Rasmussen, S. C.; Gilman, S. J.; Culver, E. W.; Wilcox, W. D. *Gen. Chem.* **2021**, *7* (2), 200019.

(10) Dou, L.; Liu, Y.; Hong, Z.; Li, G.; Yang, Y. *Chem. Rev.* **2015**, *115* (23), 12633–12665.

(11) Li, Q.; Guo, Y.; Liu, Y. *Chem. Mater.* **2019**, *31* (17), 6359–6379.

(12) Kenning, D. D.; Rasmussen, S. C. *Macromolecules* **2003**, *36* (17), 6298–6299.

(13) Wen, L.; Duck, B. C.; Dastoor, P. C.; Rasmussen, S. C. *Macromolecules* **2008**, *41* (13), 4576–4578.

(14) Mulholland, M. E.; Wen, L.; Rasmussen, S. C. *Topol. Supramol. Polym. Sci.* **2015**, *2* (1) 18–29.

(15) Rasmussen, S. C.; Schwiderski, R. L.; Mulholland, M. E. *Chem. Commun.* **2011**, *47* (41), 11394–11410.

(16) Kenning, D. D.; Mitchell, K. A.; Calhoun, T. R.; Funfar, M. R.; Sattler, D. J.; Rasmussen, S. C. *J. Org. Chem.* **2002**, *67* (25), 9073–9076.

(17) Wudl, F.; Kobayashi, M.; Heeger, A. J. *J. Org. Chem.* **1984**, *49* (18), 3382–3384.

(18) Nayak, K.; Marynick, D. S. *Macromolecules* **1990**, *23* (8), 2237–2245.

(19) Ferraris, J. P.; Bravo, A.; Kim, W.; Hrncir, D. C. *J. Chem. Soc., Chem. Commun.* **1994**, *8*, 991–992.

(20) Pomerantz, M.; Chaloner-Gill, B.; Harding, L. O.; Tseng, J. J.; Pomerantz, W. J. *J. Chem. Soc., Chem. Commun.* **1992**, *22*, 1672–1673.

(21) Van Asselt, R.; Hoogmartens, I.; Vanderzande, D.; Gelan, J.; Froehling, P. E.; Aussems, M.; Aagaard, O.; Schellekens, R. *Synth. Met.* **1995**, *74* (1), 65–70.

(22) Huskić, M.; Vanderzande, D.; Gelan, J. *Synth. Met.* **1999**, *99*, 143–147.

(23) Hagan, A. J.; Moratti, S. C.; Sage, I. C. *Synth. Met.* **2001**, *119*, 147–148.

(24) H. Tamura, S. Yamanaka, K. Matsuda and T. Konishi, *Jpn. J. Polym. Sci.* **1998**, *55*, 277–283.

(25) Willot, P.; Moerman, D.; Leclère, P.; Lazzaroni, R.; Baeten, Y.; Van Der Auweraer, M.; Koeckelberghs, G. *Macromolecules* **2014**, *47* (19), 6671–6678.

(26) Ho, K.-S.; Bartus, J.; Levon, K.; Mao, J.; Zheng, W.-Y.; Laakso, J.; Taka, T. *Synth. Met.* **1993**, *55* (1), 384–387.

(27) Nguyen, L. H.; Hoppe, H.; Erb, T.; Günes, S.; Gobsch, G.; Sariciftci, N. S. *Adv. Funct. Mater.* **2007**, *17* (7), 1071–1078.

(28) Izumi, T.; Kobashi, S.; Takimiya, K.; Aso, Y.; Otsubo, T. *J. Am. Chem. Soc.* **2003**, *125* (18), 5286–5287.

(29) Ma, J.; Li, S.; Jiang, Y. *Macromolecules* **2002**, *35* (3), 1109–1115.

(30) Sheina, E. E.; Liu, J.; Iovu, M. C.; Laird, D. W.; McCullough, R. D. *Macromolecules* **2004**, *37* (10), 3526–3528.

(31) Yokoyama, A.; Miyakoshi, R.; Yokozawa, T. *Macromolecules* **2004**, *37* (4), 1169–1171.

(32) Lutz, J. P.; Hannigan, M. D.; McNeil, A. J. *Coord. Chem. Rev.* **2018**, *376*, 225–247.

(33) Geng, Y.; Huang, L.; Wu, S.; Wang, F. *Sci. China Chem.* **2010**, *53* (8), 1620–1633.

(34) Leone, A. K.; McNeil, A. J. *Acc. Chem. Res.* **2016**, *49* (12), 2822–2831.

(35) Jarrett-Wilkins, C. N.; Pollit, A. A.; Seferos, D. S. *Trends Chem.* **2020**, *2* (6), 493–505.

(36) Baker, M. A.; Tsai, C.; Noonan, K. J. T. *Chem. Eur. J.* **2018**, *24* (50), 13078–13088.

(37) Aplan, M. P.; Gomez, E. D. *Ind. Eng. Chem. Res.* **2017**, *56* (28), 7888–7901.

(38) Bryan, Z. J.; McNeil, A. J. *Macromolecules* **2013**, *46* (21), 8395–8405.

(39) Leone, A. K.; Mueller, E. A.; McNeil, A. J. *J. Am. Chem. Soc.* **2018**, *140* (45), 15126–15139.

(40) Lei, T.; Wang, J.-Y.; Pei, J. *Chem. Mater.* **2014**, *26* (1), 594–603.

(41) Mei, J.; Bao, Z. *Chem. Mater.* **2014**, *26* (1), 604–615.

(42) Zhang, Z.-G.; Li, Y. *Sci. China Chem.* **2015**, *58* (2), 192–209.

(43) Luo, N.; Ren, P.; Feng, Y.; Shao, X.; Zhang, H.-L.; Liu, Z. *J. Phys. Chem. Lett.* **2022**, *13* (4), 1131–1146.

(44) Yang, Y.; Liu, Z.; Zhang, G.; Zhang, X.; Zhang, D. *Adv. Mater.* **2019**, *31* (46), 1903104.

(45) Lv, S.; Li, L.; Mu, Y.; Wan, X. *Polym. Rev.* **2021**, *61* (3), 520–552.

(46) Reid, D. R.; Jackson, N. E.; Bourque, A. J.; Snyder, C. R.; Jones, R. L.; de Pablo, J. J. *J. Phys. Chem. Lett.* **2018**, *9* (16), 4802–4807.

(47) Culver, E. W.; Anderson, T. E.; López Navarrete, J. T.; Ruiz Delgado, M. C.; Rasmussen, S. C. *ACS Macro Lett.* **2018**, *7* (10), 1215–1219.

(48) Drozdov, F. V.; Surin, N. M.; Peregudova, S. M.; Trukhanov, V. A.; Dmitryakov, P. V.; Chvalun, S. N.; Parashchuk, D. Yu.; Ponomarenko, S. A. *Polym. Sci. Ser. B* **2019**, *61* (1), 56–76.

(49) Tsubogo, T.; Aoyama, S.; Takeda, R.; Uchiro, H. *Chem. Pharm. Bull.* **2018**, *66* (9), 843–846.

(50) Miyakoshi, R.; Shimono, K.; Yokoyama, A.; Yokozawa, T. *J. Am. Chem. Soc.* **2006**, *128* (50), 16012–16013.

(51) Stefan, M. C.; Javier, A. E.; Osaka, I.; McCullough, R. D. *Macromolecules* **2009**, *42*, 30–32.

(52) Krasovskiy, A.; Knochel, P. *Angew. Chem. Int. Ed.* **2004**, *43*, 3333–3336.

(53) Rasmussen, S. C.; Sattler, D. J.; Mitchell, K. A.; Maxwell, J. *J. Lumin.* **2004**, *109* (2), 111–119.

(54) Beaujuge, P. M.; Amb, C. M.; Reynolds, J. R. *Acc. Chem. Res.* **2010**, *43* (11), 1396–1407.

(55) Wen, L.; Heth, C. L.; Rasmussen, S. C. *Phys. Chem. Chem. Phys.* **2014**, *16* (16), 7231–7240.

(56) Audebert, P.; Hapiot, P. *Synth. Met.* **1995**, *75*, 95–102.

(57) Rasmussen, S. C.; Pickens, J. C.; Hutchison, J. E. *Chem. Mater.* **1998**, *10* (7), 1990–1999.

(58) Armand, J.; Bellec, C.; Boulares, L.; Chaquin, P.; Masure, D.; Pinson, J. *J. Org. Chem.* **1991**, *56* (16), 4840–4845.

(59) Bredas, J.-L. *Mater. Horiz.* **2014**, *1* (1), 17–19.

(60) Duck, B. C.; Vaughan, B.; Wen, L.; Heth, C. L.; Rasmussen, S. C.; Zhou, X.; Belcher, W. J.; Dastoor, P. C. *Sol. Energy Mater. Sol. Cells* **2013**, *110*, 8–14.

(61) Mazzio, K. A.; Luscombe, C. K. *Chem. Soc. Rev.* **2015**, *44* (1), 78–90.

(62) Duck, B. C.; Vaughan, B.; Cooling, N.; Zhou, X.; Holdsworth, J. L.; Wen, L. L.; Rasmussen, S. C.; Dastoor, P. C.; Belcher, W. J. *Sol. Energy Mater. Sol. Cells* **2013**, *114*, 65–70.

(63) Oku, T.; Nagaoka, S.; Suzuki, A.; Kikuchi, K.; Hayashi, Y.; Inukai, H.; Sakuragi, H.; Soga, T. *J. Phys. Chem. Solids* **2008**, *69*, 1276–1279.

(64) Pan, M.-A.; Lau, T.-K.; Tang, Y.; Wu, Y.-C.; Liu, T.; Li, K.; Chen, M.-C.; Lu, X.; Ma, W.; Zhan, C. *J. Mater. Chem. A* **2019**, *7* (36), 20713–20722.

(65) Kippelen, B.; Brédas, J.-L. *Energy Environ. Sci.* **2009**, *2* (3), 251–261.

(66) Chow, P. C. Y.; Someya, T. *Adv. Mater.* **2020**, *32* (15), 1902045.

(67) Liu, X.; Lin, Y.; Liao, Y.; Wu, J.; Zheng, Y. *J. Mater. Chem. C* **2018**, *6* (14), 3499–3513.

(68) Li, N.; Lan, Z.; Cai, L.; Zhu, F. *J. Mater. Chem. C* **2019**, *7* (13), 3711–3729.

(69) Yang, D.; Ma, D. *Adv. Opt. Mater.* **2019**, *7* (1), 1800522.

(70) Han, J.; Yang, D.; Ma, D.; Qiao, W.; Wang, Z. Y. *Adv. Opt. Mater.* **2018**, *6* (15), 1800038.

(71) Po, R.; Bianchi, G.; Carbonera, C.; Pellegrino, A. *Macromolecules*, **2015**, *48*, 453–461.

(72) Chen, C.-H.; Hsieh, C.-H.; Dubosc, M.; Cheng, Y.-J.; Hsu, C.-S. *Macromolecules* **2010**, *43*, 697–708.

(73) Cardona, C. M.; Li, W.; Kaifer, A. E.; Stockdale, D.; Bazan, G. C. *Adv. Mater.* **2011**, *23* (20), 2367–2371.

(74) Han, J.; Qi, J.; Zheng, X.; Wang, Y.; Hu, L.; Guo, C.; Wang, Y.; Li, Y.; Ma, D.; Qiao, W.; Wang, Z. Y. *J. Mater. Chem. C* **2017**, *5* (1), 159–165.

(75) Evenson, S. J.; Rasmussen, S. C. *Org. Lett.* **2010**, *12* (18), 4054–4057.

(76) Koeckelberghs, G.; De Cremer, L.; Vanormelingen, W.; Dehaen, W.; Verbiest, T.; Persoons, A.; Samyn, C. *Tetrahedron* **2005**, *61* (3), 687–691.

(77) Evenson, S. J.; Pappenfus, T. M.; Delgado, M. C. R.; Radke-Wohlers, K. R.; Navarrete, J. T. L.; Rasmussen, S. C. *Phys. Chem. Chem. Phys.* **2012**, *14* (17), 6101–6111.

(78) Wu, J.; Lai, G.; Li, Z.; Lu, Y.; Leng, T.; Shen, Y.; Wang, C. *Dyes Pigments* **2016**, *124*, 268–276.

(79) Heiskanen, J. P.; Vivo, P.; Saari, N. M.; Hukka, T. I.; Kastinen, T.; Kaunisto, K.; Lemmetyinen, H. J.; Hormi, O. E. O. *J. Org. Chem.* **2016**, *81* (4), 1535–1546.

(80) Qi, J.; Fang, Y.; Kwok, R. T. K.; Zhang, X.; Hu, X.; Lam, J. W. Y.; Ding, D.; Tang, B. Z. *ACS Nano* **2017**, *11* (7), 7177–7188.

(81) Perzon, E.; Wang, X.; Admassie, S.; Inganäs, O.; Andersson, M. R. *Polymer* **2006**, *47* (12), 4261–4268.

(82) Perzon, E.; Zhang, F.; Andersson, M.; Mammo, W.; Inganäs, O.; Andersson, M. R. *Adv. Mater.* **2007**, *19*, 3308–3311.

(83) Liu, J.; Geng, J.; Liao, L.-D.; Thakor, N.; Gao, X.; Liu, B. *Polym. Chem.* **2014**, *5* (8), 2854–2862.

(84) Yiu, A. T.; Beaujuge, P. M.; Lee, O. P.; Woo, C. H.; Toney, M. F.; Fréchet, J. M. J. *J. Am. Chem. Soc.* **2012**, *134* (4), 2180–2185.

(85) Kirkus, M.; Wang, L.; Mothy, S.; Beljonne, D.; Cornil, J.; Janssen, R. A. J.; Meskers, S. C. J. *J. Phys. Chem. A* **2012**, *116* (30), 7927–7936.

(86) Bürgi, L.; Turbiez, M.; Pfeiffer, R.; Bienewald, F.; Kirner, H.-J.; Winnewisser, C. *Adv. Mater.* **2008**, *20* (11), 2217–2224.

(87) Randell, N. M.; Radford, C. L.; Yang, J.; Quinn, J.; Hou, D.; Li, Y.; Kelly, T. L. *Chem. Mater.* **2018**, *30* (14), 4864–4873.

(88) Kitamura, C.; Tanaka, S.; Yamashita, Y. *Chem. Mater.* **1996**, *8* (2), 570–578.

(89) Wan, L.; Li, X.; Song, C.; He, Y.; Zhang, W. *Sol. Energy Mater. Sol. Cells* **2019**, *191*, 437–443.

(90) Yuen, J. D.; Kumar, R.; Zakhidov, D.; Seifter, J.; Lim, B.; Heeger, A.; Wudl, F. *Adv. Mater.* **2011**, *23*, 3780–3785.

(91) Imin, P.; Imit, M.; Adronov, A. *Macromolecules* **2011**, *44* (23), 9138–9145.

(92) Fallahi, A.; Taromi, F. A.; Mohebbi, A.; Yuen, J. D.; Shahinpoor, M. *J. Mater. Chem. C* **2014**, *2* (32), 6491–6501.

(93) Zheng, L.; Zhu, T.; Xu, W.; Liu, L.; Zheng, J.; Gong, X.; Wudl, F. *J. Mater. Chem. C* **2018**, *6* (14), 3634–3641.

(94) Fuller, L. S.; Iddon, B.; Smith, K. A. *J. Chem. Soc., Perkin Trans. 1* **1997**, 22, 3465–3470.

(95) Li, Y.; Sonar, P.; Singh, S. P.; Ooi, Z. E.; Lek, E. S. H.; Loh, M. Q. Y. *Phys. Chem. Chem. Phys.* **2012**, *14* (19), 7162–7169.

(96) Verstraeten, F.; Gielen, S.; Verstappen, P.; Kesters, J.; Georgitzikis, E.; Raymakers, J.; Cheyns, D.; Malinowski, P.; Daenen, M.; Lutsen, L.; Vandewal, K.; Maes, W. *J. Mater. Chem. C* **2018**, *6* (43), 11645–11650.

CHAPTER 3. ACENAPHTHO[1,2-*b*]THIENO[3,4-*e*]PYRAZINE-BASED SOLUTION PROCESSABLE CONJUGATED POLYMERS WITH BANDGAPS BELOW 0.7 eV

3.1. Introduction

Researchers in the field of conjugated polymers have aimed to create polymers with a zero bandgap or very low bandgap.[1] This is because a lower bandgap requires less thermal energy to populate the conduction band, theoretically resulting in better conductivity.[1–3] Additionally, reducing the bandgap of the polymer causes its absorption to shift towards the near-infrared (NIR) portion of the spectrum, which creates the possibility for a colorless transparent conducting material.[1] Moreover, by pushing the polymer absorption into the NIR part of the spectrum, these materials can be used for NIR photodetection[4] and bioimaging.[5–7] Finally, as low bandgap polymers usually have a high HOMO and a low LUMO, it is possible to make ambipolar (i.e., hole and electron transporting) organic field-effect transistors (OFETs) from these materials.[8]

Very low bandgaps are commonly achieved by destabilizing the HOMO energy level and stabilizing the LUMO energy level. However, when the HOMO level is significantly destabilized, the resulting material generally exhibits low ambient stability. As a result, many of the very low bandgap polymers that have been created are oxidatively unstable and cannot be used under ambient conditions.[1] Furthermore, low bandgap polymers typically consist of rigid fused-ring units, which often leads to low solubility and makes processing difficult. As a consequence, this limits the application of such polymers to devices.[9]

3.1.1. Low Bandgap Conjugated Polymer History

After the discovery of organic semiconducting materials, researchers became interested in producing low bandgap polymers. As previously introduced in chapter 3, Wudl and coworkers

synthesized the first low bandgap polymer, polyisothianaphthene (**3.1**), by electrochemical polymerization in 1984, which had a bandgap of 1.0 eV.[10–13] Since **3.1**, other benzothiophene analogs have been made to produce low bandgap materials.[14] However, as discussed in chapter 2, benzothiophene-based polymers have a limitation due to the steric interaction between the neighboring H on the benzene ring and the S of the thiophene ring. This causes a deviation from planarity, which results in a decreased electron delocalization.[15]

Researchers then shifted their focus from benzothiophene-based polymers to polymers containing units like thieno[3,4-*b*]pyrazine (TP) and thieno[3,4-*c*][1,2,5]thiadiazole, as these polymers exhibit enhanced planarity since they do not have the steric H···S interaction. In 1992, Pomerantz and coworkers produced poly(2,3-dihexylthieno[3,4-*b*]pyrazine) (**3.2**) by chemical oxidative polymerization. This polymer had a bandgap of 0.95 eV, which was one of the lowest bandgaps reported at the time.[16,17]

In 1992, reports started emerging about bithiophene-based copolymers that contained fused-ring units such as isothianaphthene (ITN) and TP.[1,18] These copolymers were often synthesized through oxidative polymerization of the corresponding terthienyls. One such example is poly(naphtho[2,3-*c*]thiophene-*alt*-bithiophene) (**3.3**), which was reported in 1993 and exhibited an optical bandgap of 0.65 eV.[19] Another report in 1995 by Karikomi et al. discussed a benzobisthiadiazole-bithiophene alternating copolymer (**3.4**) with an optical bandgap less than 0.5 eV.[20,21] However, accurate measurement of the bandgap was not possible due to overlap with the absorption of the indium tin oxide (ITO) electrode.

In 1995, Tanaka and Yamashita reported [1,2,5]thiadiazolo[3,4-*b*]thieno[3,4-*e*]pyrazine-based polymer **3.5**, which they made by electropolymerization of thiophene-flanked [1,2,5]thiadiazolo[3,4-*b*]thieno[3,4-*e*]pyrazine.[22] Due to the lack of solubilizing side chains this

polymer was insoluble. However, they were above to determine that the polymer exhibited an electrochemical bandgap of 0.3 eV, which agreed well with optical data that showed that the dedoped polymer film exhibited an absorption onset below 0.5 eV, but accurate measurement of the optical bandgap was not possible due to overlap with the absorption of the indium tin oxide (ITO) electrode. Later in 1997, Tanaka and Yamashita reported the pyrrole analog of polymer **3.5** (polymer **3.6**) again by electropolymerization of the corresponding terthienyl.[23] The polymer's cyclic voltammogram suggested that the polymer had an electrochemical bandgap of ~0 eV. However, cyclic voltammetry is not an ideal method to determine the bandgap of a very low bandgap polymer. The bandgap should have been determined by an additional method to confirm their findings. Nevertheless, as is the case with all the polymers discussed thus far (with the exception of **3.2**) they do not have solubilizing side chains and thus are impractical for use in devices.

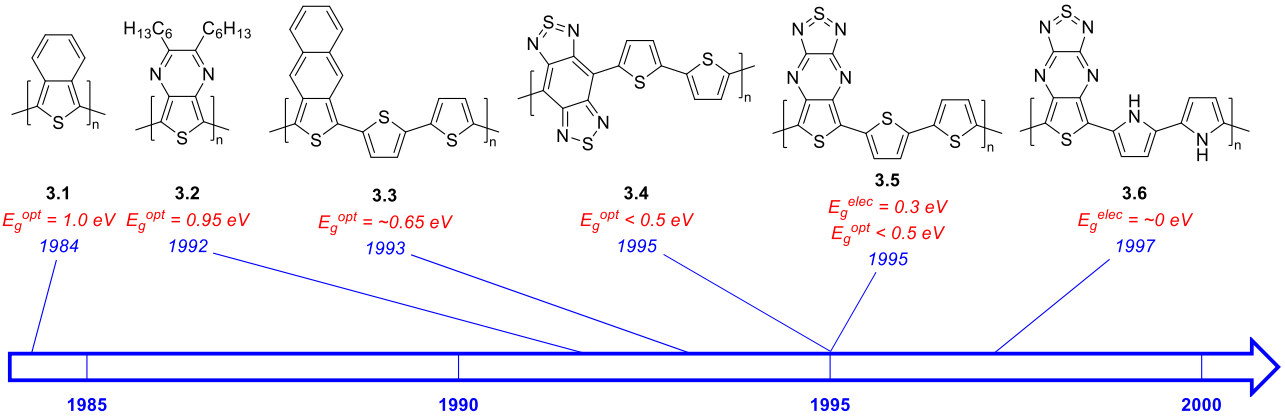

Figure 3.1. Record low bandgap polymers reported before the year 2000.

3.1.2. Record Low Bandgap Processable Conjugated Polymers

Low bandgap polymers have gained interest in applications such as OFETs and NIR photodetectors, where the polymer active layer needs to be processed from solution. Thus, low

bandgap polymers that exhibit good solubility in common organic solvents are desirable. Generally, at least 10 mg of the polymer should be soluble in 1.0 mL of solvent to be useful.[24]

In 2009, Steckler et al. prepared the low bandgap solution-processable polymer, poly(4,8-dithien-2-yl-2$\lambda^4\delta^2$-benzo[1,2-*c*;4,5*c'*]bis[1,2,5]thiadiazole-*alt*-*N*-(3,4,5-tris(dodecyloxy)phenyl)-dithieno[3,2-*b*:2',3'-*d*]pyrrole) (**3.7a**).[25] Polymer **3.7a** had a bandgap of 0.54 eV, which at the time was the lowest bandgap reported for a solution-processable conjugated polymer. The polymer was made up of the strong acceptor unit, benzo[1,2-*c*;4,5-*c'*]bis[1,2,5]thiadiazole and a strong donor unit dithieno[3,2-*b*:2′,3′-*d*]pyrrole (DTP), which was functionalized with a trialkoxyphenyl group. The alkoxy substituents were used to give the polymer good solubility, and to enhance the electron-rich nature of the DTP unit. They found that the polymer exhibited electrochromism, with four different colored states that could be accessed by changing the potential. They also made OFETs from the polymer and found that it exhibited ambipolar character with a hole and electron mobility of 1.2 x 10^{-3} and 5.8 x 10^{-4} cm^2 V^{-1} s^{-1}, respectively.

In 2016, Hasegawa et al. made two low bandgap polymers based on the thiophene-based analogue of isoindigo (TII).[26] Polymer **3.8a** was functionalized with 2-butyloctyl side chains while polymer **3.8b** was functionalized with siloxane-terminated undecyl groups. The TII has been used to make low bandgap polymers due to its quinoid nature. Additionally, the authors suggest that the TII homopolymer should have some D–A character due to the electron-rich nature of thiophene and the electron-poor nature of the carbonyl group. Polymers **3.8a** and **3.8b** exhibited a solid-state λ_{max} of 1369 and 1302 nm, respectively, and an optical bandgap of 0.59 and 0.57 eV, respectively. One possible reason why **3.8b** exhibits a lower bandgap is because the branching point of the side chain is further away from the polymer backbone, resulting in better

π-stacking. They also made OFETs from the polymers, which exhibited hole mobilities of 10^{-3} to 10^{-2} cm^2 V^{-1} s^{-1}.

In 2018, Wudl and coworkers synthesized and analyzed polymer **3.7b**, a hexyl-functionalized analog of polymer **3.7a**.[27] Polymer **3.7b** exhibited an optical bandgap of 0.50 eV, which is one of the lowest bandgaps for a solution-processable polymer. They used this material in NIR photodetectors, pairing it with tri-$PC_{61}BM$ as the acceptor material. The resulting devices had a wide spectral response region from 350 to 2500 nm, which is one of the widest for a polymer-based NIR photodetector.[4] They also determined specific detectivity values at 800 and 1500 nm, which were 1.4 x 10^{11} and 2.2 x 10^{11} Jones, respectively. However, it is important to note that these detectivity values were determined using only the dark current, which does not account for thermal noise and can overestimate detectivity.[28–31]

In 2019, Hasegawa et al. synthesized and characterized a low bandgap polymer that was made up of the thiadiazoloquinoxalinimide (TzQI) and thiophene-flanked diketopyrrolopyrrole (TDPP) units (**3.9**).[32] The electron-poor character of TzQI and DPP led polymer **3.9** to exhibit a low-lying LUMO energy level of –4.17 eV. In addition, polymer **3.9** had an optical bandgap of 0.60 eV. They also made OFETs from **3.9** and found that the resulting devices exhibited ambipolar character with a maximum hole and electron mobility while under vacuum of 2.5 x 10^{-2} and 8.7 x 10^{-2} cm^2 V^{-1} s^{-1}, respectively. Moreover, the devices exhibited good stability in air with a hole and electron mobility of 9.8 x 10^{-3} and 5.8 x 10^{-3} cm^2 V^{-1} s^{-1}, respectively, after the device was stored under air for 30 days. The authors suggest that the good ambient stability of these devices is due to the low-lying LUMO of **3.9**.

In 2020, Tam et al. synthesized a polymer composed of the units benzo[1,2-*c*;4,5-*c′*]bisthiadiazole and thiophene-flanked thieno[3,2-*b*]thiophene (**3.10**).[33] They found that

polymer **3.10** exhibited an optical bandgap of 0.52 eV. They also investigated whether polymer **3.10** could be used in thermoelectrics and found that it was one of the highest performing solution-phase doped conjugated polymers for this purpose.

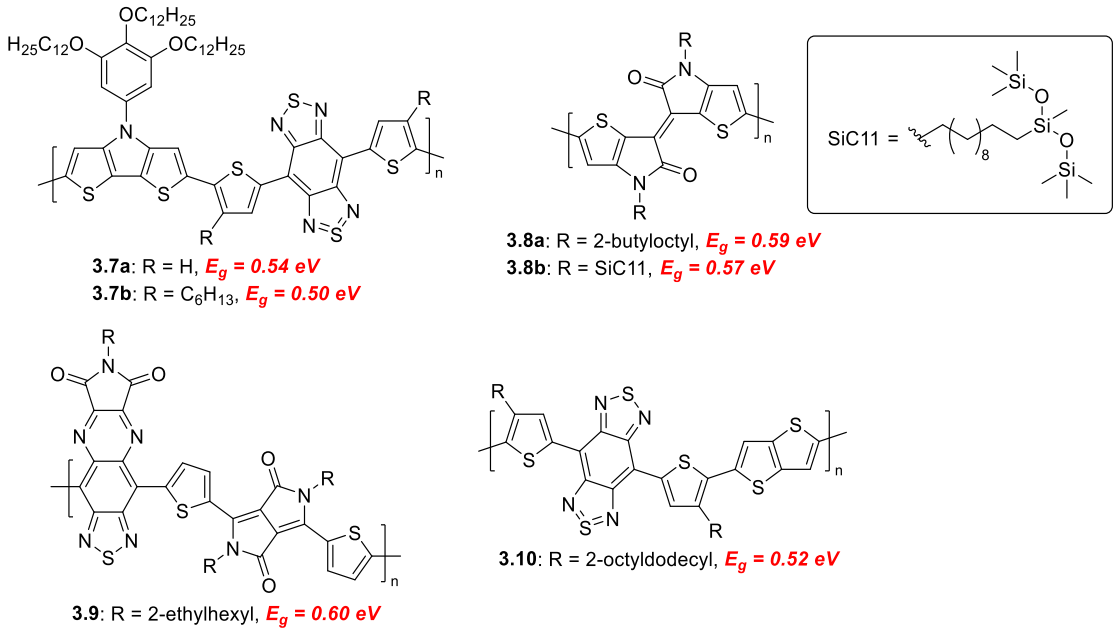

Figure 3.2. Record low bandgap solution-processable conjugated polymers.

3.1.3. Extended Thieno[3,4-b]pyrazines

As mentioned in chapter 1 and 2, TP has been successful in producing low bandgap materials. Researchers have explored extending the conjugation of TP in an attempt to produce useful materials for various applications.[22,23,34–62] Examples of extended TP-based conjugated compounds are displayed in Figure 3.3. Additionally, the majority of extended TPs are synthesized from a 3,4-diaminothiophene analog and a cyclic α-dione through a double condensation reaction (Figure 3.4).

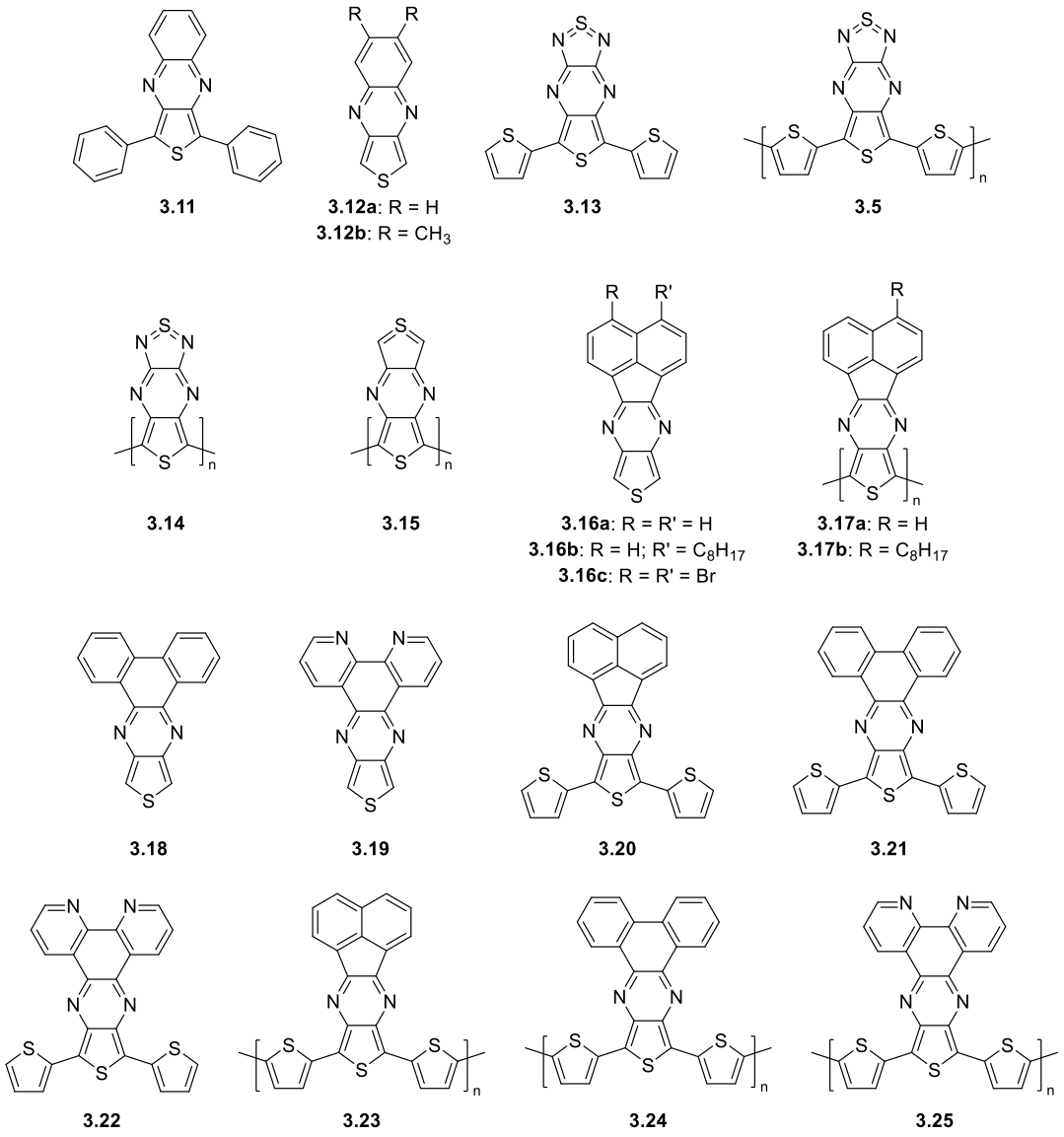

Figure 3.3. Examples of extended thieno[3,4-*b*]pyrazine-based compounds.

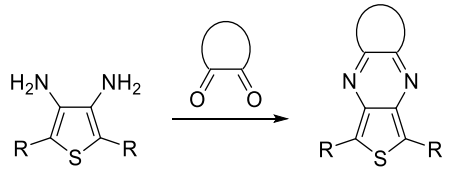

Figure 3.4. Double condensation reaction commonly used to synthesize extended thieno[3,4-*b*]pyrazines.

In 1974, Haddadin et al. prepared and isolated one of the first extended TPs, namely 1,3-diphenylthieno[3,4-*b*]quinozaline (**3.11**). Extended TP **3.11** was prepared by reacting 2,3-dibenzoylquinoxaline with phosphorus pentasulfide in pyridine.[34] They provided data on the melting point, IR spectrum, and elemental analysis for TP **3.11**.

In 1977, Roland and Anderson attempted to synthesize and purify thieno[3,4-*b*]quinoxaline (**3.12a**). However, they were unsuccessful due to its poor stability.[35] Despite that, they were able to show the existence of **3.12a** through trapping experiments. To achieve this, they heated 1,3-dihydrothieno[3,4-*b*]quinoxaline 2-oxide in acetic anhydride and trapped it with *N*-phenylmaleimide or dimethyl acetylenedicarboxylate.

In 1995, Pohmer et al. became the first to successfully synthesize and isolate an extended TP monomer.[36] They made thieno[3,4-*b*]quinoxalines **3.12a** and **3.12b** through base-catalyzed Pummerer dehydration, which involved treating the corresponding 1,3-dihydrothieno[3,4-*b*]quinoxaline 2-oxide with KOH in benzene. The resulting products were collected as an orange crystalline material, which were stable for at least several days when protected from light and oxygen.

As mentioned in section 3.1.1, Tanaka and Yamashita reported polymer **3.5** in 1995, which was one of the first extended TP-based polymers.[22] Additionally, in their report, they compared the extended TP trimer **3.13** with the non-extended TP trimer **3.27**, which they synthesized from diamine **3.26** (Figure **3.5**). They found that the extended TP exhibited a significant redshift in absorption (990 vs 529 nm). Moreover, electrochemical results showed that the extended TP a small decrease in the oxidation potential, but there was a significant increase in the reduction potential, possibly due to the electron poor character of the thiadiazole ring.

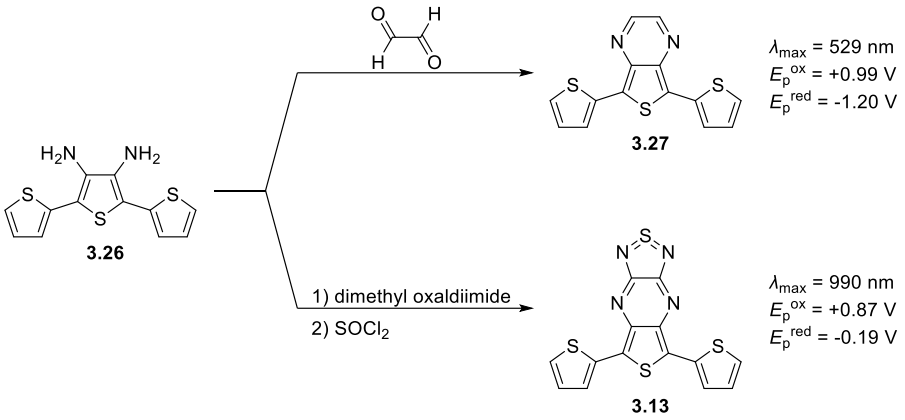

Figure 3.5. Preparation of TP trimers **3.27** and **3.13** by Tanaka and Yamashita.

Following these initial reports, more extended TP-based polymers were reported.[37,38] However, these polymers were copolymers that contained thiophene units between the extended TP units. This limited the extent to which the bandgap could be lowered. Ideally, an extended TP homopolymer would exhibit a very low bandgap. In 2002, a computational study determined the calculated bandgaps for poly([1,2,5]thiadiazolo[3,4-*b*]thieno[3,4-*e*]pyrazine) (**3.14**) and poly(dithieno[3,4-*b*:3′,4′-*e*]pyrazine) (**3.15**) to be 0.10 and 0.14 eV, respectively.[39] However, these homopolymers are not practical as they lack solubilizing side chains. Moreover, most of the extended TPs that have been reported are relatively large, and only a few are small enough to allow for homopolymerization.

In 2008, Rasmussen and coworkers made poly(acenaphtho[1,2-*b*]thieno[3,4-*e*]pyrazine) (**3.17a**), the first reported extended TP homopolymer.[40] They achieved this through the electropolymerization of acenaphto[1,2-*b*]thieno[3,4-*e*]pyrazine (**3.16a**), with this also the first report of monomer **3.16a**. They found that compared to other poly(thieno[3,4-*b*]pyrazine)s (PTPs), conjugation extension with the acenaphtho functionality resulted in LUMO stabilization with limited impact on the HOMO. This resulted in a low bandgap polymer that exhibited good

stability. They determined the bandgap to be ~0.50 eV. Additionally, **3.17a** exhibited a solid-state λ_{max} at ~910 nm with the film absorbing out past 2700 nm. However, **3.17a** was insoluble in common organic solvents, which limits its application to devices.

In 2009, Rasmussen and coworkers attempted to enhance to solubility of polymer **3.17a** by functionalizing it with an alkyl side chain.[41] They synthesized poly(3-octylacenaphtho[1,2-*b*]thieno[3,4-*e*]pyrazine) (**3.17b**) by electropolymerization of **3.16b**. However, polymer **3.17b** displayed almost no solubility in common organic solvents.[42] Moreover, **3.17b** exhibited an increased electrochemical bandgap (0.65 eV) compared to **3.17a**. They attributed the large increase in bandgap to the regiorandom nature of the polymer, which led to disorder in the polymer film.

In 2011, Rasmussen and coworkers synthesized and characterized several extended TP monomers.[43] The compounds synthesized included acenaphtho[1,2-*b*]thieno[3,4-*e*]pyrazine (**3.16a**), 3,4-dibromoacenaphtho[1,2-*b*]thieno[3,4-*e*]pyrazine (**3.16c**), 3-octylacenaphtho[1,2-*b*]thieno[3,4-*e*]pyrazine (**3.16b**), dibenzo[*f, h*]thieno[3,4-*b*]quinoxaline (**3.18**), and thieno[3',4':5,6]pyrazino[2,3-*f*][1,10]phenanthroline (**3.19**). All the extended TPs were prepared by double condensation reaction between 3,4-diaminothiophene and the corresponding cyclic α-dione (Figure 3.4). However, **3.16c** was of very low solubility, limiting its applications. **3.16b** was slightly more soluble than **3.16a**, but they mentioned that more soluble analogs of **3.16a** are still needed. They found that all the extended TPs, except **3.16c** and **3.19**, exhibited a higher HOMO than 2,3-dimethylthieno[3,4-*b*]pyrazine due to the increased π-electron delocalization. Extended TP **3.16c** exhibits a stabilized HOMO due to the electron-withdrawing character of the bromo functionalities, while extended TP **3.19** exhibits a stabilized HOMO due to the electron-withdrawing character of the sp^2 N atoms. In addition, extended TPs **3.16c** and **3.19** exhibit the

lowest LUMO levels due to the electron-withdrawing nature of the bromine functionalities and sp^2 N atoms. Moreover, they analyzed extended TPs **3.16a**, **3.18**, and **3.19** by absorption spectroscopy. They found that extended TP **3.18** exhibited the most redshifted low energy solution-state λ_{max} value (426 nm). In addition, extended TPs **3.16a**, **3.18**, and **3.19** exhibit a redshifted absorption onset compared to 2,3-diphenylthieno[3,4-*b*]pyrazine.

In 2016, Rasmussen and coworkers synthesized terthienyls **3.20**, **3.21**, and **3.22**, and their corresponding polymers (**3.23**, **3.24**, and **3.25**).[44] The terthienyls were made using a double condensation reaction between 3',4'-diamino-2,2':5',2"-terthiophene and the corresponding cyclic α-dione. Polymers **3.23**, **3.24**, and **3.25** were produced through electropolymerization of **3.20**, **3.21**, and **3.22**, respectively. The resulting materials displayed low optical bandgaps ranging from 0.82 to 0.99 eV, with the lowest bandgap observed for polymer **3.25**.

3.1.4. Motivation for This Work

Extended TPs have been used to create a variety of low bandgap materials. However, two issues arise when using extended TPs. The first is the low solubility of the extended TP monomers and polymers, which limits their practical use. The second issue is the large size of the monomeric units limit the number of polymers that can be produced. For example, the large size of extended TPs **3.18** and **3.19** makes homopolymerization difficult due to steric issues. Thus, TPs **3.18** and **3.19** needs to be copolymerized with a "spacer" unit like thiophene (which increases bandgap).

Considering the shortcomings of extended TPs a copolymer made up of the extended TP **3.16a** and a very soluble TP analog, 2,3-bis(2-octyldodecyl)thieno[3,4-*b*]pyrazine (**3.28**) was targeted. The long and branched side chains of **3.28** result in enhanced solubility, making it a suitable pair for the very insoluble **3.16a** unit. A random and alternating copolymer using TPs

3.16a and **3.28** was targeted. A random copolymer is a copolymer where the monomeric units are distributed randomly along the polymer backbone (Figure 3.6). Random copolymers offer a straightforward way to adjust polymer properties by changing the ratio of the comonomers.[63–65] An alternating copolymer is a copolymer where the monomeric units alternate along the polymer backbone (Figure 3.6).

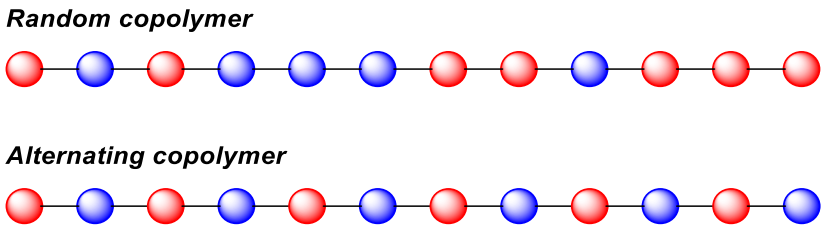

Figure 3.6. Random and alternating copolymer of two components.

Conjugated random copolymers are often made by cross-coupling polymerizations (Stille, Suzuki, Kumada, etc.).[63–66] Through this route, random copolymers are made by functionalizing each monomeric unit with a halide function and an organometallic function, combining them in one pot, and adding a metal precatalyst (Figure 3.7).[67,68] GRIM polymerization is an especially straightforward way to make random copolymers as the halogenated monomers can be activated in the same reaction pot.[69,70]

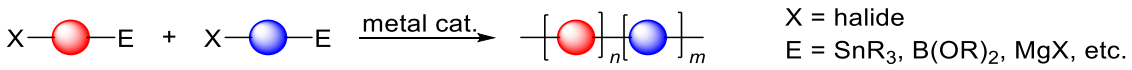

Figure 3.7. Common one-pot synthesis of conjugated random copolymers by cross coupling.

Conjugated alternating copolymers are often made by cross-coupling polymerizations (Stille, Suzki, Kumada, etc.).[71–73] Through this route, one monomeric unit is difunctionalized with halide functions and the other monomeric unit is difunctionalized with organometallic functions. The functionalized monomers are then combined in one pot, and a metal precatalyst is

added resulting in polymerization (Figure 3.8). However, the traditional cross-coupling polymerizations listed above have several drawbacks including the need for the organometallic functions and in the case of Stille coupling the formation of toxic byproducts.[71] An alternative polymerization method has been developed in recent years, namely direct arylation polymerization (DArP), in which coupling occurs between a monomeric unit difunctionalized with halide functions and an unfunctionalized arene (Figure 3.8).[74,75] This avoids preparation of the organometallic functionalized monomer, reducing the number of synthetic steps and increasing atom economy. The Rasmussen group has previously made several TP-based alternating copolymers using DArP[76,77] allowing their conditions to be applied to produce an alternating copolymer of TPs **3.16a** and **3.28**.

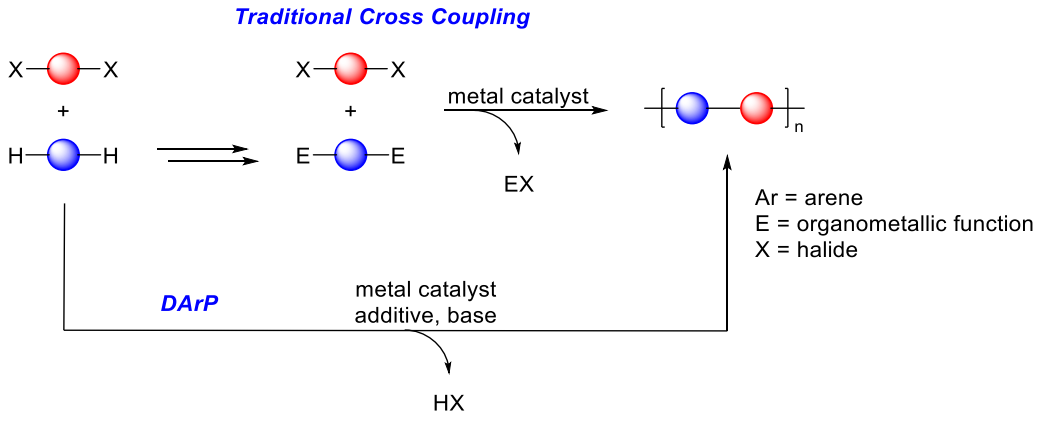

Figure 3.8. Comparison of traditional cross-coupling polymerizations and DArP.

3.2. Results and Discussion

3.2.1. Design and Synthesis

First, the random copolymer composed of TPs **3.16a** and **3.28** was produced using GRIM polymerization. The work reported in chapter 2 demonstrats the effectiveness of GRIM polymerization for producing TP random copolymers. The synthesis of polymer **3.22** began by

making monomeric units **3.16a** and **3.28**. Monomer **3.16a** was prepared by previous methods reported by Rasmussen and coworkers.[40] The preparation of monomer **3.28** was discussed in chapter 2.

Bromination of **3.16a** had previously been reported by Bao and coworkers.[45] However, their procedure required a 2-day reaction time to yield 8,10-dibromoacenaphtho[1,2-*b*]thieno[3,4-*e*]pyrazine (**3.29**) in a 69.3% yield. Based on previous work done by Rasmussen and coworkers,[78,79] the reaction time was reduced to 3.5 hours to yield **3.29** in 84% (Figure 3.9).

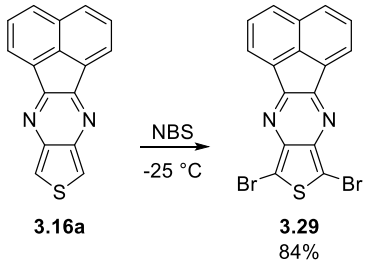

Figure 3.9. Bromination of acenaphtho[1,2-*b*]thieno[3,4-*e*]pyrazine.

A similar procedure was used to brominate **3.28**. Due to the low solubility of TP **3.29** the reaction was worked up by pouring over ice and filtering. However, pouring the reaction of 5,7-dibromo-2,3-bis(2-octyldodecyl)thieno[3,4-*b*]pyrazine (**3.30**) over ice did not result in product precipitation, likely due to the branched side chains on **3.30**. As a result, the reaction was worked up by extraction with ethyl acetate followed by purification with a short silica plug to give **3.30** in 82% yield (Figure 3.10).

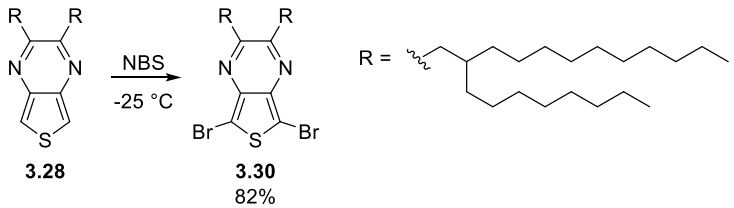

Figure 3.10. Bromination of 2,3-bis(2-octyldodecyl)thieno[3,4-*b*]pyrazine.

GRIM polymerization was used to copolymerize **3.29** and **3.30**. First, 0.5 equivalents of both brominated monomers were added to the reaction pot and dissolved in THF. Then, 1.05 equivalents of MeMgBr was added, and the reaction was heated at reflux for 1 h, resulting in Grignard metathesis. Next, the precatalyst, [1,3-bis(diphenylphosphino)propane]dichloronickel(II) was added, followed by reflux for another 1 h, causing polymerization by Kumada coupling. The reaction was heated at reflux because previous work has found that this gives a higher soluble-fraction yield for polymer **3.2**.[78] Finally, the polymer was precipitated in methanol, purified using a Soxhlet apparatus, extracted in chloroform, and concentrated to give the black solid polymer, poly(acenaphtho[1,2-*b*]thieno[3,4-*e*]pyrazine-*ran*-2,3-bis(2-octyldodecyl)thieno[3,4-*b*]pyrazine) (**3.31**) in 52% yield (Figure 3.11). This polymerization was found to be repeatable.

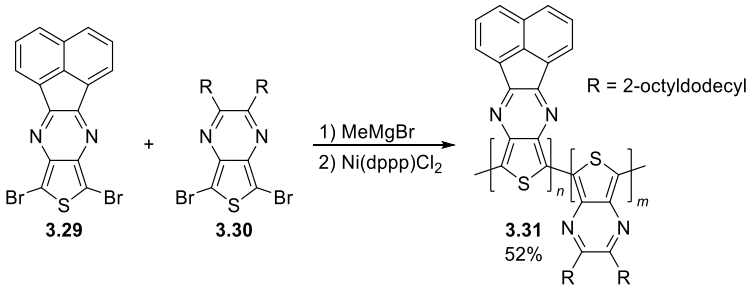

Figure 3.11. GRIM polymerization of poly(acenaphtho[1,2-*b*]thieno[3,4-*e*]pyrazine-*ran*-2,3-bis(2-octyldodecyl)thieno[3,4-*b*]pyrazine).

Using gel permeation chromatography with 1,2,4-trichlorobenzene at 100 °C and comparing to polystyrene standards, number and weight average molecular weights (M_n and M_w) of 5700, and 7000 were determined, respectively. This gave a low polydispersity index (PDI) of 1.23. If it is assumed that polymer **3.31** is composed of a completely 1-to-1 ratio of monomers **3.16a** and **3.28**, the polymer chains would consist of about 12 repeat units, which is well below the effective conjugation length of polythiophene.[80,81] Initially it was thought that the low

molecular weight of this polymer was due to its low solubility. However, further experiments determined that the polymer exhibited good solubility in chloroform (32.5 ± 2.5 mg/mL). A possible explanation for the low molecular weight is the poor compatibility of brominated monomers **3.29** and **3.30** with the GRIM mechanism leading to termination processes.[82–84]

The alternating copolymer, poly(acenaphtho[1,2-*b*]thieno[3,4-*e*]pyrazine-*alt*-2,3-bis(2-octyldodecyl)thieno[3,4-*b*]pyrazine) (**3.32**), was prepared using direct arylation polymerization (DArP) (Figure 3.12). The Rasmussen group has developed a procedure for the production of alternating copolymers using the TP unit.[76,77] Dibromide **3.29** and TP **3.28** were chosen as the starting materials for this polymerization. TP **3.28** was used as the unfunctionalized aromatic unit as previous work by the Rasmussen group shows that the C-H of the TP unit is viable for DArP. However, they have not attempted DArP with the extended TP, **3.16a**. The polymerization was carried out by adding the monomers, $Pd(OAc)_2$, tris(2-methoxyphenyl)phosphine (TOMPP), K_2CO_3, pivalic acid, and THF to a microwave vial, sealing the vial under N_2 atmosphere, and heating the reaction to 120 °C for 24 h. Finally, the polymer was precipitated in methanol, purified using a Soxhlet apparatus, extracted in chloroform, and concentrated to give polymer **3.32** as a black solid in 60% yield. Polymer **3.32** exhibited good solubility in chloroform (22.5 ± 2.5 mg/mL).

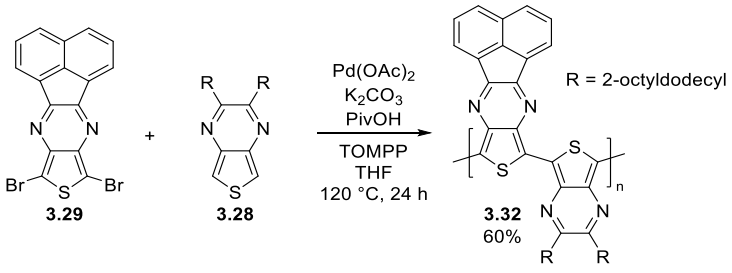

Figure 3.12. DArP polymerization of poly(acenaphtho[1,2-*b*]thieno[3,4-*e*]pyrazine-*alt*-2,3-bis(2-octyldodecyl)thieno[3,4-*b*]pyrazine).

Using gel permeation chromatography with the same methods discussed above the M_n, M_w, and PDI for polymer **3.32** were determined to be 3400, 4900, and 1.43, respectively. A M_n of 3400 corresponds to about seven repeat units, which is relatively low. The low molecular weight of this polymer could be due to the polymer's incompatibility with the DArP conditions used.

3.2.2. UV-vis-NIR Absorption Spectroscopy

Shown in Table 3.1 are the solution and solid-state UV-vis-NIR absorption data for polymers **3.31** and **3.32** along with polymer **3.2** made by GRIM polymerization and **3.17a** made by electropolymerization for comparison. Shown in Figure 3.13 are the solution and solid-state UV-vis-NIR absorption spectra of polymers **3.31** and **3.32**. The absorption spectra of polymers **3.31** and **3.32** exhibit the characteristic two band structure, which is commonly observed in donor-acceptor systems.[85] The low energy band stems from intramolecular charge transfer and the high energy band stems from the π-π* transition.[85] The solid-state spectra for both polymers redshifted and broader than the corresponding solution-state spectrum, which is due to intermolecular interactions in the solid state.[2,24]

Table 3.1 Visible-NIR absorbance data for PTPs.

Material	λ_{max} (nm, $CHCl_3$)[a]	λ_{max} (nm, film)[a,b]	E_g (eV)
3.2	862, (940)	886, (990)	1.07
3.31	1184	1250	0.64
3.32	1190	1259	0.67
3.17a[c]	-	~910	~0.55

[a] Values in parentheses denote prominent shoulders. [b] Unannealed films. [c] Ref. 40.

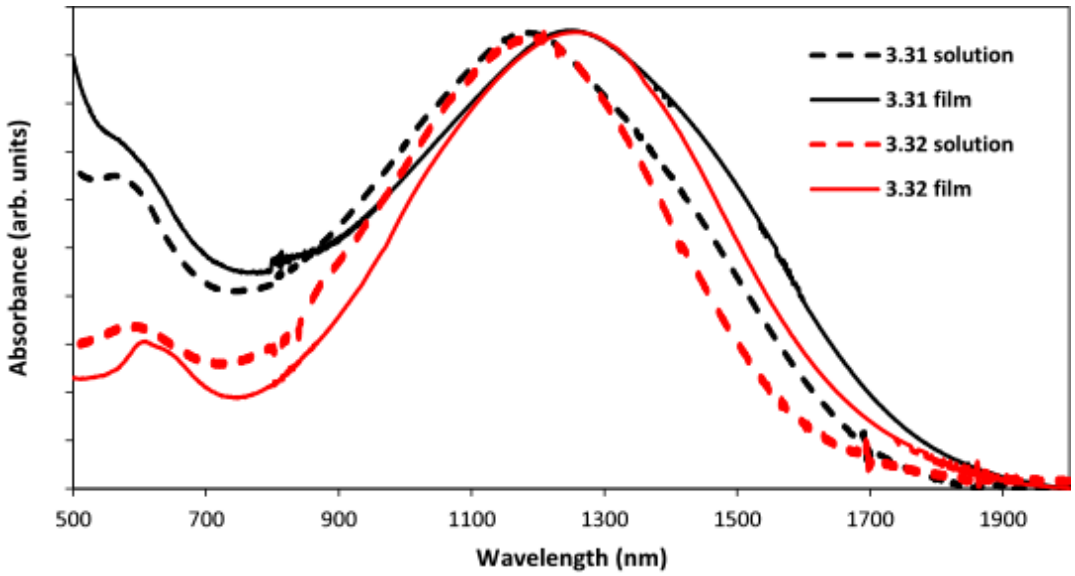

Figure 3.13. Solution- and solid-state UV-vis-NIR spectra of poly(acenaphtho[1,2-*b*]thieno[3,4-*e*]pyrazine-*ran*-2,3-bis(2-octyldodecyl)thieno[3,4-*b*]pyrazine) and poly(acenaphtho[1,2-*b*]thieno[3,4-*e*]pyrazine-*alt*-2,3-bis(2-octyldodecyl)thieno[3,4-*b*]pyrazine).

Polymers **3.31** and **3.32** exhibit a solution-state λ_{max} value of 1184 and 1190 nm, respectively, which are significantly redshifted compared to polymer **3.2** (970 nm). However, comparison to solution data of polymer **3.17a** is not possible due to the insolubility of the polymer. Polymers **3.31** and **3.32** exhibit a solid-state λ_{max} value of 1250 and 1259 nm, respectively, which is significantly redshifted compared to both polymers **3.2** (890 nm) and **3.17a** (~910 nm). Furthermore, polymers **3.31** and **3.32** exhibit an optical bandgap of 0.64 and 0.67 eV, which are some of the lowest bandgaps reported for solution-processable polymers. The larger bandgap of polymer **3.2** is likely due to the smaller size of the conjugated portion of the monomeric unit, 2,3-dihexylthieno[3,4-*b*]pyrazine, which limits electron delocalization. In addition, polymer **3.2** is functionalized with side chains on every monomeric unit, which disrupts π-stacking resulting in an increase in bandgap. The smaller bandgap of **3.17a** is likely a result of the extended conjugation of the monomeric units and the lack of side chains, leading to better π-stacking in the solid state and enhanced electron delocalization. Comparing the solution and

solid-state UV vis spectra of polymer **3.31** and **3.32** the random copolymer exhibits a wider spectral profile with a lower energy onset of absorption giving a slightly lower bandgap, which is potentially due to the higher molecular weight of the random copolymer.

3.2.3. Electrochemistry

Cyclic voltammetry was used to estimate the frontier molecular orbital energy levels of polymers **3.31** and **3.32**. Shown in Table 3.2 is the electrochemical data for polymers **3.31** and **3.32** along with polymer **3.2** made by GRIM polymerization and polymer **3.17a** made by electropolymerization for comparison. The cyclic voltammogram for polymers **3.31** and **3.32** are shown in Figure 3.14. Polymers **3.31** and **3.32** exhibit a HOMO in between that of polymers **3.2** and **3.17a**, which is potentially because the extended TP content of **3.31** and **3.32** is in between that of polymers **3.2** and **3.17a**, and extending the conjugation path generally raises the HOMO.[2,24] The LUMO of polymers **3.31** and **3.32** is higher than polymer **3.17a** and about the same as polymer **3.2**. The HOMO and LUMO level of **3.31** and **3.32** suggest that these polymers could function in a photonic device with common acceptors such as PCBM, Y6, and IT-4F. The electrochemical bandgap of polymers **3.31** and **3.32** was determined to be 0.9 eV. The difference in energy between the electrochemical bandgap and the optical bandgap is due to the exciton binding energy.[86]

Table 3.2. PTP electrochemical data.

Material	E_{HOMO} (eV)[a]	E_{LUMO} (eV)[b]	E_g^{elec} (eV)
3.2	-5.2	-3.6	1.6
3.31	-4.8	-3.9	0.9
3.32	-4.8	-3.9	0.9
3.17a[c]	-4.7	-4.2	0.5

[a] $E_{HOMO} = -(E_{[onset,ox\ vs.\ Fc+/Fc]} + 5.1)(eV)$. [b] $E_{LUMO} = -(E_{[onset,red\ vs.\ Fc+/Fc]} + 5.1)(eV)$. [c] Ref. 40.

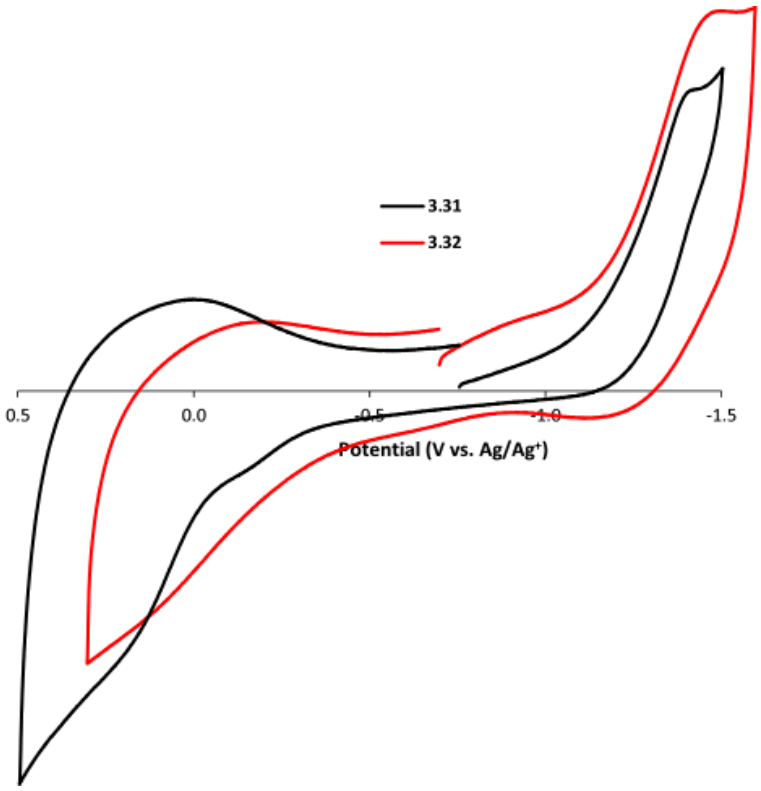

Figure 3.14. Cyclic voltammogram of poly(acenaphtho[1,2-*b*]thieno[3,4-*e*]pyrazine-*ran*-2,3-bis(2-octyldodecyl)thieno[3,4-*b*]pyrazine) and poly(acenaphtho[1,2-*b*]thieno[3,4-*e*]pyrazine-*alt*-2,3-bis(2-octyldodecyl)thieno[3,4-*b*]pyrazine).

3.2.4. Synthetic Complexity

The synthetic complexity of polymer **3.31** was compared with some of the top performing solution processible low bandgap conjugated polymers (Figure 3.15). The values used to calculate synthetic complexity can be found in Table 3.3. An example calculation for polymer **3.31** can be found in Figure 3.16. Of the six polymers shown, polymer **3.31** has a relatively low synthetic complexity with only polymer **3.8a** having a lower value. However, the synthetic complexity of polymer **3.31** could be lowered significantly by improving the yield of the double condensation reaction used to make the 2,3-bis(2-octyldodecyl)thieno[3,4-*b*]pyrazine discussed in chapter 2.

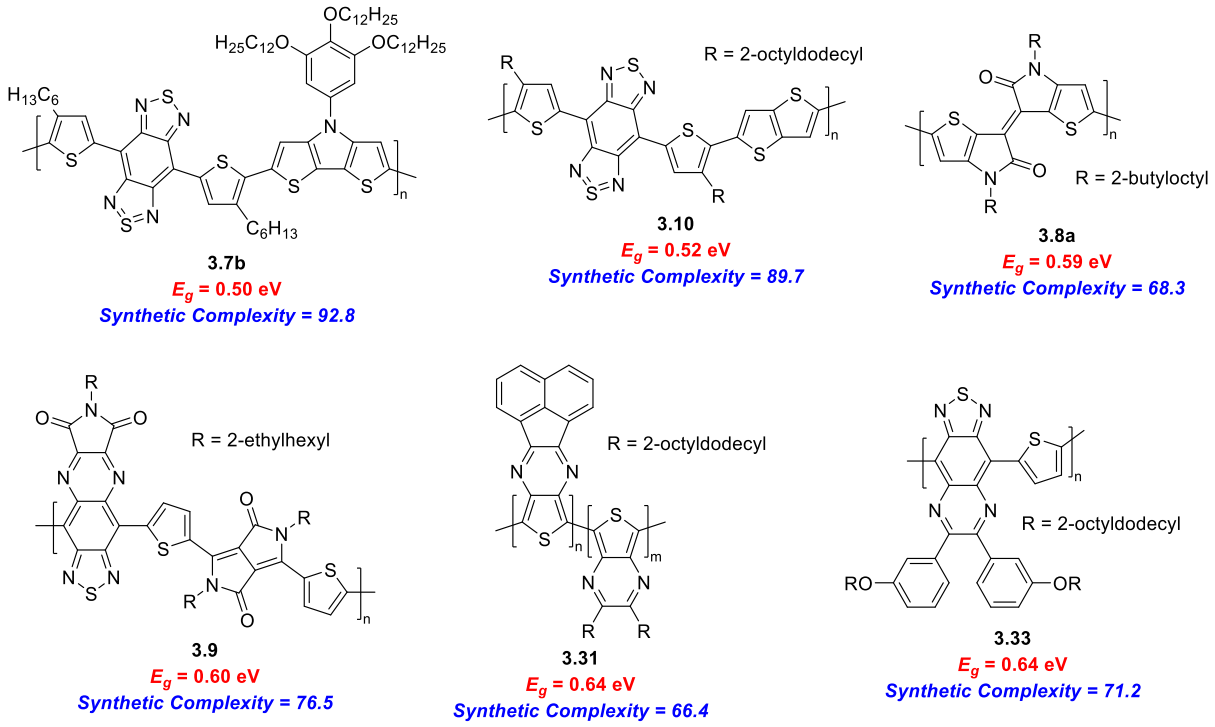

Figure 3.15. Bandgap and relative synthetic complexity of some of the top-performing solution processable low bandgap conjugated polymers.

3.3. Conclusion

TPs **3.16a** and **3.28** were brominated in good yield (80-85%) using NBS at low temperature. A random copolymer (**3.31**) composed of monomeric units **3.16a** and **3.28** was prepared by GRIM polymerization in moderate yield (52%). However, polymer **3.31** was of relatively low molecular weight (M_n = 5700). If the polymer was a true 1:1 copolymer, the number of monomeric units in the polymer would be about 12, which is well below the effective conjugation length of polythiophene.[80,81] Thus, increasing the molecular weight of this polymer should be targeted as it could result in a further decrease in bandgap. A possible explanation for the low molecular weight is the poor compatibility of brominated monomers **3.29** and **3.30** with the GRIM mechanism leading to termination processes.[82–84]

An alternating copolymer (**3.32**) composed of monomeric units **3.16a** and **3.28** was prepared by DArP in moderate yield (60%). However, polymer **3.32** was of relatively low number average molecular weight of 3400, which corresponds to about seven repeat units, which is well below the effective conjugation length of polythiophene.[80,81] The low molecular weight of this polymer could be due to the polymer's incompatibility with the DArP conditions used.

Polymers **3.31** and **3.32** exhibited red-shifted solution and solid state λ_{max} values compared to polymer **3.2** prepared by GRIM polymerization and polymer **3.17a** prepared by electropolymerization. The optical bandgap of polymers **3.31** and **3.32** was determined to be 0.64 and 0.67 eV, which are some of the lowest bandgaps for a solution-processible conjugated polymer. The lower bandgap of polymer **3.31** is potentially due to the higher molecular weight of this polymer. In addition, polymer **3.31** is of low synthetically complexity compared to some of the top-performing solution processable low bandgap polymers. Future work consists of fabricating NIR photodetectors from polymers **3.31** and **3.32**.

3.4. Experimental

3.4.1. General

All materials were reagent grade and used without further purification unless noted. DMF was dried by mixing with $MgSO_4$ and flushing through a silica gel plug. THF was dried by distillation over sodium/benzophenone. All dry solvents were transferred via standard syringe techniques. All reactions were carried out under a dry nitrogen stream. Reaction glassware was oven dried before use. ^1H and ^{13}C NMR were collected using a 400 MHz spectrometer using $CDCl_3$ as the solvent. NMR peak multiplicity is reported as follows: d = doublet and m = multiplet. A digital thermal couple with a 0.1 °C resolution was used to determine melting points. Acenaphtho[1,2-*b*]thieno[3,4-*e*]pyrazine was prepared following a previously reported

procedure.[40] The preparation of 2,3-bis(2-octyldodecyl)thieno[3,4-*b*]pyrazine was discussed in chapter 2.

8,10-Dibromoacenaphtho[1,2-*b*]thieno[3,4-*e*]pyrazine (3.29). Compound **3.29** was prepared by the modification of a previously reported procedure.[78] **3.16a** (0.92 g, 3.53 mmol) was added to a 250 mL three-neck round-bottom flask equipped with an addition funnel. Dry DMF (105 mL) was added and the solution was cooled to -78 °C in an acetone/dry ice bath. In a separate flask, NBS (1.57 g, 8.82 mmol) was dissolved in dry DMF (35 mL) and put under dry N_2. The NBS solution was added dropwise to the **3.16a** solution (ca. 1 h addition). The mixture was then warmed to -20 °C in a brine/dry ice bath and stirred for 3.5 h. The mixture was poured onto ice and stirred until the ice melted. The yellow precipitate was filtered, washed with water, and dried in vacuo (1.24 g, 84%). Mp ~190 °C (dec); ^{1}H NMR ($CDCl_3$, 400 MHz): δ 8.45 (d, *J* = 7.1 Hz, 2H), 8.15 (d, *J* = 8.2 Hz, 2H), 7.86 (dd, *J* = 8.2, 7.1 Hz, 2H). NMR data agree well with previously reported values.[45]

Poly(acenaphtho[1,2-*b*]thieno[3,4-*e*]pyrazine-*ran*-2,3-bis(2-octyldodecyl)thieno[3,4-*b*]pyrazine) (3.32). Polymer **3.32** was prepared by the modification of a previously reported procedure.[78] To a 50 mL three neck round bottom flask equipped with a condenser was added, **3.29** (0.418 g, 1.0 mmol), **3.30** (0.855 g, 1.0 mmol), and dry THF (10 mL). Methylmagnesium bromide (0.7 mL, 3.0 M solution in diethyl ether) was added via syringe dropwise. The reaction was heated at reflux for 1 h. Ni(dppp)Cl_2 (0.0054 g, 0.010 mmol) was added and the reaction was heated at reflux for another 1 h. The reaction was let cool to room temperature and precipitated by adding dropwise via Pasteur pipette to MeOH (~100 mL) at 0 °C. The mixture was stirred at 0 °C for 2 h. The precipitate was loaded onto a glass frit and washed with methanol via Soxhlet apparatus for 48 h. The soluble fraction was extracted with $CHCl_3$ and concentrated

to give a black solid. The solid was pumped for 4 h to yield the desired product (0.50 g, 52%). ^{1}H NMR ($CDCl_3$, 400 MHz): δ 8.44, 8.14, 7.87, 2.84, 2.03, 1.26, 0.89. GPC: Mw = 7000, Mn = 5700, PDI = 1.23.

Poly(acenaphtho[1,2-*b*]thieno[3,4-*e*]pyrazine-*alt*-2,3-bis(2-octyldodecyl)thieno[3,4-*b*]pyrazine) (3.32). Polymer **3.32** was prepared by the modification of a previously reported procedure.[76] To a microwave vial was added, **3.29** (0.153 g, 0.367 mmol), palladium(II) acetate (0.016 g, 0.0717 mmol), potassium carbonate (0.149 g, 1.08 mmol), pivalic acid (0.041 g, 0.397 mmol), and tris(*o*-methoxyphenyl)phosphine (0.025 g, 0.071 mmol). The vial was transferred to a glovebox where **3.28** (0.267 g, 0.383 mmol) and dry THF (7 mL) were added. A cap was crimped on the vial and the vial was removed from the glovebox. The reaction was heated at 120 °C for 24 hours. The reaction was let cool to room temperature and precipitated by adding dropwise via Pasteur pipette to MeOH (~200 mL) at 0 °C. The mixture was stirred at 0 °C for 2 h. The precipitate was loaded onto a glass frit and washed with methanol and acetone via Soxhlet apparatus. The soluble fraction was extracted with $CHCl_3$ and concentrated to give a black solid. The solid was pumped for 4 h to yield the desired product (0.219 g, 60%). ^{1}H NMR ($CDCl_3$, 400 MHz): δ 3.31, 1.28, 1.19, 0.91, 0.78. GPC: Mw = 4900, Mn = 3400, PDI = 1.43.

3.4.2. Electrochemistry

Electrochemical analysis was performed using a three-electrode cell with a platinum disc working electrode and a platinum wire auxiliary electrode. The Ag/Ag^+ reference electrode was prepared with a 0.01 M $AgNO_3$ and 0.1 M tetrabutylammonium hexafluorophosphate ($TBAPF_6$) solution in dry MeCN. MeCN used for electrochemistry was dried by distillation over CaH_2 under dry N_2. Polymer films were prepared by drop casting a polymer solution in $CHCl_3$ onto the working electrode. Electrochemical cells were oven dried. Solutions of 0.10 M $TBAPF_6$ in dry

MeCN were deoxygenated by sparging with argon before each scan and blanked with argon during the scan. Measurements were taken with a sweep rate of 100 mV s^{-1}. E_{HOMO} and E_{LUMO} values were estimated by taking the onsets of first oxidation and reduction and referencing to ferrocene (5.1 V vs. vacuum).[87]

3.4.3. Absorption Spectroscopy

Absorption spectroscopy measurements were collected using a Carry 500 dual-beam UV-vis-NIR spectrophotometer. Solution-state spectra were collected with the analyte dissolved in $CHCl_3$. Spin coated polymer films on glass plates were used for solid-state analysis. Optical bandgaps were determined from the solid-state spectra by extending the steepest part of the low energy absorption onset to the baseline.

3.4.4. Synthetic Complexity

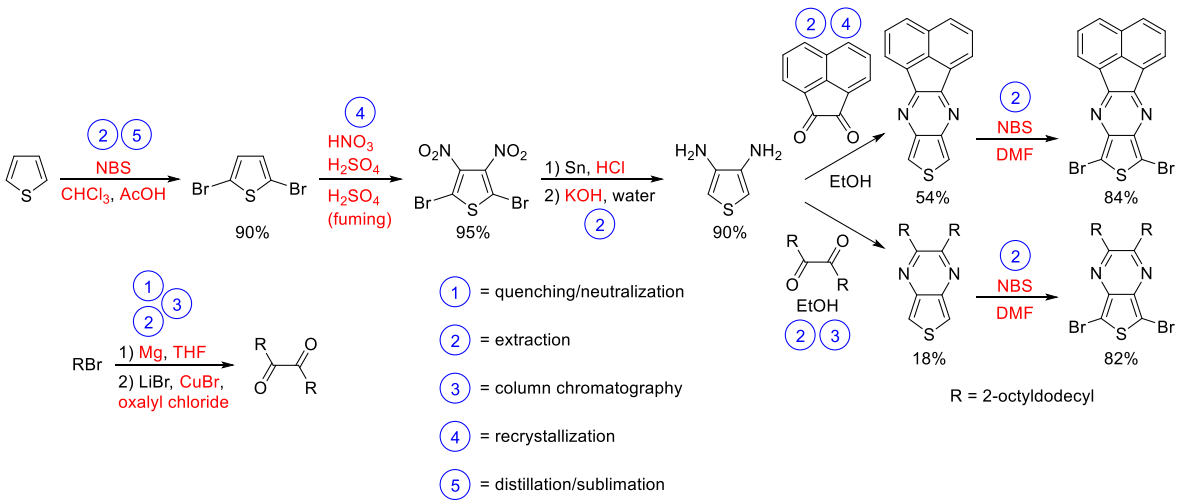

Figure 3.16. Example synthetic complexity calculation for polymer **3.31** with unit operations represented by the blue numbers and hazardous chemicals in red.

Synthetic complexity was calculated following the guidelines discussed in chapter 2. Values used for the calculation are given in Table 3.3 and an example calculation for polymer **3.31** is given in Figure 3.16.

Table 3.3. Values used for synthetic complexity calculations for solution processable low bandgap polymers with the values in red used as the max values.

			Number of Purification Steps							
Polymer	Synthetic Steps	Reciprocal yield (100/yield of the comonomers)	Quenching/neutralization	Extraction	Column Chromatography	Recrystallization	Distillation/sublimaiton	Number of hazardous chemicals	Synthetic Complexity (relative)	References used for calculation
3.31	9	9.64	1	7	2	2	1	32	66.4	88, This Work
3.7b	14	12.99	3	6	3	5	0	60	92.8	5, 21, 27, 89-96
3.10	15	8.676	4	7	3	2	1	50	89.7	33, 90-92, 97-102
3.8a	6	14.65	1	4	4	0	0	38	68.3	26, 103
3.9	13	6.24	1	4	3	2	0	54	76.5	32, 90-92, 104-108
3.33	11	5.96	1	5	3	2	0	48	71.2	90-92, 109-111

3.5. References

(1) Rasmussen, S. C.; Pomerantz, M. In *Handbook of Conducting Polymers: Theory, Synthesis, Properties, and Characterization*, 3rd ed.; Skotheim, T. A.; Reynolds, J. R., Eds.; CRC Press: Boca Raton, FL, 2007, Chapter 12.

(2) Rasmussen, S. C. Low Bandgap Polymers. In *Encyclopedia of Polymeric Nanomaterials*; Mullen, K., Ed.; Springer: Berlin, 2013; pp 1-13.

(3) Roncali, J. *Chem. Rev.* **1997**, *97* (1), 173–206.

(4) Rasmussen, S. C.; Gilman, S. J.; Culver, E. W.; Wilcox, W. D. *Gen Chem* **2021**, *7* (2), 200019.

(5) Kenry; Duan, Y.; Liu, B. *Adv. Mater.* **2018**, *30* (47), 1802394.

(6) Mu, J.; Xiao, M.; Shi, Y.; Geng, X.; Li, H.; Yin, Y.; Chen, X. *Angew. Chem. Int. Ed.* **2022**, *61* (14), e202114722.

(7) Ding, F.; Zhan, Y.; Lu, X.; Sun, Y. *Chem. Sci.* **2018**, *9* (19), 4370–4380.

(8) Dou, L.; Liu, Y.; Hong, Z.; Li, G.; Yang, Y. *Chem. Rev.* **2015**, *115* (23), 12633–12665.

(9) Rasmussen, S. C.; Gilman, S. J.; Wilcox, W. D. *Gen. Chem.* **2023**, *9*, 220010.

(10) Kobayashi, M.; Colaneri, N.; Boysel, M.; Wudl, F.; Heeger, A. J. *J. Chem. Phys.* **1985**, *82* (12), 5717–5723.

(11) Wudl, F.; Kobayashi, M.; Heeger, A. J. *J. Org. Chem.* **1984**, *49* (18), 3382–3384.

(12) Kobayashi, M.; Chen, J.; Chung, T.-C.; Moraes, F.; Heeger, A. J.; Wudl, F. *Synth. Met.* **1984**, *9* (1), 77–86.

(13) Bredas, J. L.; Themans, B.; Andre, J. M.; Heeger, A. J.; Wudl, F. *Synth. Met.* **1985**, *11* (6), 343–352.

(14) Mishra, A.; Ma, C.-Q.; Segura, J. L.; Bauerle, P. In *Handbook of Thiophene-Based Materials: Applications in Organic Electronics and Photonics*; Perepichika, I. F., Perepichka, D. F., Eds.; Wiley: West Sussex, U.K., 2009; Vol 1, pp 1-157.

(15) Nayak, K.; Marynick, D. S. *Macromolecules* **1990**, *23* (8), 2237–2245.

(16) Pomerantz, M.; Chaloner-Gill, B.; Harding, L. O.; Tseng, J. J.; Pomerantz, W. J. *J. Chem. Soc., Chem. Commun.* **1992**, *22*, 1672–1673.

(17) Pomerantz, M.; Chaloner-Gill, B.; Harding, L. O.; Tseng, J. J.; Pomerantz, W. J. *Synth. Met.* **1993**, *55-57*, 960–965.

(18) Lorcy, D.; Cava, M. P. *Adv. Mater.* **1992**, *4* (9), 562–564.

(19) Lakshmikantham, M. V.; Lorcy, D.; Scordilis-Kelley, C.; Wu, X.-L.; Parakka, J. P.; Metzger, R. M.; Cava, M. P. *Adv. Mater.* **1993**, *5* (10), 723–726.

(20) Karikomi, M.; Kitamura, C.; Tanaka, S.; Yamashita, Y. *J. Am. Chem. Soc.* **1995**, *117* (25), 6791–6792.

(21) Kitamura, C.; Tanaka, S.; Yamashita, Y. *Chem. Mater.* **1996**, *8* (2), 570–578.

(22) Tanaka, S.; Yamashita, Y. *Synth. Met.* **1995**, *69*, 599–600.

(23) Tanaka, S.; Yamashita, Y. *Synth. Met.* **1997**, *84* (1–3), 229–230.

(24) Rasmussen, S. C.; Gilman, S. J.; Wilcox, W. D. *Conjugated Polymers – Synthesis and Design*; ACS In Focus, American Chemical Society: Washington, D.C., 2023, *Submitted*.

(25) Steckler, T. T.; Zhang, X.; Hwang, J.; Honeyager, R.; Ohira, S.; Zhang, X.-H.; Grant, A.; Ellinger, S.; Odom, S. A.; Sweat, D.; Tanner, D. B.; Rinzler, A. G.; Barlow, S.; Brédas, J.-L.; Kippelen, B.; Marder, S. R.; Reynolds, J. R. *J. Am. Chem. Soc.* **2009**, *131* (8), 2824–2826.

(26) Hasegawa, T.; Ashizawa, M.; Hiyoshi, J.; Kawauchi, S.; Mei, J.; Bao, Z.; Matsumoto, H. *Polym. Chem.* **2016**, *7* (5), 1181–1190.

(27) Zheng, L.; Zhu, T.; Xu, W.; Liu, L.; Zheng, J.; Gong, X.; Wudl, F. *J. Mater. Chem. C* **2018**, *6* (14), 3634–3641.

(28) Li, Q.; Guo, Y.; Liu, Y. *Chem. Mater.* **2019**, *31* (17), 6359–6379.

(29) Chow, P. C. Y.; Someya, T. *Adv. Mater.* **2020**, *32* (15), 1902045.

(30) Liu, X.; Lin, Y.; Liao, Y.; Wu, J.; Zheng, Y. *J. Mater. Chem. C* **2018**, *6* (14), 3499–3513.

(31) Yang, D.; Ma, D. *Adv. Opt. Mater.* **2019**, *7* (1), 1800522.

(32) Hasegawa, T.; Ashizawa, M.; Hayashi, Y.; Kawauchi, S.; Masunaga, H.; Hikima, T.; Manaka, T.; Matsumoto, H. *ACS Appl. Polym. Mater.* **2019**, *1* (3), 542–551.

(33) Tam, T. L. D.; Wu, G.; Chien, S. W.; Lim, S. F. V.; Yang, S.-W.; Xu, J. *ACS Mater. Lett.* **2020**, *2* (2), 147–152.

(34) Haddadin, M. J.; Chelhot, N. C.; Pieridou, M. *J. Org. Chem.* **1974**, *39* (22), 3278–3281.

(35) Roland, M. M.; Anderson, R. C. *J. Heterocycl. Chem.* **1977**, *14* (4), 541–543.

(36) Pohmer, J.; Lakshmikantham, M. V.; Cava, M. P. *J. Org. Chem.* **1995**, *60* (25), 8283–8288.

(37) Čík, G.; Krajčovič, J.; Veis, P.; Végh, D.; Šeršen, F. *Synth. Met.* **2001**, *118*, 111–119.

(38) Petersen, M.; Hagemann, O.; Nielsen, K.; Jorgensen, M.; Krebs, F. *Sol. Energy Mater. Sol. Cells* **2007**, *91* (11), 996–1009.

(39) Tachibana, M.; Tanaka, S.; Yamashita, Y.; Yoshizawa, K. *J. Phys. Chem. B* **2002**, *106* (14), 3549–3556.

(40) Nietfeld, J. P.; Heth, C. L.; Rasmussen, S. C. *Chem. Commun.* **2008**, 981–983.

(41) Wen, L.; Nietfeld, J. P.; Amb, C. M.; Rasmussen, S. C. *Synth. Met.* **2009**, *159*, 2299–2301.

(42) Rasmussen, S. C.; Schwiderski, R. L.; Mulholland, M. E. *Chem. Commun.* **2011**, *47* (41), 11394–11410.

(43) Nietfeld, J. P.; Schwiderski, R. L.; Gonnella, T. P.; Rasmussen, S. C. *J. Org. Chem.* **2011**, *76* (15), 6383–6388.

(44) Konkol, K. L.; Schwiderski, R. L.; Rasmussen, S. C. S *Materials* **2016**, *9*, 404.

(45) Becerril, H. A.; Miyaki, N.; Tang, M. L.; Mondal, R.; Sun, Y.-S.; Mayer, A. C.; Parmer, J. E.; McGehee, M. D.; Bao, Z. *J Mater Chem* **2009**, *19* (5), 591–593.

(45) Christl, V. M.; Krimm, S.; Kraft, A. *Angew. Chem.* **1990**, *102* (6), 704–706.

(47) Paz, M. A.; Martin, P.; Flückiger, R.; Mah, J.; Gallop, P. M. *Anal. Biochem.* **1996**, *238* (2), 145–149.

(48) Crossley, M. J.; Prashar, J. K. *Tetrahedron Lett.* **1997**, *38* (38), 6751–6754.

(49) Tachibana, M.; Tanaka, S.; Yamashita, Y.; Yoshizawa, K. *J. Phys. Chem. B* **2002**, *106* (14), 3549–3556.

(50) Nishida, J.; Murakami, S.; Tada, H.; Yamashita, Y. *Chem. Lett.* **2006**, *35* (11), 1236–1237.

(51) Peng, B.; Chao, H.; Sun, B.; Li, H.; Gao, F.; Ji, L.-N. *J. Inorg. Biochem.* **2007**, *101* (3), 404–411.

(52) Peng, B.; Chao, H.; Sun, B.; Gao, F.; Ji, L.-N.; Zhang, J. *Transit. Met. Chem.* **2007**, *32* (2), 271–277.

(53) Chen, Z.; Bouffard, J.; Kooi, S. E.; Swager, T. M. *Macromolecules* **2008**, *41* (18), 6672–6676.

(54) Mak, C. S. K.; Leung, Q. Y.; Chan, W. K.; Djurišić, A. B. *Nanotechnology* **2008**, *19* (42), 424008.

(55) Wen, L.; Nietfeld, J. P.; Amb, C. M.; Rasmussen, S. C. *J. Org. Chem.* **2008**, *73* (21), 8529–8536.

(56) Mondal, R.; Miyaki, N.; Becerril, H. A.; Norton, J. E.; Parmer, J.; Mayer, A. C.; Tang, M. L.; Brédas, J.-L.; McGehee, M. D.; Bao, Z. *Chem. Mater.* **2009**, *21* (15), 3618–3628.

(57) Mondal, R.; Ko, S.; Norton, J. E.; Miyaki, N.; Becerril, H. A.; Verploegen, E.; Toney, M. F.; Brédas, J.-L.; McGehee, M. D.; Bao, Z. *J. Mater. Chem.* **2009**, *19* (39), 7195.

(58) Karsten, B. P.; Bijleveld, J. C.; Viani, L.; Cornil, J.; Gierschner, J.; Janssen, R. A. J. *J. Mater. Chem.* **2009**, *19* (30), 5343–5350.

(59) Velusamy, M.; Huang, J.-H.; Hsu, Y.-C.; Chou, H.-H.; Ho, K.-C.; Wu, P.-L.; Chang, W.-H.; Lin, J. T.; Chu, C.-W. *Org. Lett.* **2009**, *11* (21), 4898–4901.

(60) Mondal, R.; Ko, S.; Verploegen, E.; Becerril, H. A.; Toney, M. F.; Bao, Z. *J Mater Chem* **2011**, *21* (5), 1537–1543.

(61) Wang, Z.; Gao, Z.; Feng, Y.; Liu, Y.; Yang, B.; Liu, D.; Lv, Y.; Lu, P.; Ma, Y. *Polymer* **2013**, *54* (22), 6191–6199.

(62) Keshtov, M. L.; Marochkin, D. V.; Kochurov, V. S.; Komarov, P. V.; Parashchuk, D. Yu.; Trukhanov, V. A.; Khokhlov, A. R. *Polym. Sci. Ser. B* **2014**, *56* (1), 89–108.

(63) Cheng, S.; Zhao, R.; Seferos, D. S. P*Acc. Chem. Res.* **2021**, *54* (22), 4203–4214.

(64) Lutz, J. P.; Hannigan, M. D.; McNeil, A. J. *Coord. Chem. Rev.* **2018**, *376*, 225–247.

(65) Yokozawa, T.; Ohta, Y. *Chem. Rev.* **2016**, *116* (4), 1950–1968.

(66) Verheyen, L.; Leysen, P.; Van Den Eede, M.-P.; Ceunen, W.; Hardeman, T.; Koeckelberghs, G. *Polymer* **2017**, *108*, 521–546.

(67) Lee, J.; Kim, H.; Park, H.; Kim, T.; Hwang, S.-H.; Seo, D.; Chung, T. D.; Choi, T.-L. *J. Am. Chem. Soc.* **2021**, *143* (29), 11180–11190.

(68) Burkhart, B.; Khlyabich, P. P.; Thompson, B. C. *Macromolecules* **2012**, *45* (9), 3740–3748.

(69) Hollinger, J.; Sun, J.; Gao, D.; Karl, D.; Seferos, D. S. *Macromol. Rapid Commun.* **2013**, *34* (5), 437–441.

(70) Kozycz, L. M.; Gao, D.; Seferos, D. S. *Macromolecules* **2013**, *46* (3), 613–621.

(71) Carsten, B.; He, F.; Son, H. J.; Xu, T.; Yu, L. *Chem. Rev.* **2011**, *111* (3), 1493–1528.

(72) Babudri, F.; Farinola, G. M.; Naso, F. *J. Mater. Chem.* **2004**, *14* (1), 11–34.

(73) Cheng, Y.-J.; Luh, T.-Y. *J. Organomet. Chem.* **2004**, *689* (24), 4137–4148.

(74) Pouliot, J.-R.; Grenier, F.; Blaskovits, J. T.; Beaupré, S.; Leclerc, M. *Chem. Rev.* **2016**, *116* (22), 14225–14274.

(75) Gobalasingham, N. S.; Thompson, B. C. *Prog. Polym. Sci.* **2018**, *83*, 135–201.

(76) Culver, E. W.; Anderson, T. E.; López Navarrete, J. T.; Ruiz Delgado, M. C.; Rasmussen, S. C. *ACS Macro Lett.* **2018**, *7* (10), 1215–1219.

(77) Anderson, T. E.; Culver, E. W.; Almyahi, F.; Dastoor, P. C.; Rasmussen, S. C. *Synlett* **2018**, *29* (19), 2542–2546.

(78) Wen, L.; Duck, B. C.; Dastoor, P. C.; Rasmussen, S. C. *Macromolecules* **2008**, *41* (13), 4576–4578.

(79) Mulholland, M. E.; Wen, L.; Rasmussen, S. C. *Topol. Supramol. Polym. Sci.* **2015**, *2* (1) 18–29.

(80) Ma, J.; Li, S.; Jiang, Y. *Macromolecules* **2002**, *35* (3), 1109–1115.

(81) Izumi, T.; Kobashi, S.; Takimiya, K.; Aso, Y.; Otsubo, T. *J. Am. Chem. Soc.* **2003**, *125* (18), 5286–5287.

(82) Leone, A. K.; McNeil, A. J. *Acc. Chem. Res.* **2016**, *49* (12), 2822–2831.

(83) Geng, Y.; Huang, L.; Wu, S.; Wang, F. *Sci. China Chem.* **2010**, *53* (8), 1620–1633.

(84) Baker, M. A.; Tsai, C.; Noonan, K. J. T. *Chem. Eur. J.* **2018**, *24* (50), 13078–13088.

(85) Beaujuge, P. M.; Amb, C. M.; Reynolds, J. R. *Acc. Chem. Res.* **2010**, *43* (11), 1396–1407.

(86) Bredas, J.-L. *Mater. Horiz.* **2014**, *1* (1), 17–19.

(87) Cardona, C. M.; Li, W.; Kaifer, A. E.; Stockdale, D.; Bazan, G. C. *Adv. Mater.* **2011**, *23* (20), 2367–2371.

(88) Kenning, D. D.; Mitchell, K. A.; Calhoun, T. R.; Funfar, M. R.; Sattler, D. J.; Rasmussen, S. C. *J. Org. Chem.* **2002**, *67* (25), 9073–9076.

(89) Evenson, S. J.; Rasmussen, S. C. *Org. Lett.* **2010**, *12* (18), 4054–4057.

(90) Wu, J.; Lai, G.; Li, Z.; Lu, Y.; Leng, T.; Shen, Y.; Wang, C. *Dyes Pigments* **2016**, *124*, 268–276.

(91) Heiskanen, J. P.; Vivo, P.; Saari, N. M.; Hukka, T. I.; Kastinen, T.; Kaunisto, K.; Lemmetyinen, H. J.; Hormi, O. E. O. *J. Org. Chem.* **2016**, *81* (4), 1535–1546.

(92) Qi, J.; Fang, Y.; Kwok, R. T. K.; Zhang, X.; Hu, X.; Lam, J. W. Y.; Ding, D.; Tang, B. Z. *ACS Nano* **2017**, *11* (7), 7177–7188.

(93) Wan, L.; Li, X.; Song, C.; He, Y.; Zhang, W. *Sol. Energy Mater. Sol. Cells* **2019**, *191*, 437–443.

(94) Yuen, J. D.; Kumar, R.; Zakhidov, D.; Seifter, J.; Lim, B.; Heeger, A.; Wudl, F. *Adv. Mater.* **2011**, *23*, 3780–3785.

(95) Imin, P.; Imit, M.; Adronov, A. *Macromolecules* **2011**, *44* (23), 9138–9145.

(96) Fallahi, A.; Taromi, F. A.; Mohebbi, A.; Yuen, J. D.; Shahinpoor, M. *J. Mater. Chem. C* **2014**, *2* (32), 6491–6501.

(97) Li, J.; Wang, R.; Sun, Y.; Xiao, P.; Yang, S.; Wang, X.; Fan, Q.; Wu, W.; Jiang, X. *ACS Appl. Mater. Interfaces* **2021**, *13* (46), 54830–54839.

(98) Yun, J. H.; Ahn, H.; Lee, P.; Ko, M. J.; Son, H. J. *Macromolecules* **2017**, *50* (19), 7567–7576.

(99) Leventis, A.; Chmovzh, T. N.; Knyazeva, E. A.; Han, Y.; Heeney, M.; Rakitin O.A.; Bronstein, H. *Polym. Chem.* **2020**, *11*, 581–585.

(100) Fan, J.; Yuen, J. D.; Wang, M.; Seifter, J.; Seo, J.-H.; Mohebbi, A. R.; Zakhidov, D.; Heeger, A.; Wudl, F. *Adv. Mater.* **2012**, *24* (16), 2186–2190.

(101) Fuller, L. S.; Iddon, B.; Smith, K. A. *J. Chem. Soc., Perkin Trans.* **1997**, *1*, 3465–3470.

(102) McCulloch I.; Heeney M.; Bailey C.; Genevicius K.; MacDonald I.; Shkunov M.; Sparrowe D.; Tierney S.; Wagner R.; Zhang W.; Chabinyc M. L. *Nat. Mater.* **2006**, *5* (4), 328–333.

(103) Chen, M. S.; Niskala, J. R.; Unruh, D. A.; Chu, C. K.; Lee, O. P.; Fréchet, J. M. J. *Chem. Mater.* **2013**, *25* (20), 4088–4096.

(104) Hasegawa, T.; Ashizawa, M.; Aoyagi, K.; Masunaga, H.; Hikima, T.; Matsumoto, H. *Org. Lett.* **2017**, *19* (12), 3275–3278.

(105) Hasegawa, T.; Aoyagi, K.; Ashizawa, M.; Konosu, Y.; Kawauchi, S.; Sariciftci, N. S.; Matsumoto, H. *Chem. Lett.* **2015**, *44* (8), 1128–1130.

(106) Kage, Y.; Mori, S.; Ide, M.; Saeki, A.; Furuta, H.; Shimizu, S. *Mater. Chem. Front.* **2018**, *2* (1), 112–120.

(107) Jeanbourquin, X. A.; Rahmanudin, A.; Yu, X.; Johnson, M.; Guijarro, N.; Yao, L.; Sivula, K. *ACS Appl. Mater. Interfaces* **2017**, *9* (33), 27825–27831.

(108) Fu, L.; Fu, W.; Cheng, P.; Xie, Z.; Fan, C.; Shi, M.; Ling, J.; Hou, J.; Zhan, X.; Chen, H. *J. Mater. Chem. A* **2014**, *2* (18), 6589–6597.

(109) Kroon, R.; Gehlhaar, R.; Steckler, T. T.; Henriksson, P.; Müller, C.; Bergqvist, J.; Hadipour, A.; Heremans, P.; Andersson, M. R. *Sol. Energy Mater. Sol. Cells* **2012**, *105*, 280–286.

(110) Steckler, T. T.; Henriksson, P.; Mollinger, S.; Lundin, A.; Salleo, A.; Andersson, M. R. *J. Am. Chem. Soc.* **2014**, *136* (4), 1190–1193.

(111) Heinrich, A. C. J.; Thiedemann, B.; Gates, P. J.; Staubitz, A. *Org. Lett.* **2013**, *15* (18), 4666–4669.

CHAPTER 4. DESIGN AND SYNTHESIS OF SMALL MOLECULE NEAR-INFRARED EMITTERS

4.1. Introduction

Fluorescence bioimaging has gained interest over traditional imaging methods such as positron emission tomography (PET) and magnetic resonance imaging (MRI) due to its affordability, high sensitivity, and fast feedback.[1–3] Light wavelengths of 700–900 nm and 1000–1700 nm are ideal for bioimaging due to the reduced absorption, autofluorescence, and scattering in these regions.[1] This is depicted in Figure 4.1, in which the biological tissue penetration depth of light increases as wavelength increases.[1,4] These regions have been termed the first near-infrared (NIR-I) window (700–900 nm) and second near-infrared (NIR-II) window (1000–1700 nm). The region is broken into two windows due to absorption by water and lipids around 950 nm.[4–6] However, this nomenclature is somewhat misleading as almost half of the NIR-I window is outside of the NIR region.

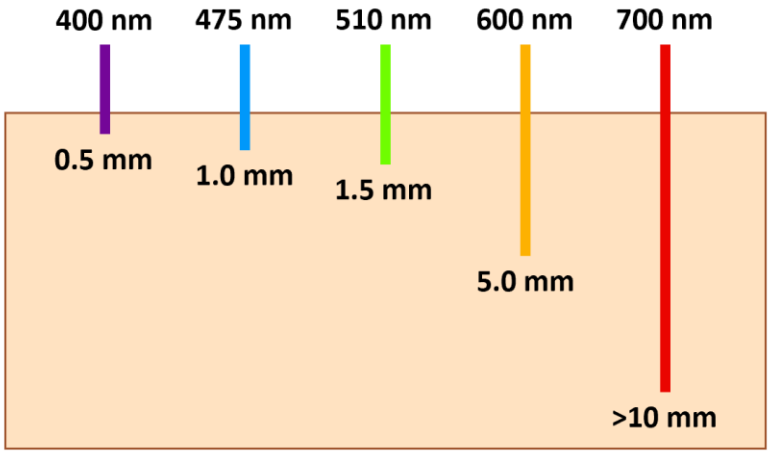

Figure 4.1. Biological tissue penetration depths for various wavelengths of light.[4]

In bioimaging, inorganic nanomaterials such as quantum dots,[7,8] single-walled carbon nanotubes,[9,10] and rare-earth-doped nanoparticles,[11,12] have drawbacks such as toxicity, poor

water solubility,[4] and slow excretion times.[1,13] Organic fluorophores, particularly small molecule fluorophores, have gained much interest due to their low toxicity, fast excretion rates, tunability through molecular design, and good biocompatibility.[1,4,14] Small molecule fluorophores also have faster excretion rates than conjugated polymers.[4]

In 1959, the U.S. Food and Drug Administration (FDA) approved the small molecule NIR fluorophore indocyanine green (ICG, Figure 4.3) for clinical applications,[1,4] which exhibits a peak emission at 830 nm. Methylene blue (MB, Figure 4.3) is another approved small molecule fluorophore that exhibits peak emission at 686 nm.[4] However, ICG and MB exhibit peak emission in the NIR-I and visible regions, which limits their application due to the lower penetration depth of these regions of light. This led to a push towards organic small molecule fluorophores that emit in the NIR-II region.

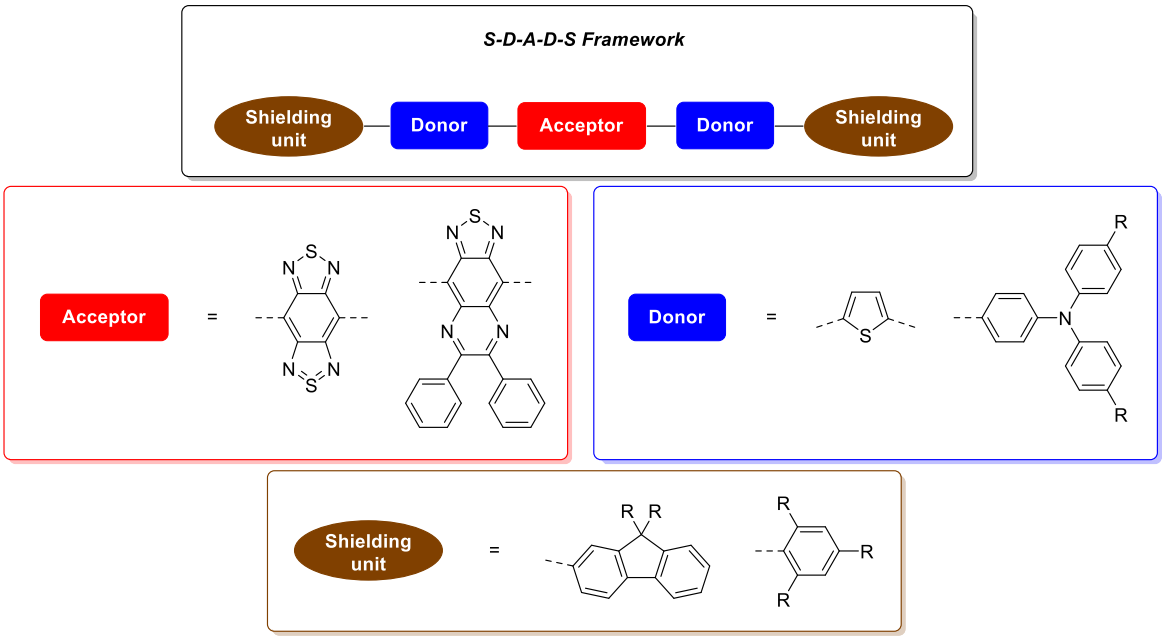

Figure 4.2. S-D-A-D-S structure and examples of common acceptors, donors, and shielding units.

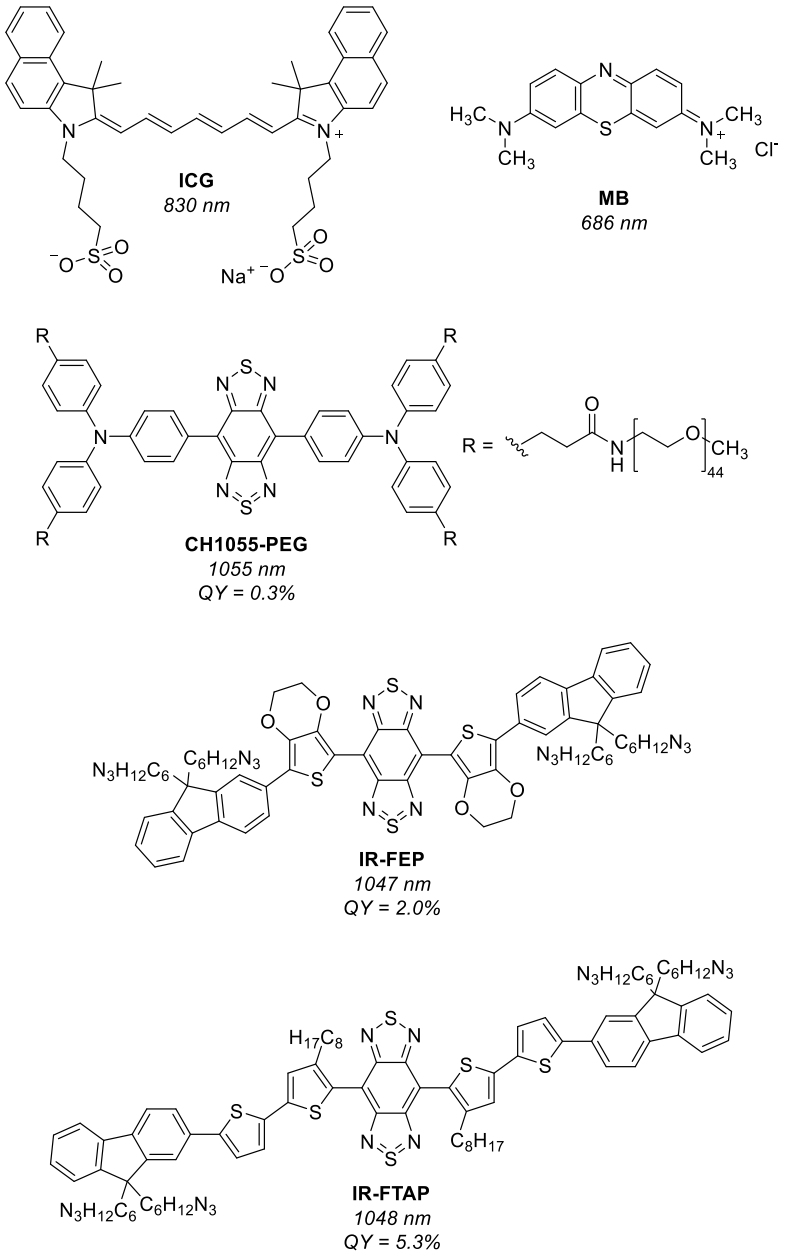

Figure 4.3. Small molecule fluorophores with corresponding emission wavelength and quantum yield in aqueous solution.

A common design for small molecule fluorophores that emit in the NIR-II region is the donor-acceptor-donor (D-A-D) framework.[1] A common central acceptor unit used in these D-A-D frameworks is benzo[1,2-*c*:4,5-*c'*]bis[1,2,5]thiadiazole (BBTD). The first example of a small molecule NIR-II emitter with a BBTD core was reported by Dai and coworkers in 2016 when

they made CH1055, which exhibits peak emission at 1055 nm.[1,15] D-A-D fluorophores exhibit relatively long wavelength absorption and emission due to the donor-acceptor interactions, resulting in a low HOMO-LUMO gap.[16–18] Furthermore, "shielding" units have been attached to the end of D-A-D fluorophores (S-D-A-D-S, Figure 4.2) to reduce aggregation between molecules and increase the quantum yield.[1]

In 2016, Dai and coworkers functionalized CH1055 with polyethylene glycol (PEG) chains, improving its aqueous solubility.[15] This differed from common methods of improving aqueous solubility, which typically involved hydrophilic encapsulation. As a result, CH1055-PEG (Figure 4.3) exhibited a fast excretion rate of ca. 90% in 24 h. Furthermore, CH1055-PEG was used to obtain high quality images of brain tumors in mice. However, the shortcomings of CH1055-PEG were the very low quantum yield (0.3%) and poor penetration depth (4 mm).

To enhance quantum yields, Dai and coworkers added a shielding unit to the D-A-D framework, preventing aggregation of the conjugated backbone.[19] Their S-D-A-D-S compound used BBTD as the core acceptor, 3,4-ethylenedioxythiophene (EDOT) as the donor, and fluorene as the shielding unit (IR-FEP, Figure 4.3). The large side chains on the fluorene unit helped break up aggregates. In water, the compound exhibited a maximum emission at 1047 nm, and a quantum yield of 2.0%.

In 2018, Dai and coworkers modified their original S-D-A-D-S design to create a new S-D'-D-A-D-D'-S compound with BBTD as the acceptor, 3-octylthiophene as the first donor (D), thiophene as the second donor (D'), and fluorene as the shielding unit (IR-FTAP, Figure 4.3).[20] The resulting NIR emitter showed a maximum emission at 1048 nm. They suggested that the large octyl side chains on the thiophene unit causes distortion of the conjugated backbone and limited interactions with water molecules. IR-FTAP exhibited a quantum yield of 5.3% in

aqueous solution, which was one of the highest for a small molecule NIR-II fluorophore at that time.

4.1.1. Tricyclic-Fused Bithiophenes

A family of compounds known as tricyclic-fused bithiophenes have gained interest for their ability to produce fluorescent materials.[21,22] These compounds are utilized as monomeric units in oligomers and polymers,[21–24] and are made up of 2,2'-bithiophene with a bridging unit attached to the 3- and 3'-positions of the thiophene rings (Figure 4.4). Examples of such compounds include dithieno[3,2-*b*:2',3'-*d*]pyrrole (DTP), dithieno[3,2-*b*:2',3'-*d*]thiophene (DTT), and 4*H*-cyclopenta[2,1-*b*:3,4-*b'*]dithiophene (CPDT). Due to their added rigidity relative to 2,2'-bithiophene, these units generally exhibit enhanced electron delocalization and a reduced bandgap.[21–23,25] In addition, they generally exhibit less vibrational relaxion from the excited state, resulting in enhanced emission.[21,26] Finally, the side chains of these compounds are placed in the center of the unit, which reduces the likelihood of regioirregularity issues in the polymers and allows for the use of larger substituents due to the reduced likelihood of steric interactions.[21,23,26]

4.1.2. Dithieno[3,2-b:2',3'-d]pyrrole

The tricyclic-fused bithiophene, DTP, has been used to produce a variety of fluorescent materials.[23,26] DTP was first reported in 1983 by Zanirato and coworkers.[28] However, DTP did not have much interest until 2003, when Rasmussen and coworkers reintroduced these units.[23,26,29] Since then many fluorescent DTP-based oligomers have been reported.[26,30–32]

Most reported DTP-based materials use first-generation DTPs, which have alkyl and aryl groups attached to the pyrrole nitrogen.[21,23,24] In 2010, Rasmussen and coworkers introduced second-generation DTPs,[33] which are functionalized with acyl groups. Due to the electron-withdrawing nature of acyl groups, second generation DTPs generally exhibit stabilized HOMO

and LUMO energy levels relative to first generation DTPs.[23,33] They also found that second-generation DTPs exhibited a red-shifted absorption onset.[33]

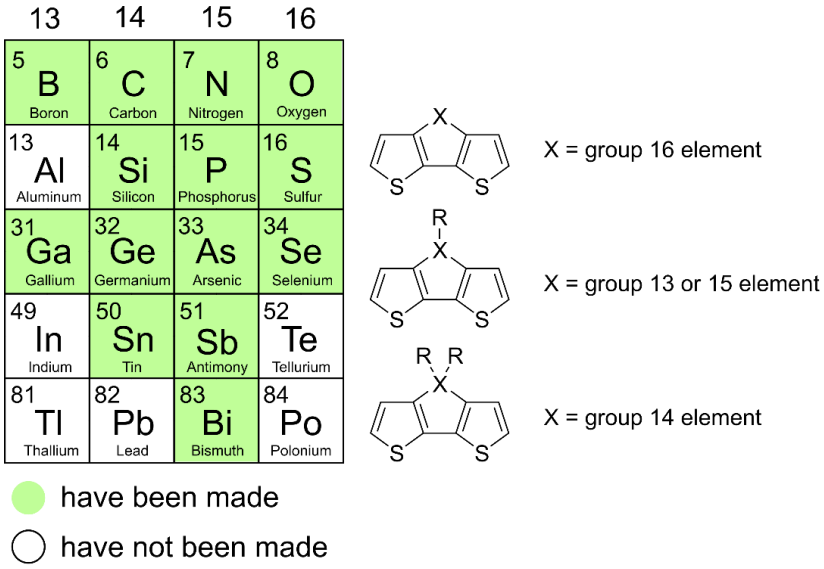

Figure 4.4. Tricyclic-fused bithiophenes.[21,27]

Figure 4.5 illustrates the production of first- and second-generation DTPs from 3-bromothiophene (**4.1**). First, the lithiation of **4.1** is achieved by the addition of LDA. Then $ZnCl_2$ and $CuCl_2$ are added to undergo transmetalation to the organocopper species. The organocopper species undergoes oxidative coupling, which is assisted by dry O_2, to give 3,3'-dibromo-2,2'-bithiophene (**4.2**) in high yield (85-90%).[33] First-generation DTPs are then made by Buchwald-Hartwig coupling between **4.2** and a primary amine to give DTP in high yield (up to 99%).[34,35] Second-generation DTPs are made by copper-catalyzed amidation of **4.2** to yield acyl-DTPs in a yield of ca. 20–40%.[33]

In 2012, Rasmussen and coworkers synthesized first and second generation DTP-based oligomers (Figure 4.6).[30] The first generation DTP-based oligomers were made by Stille coupling between the distannyl-DTP and 2-bromothiophene or bromobenzene to give oligomers **4.5** and **4.6** in 41–81% yield. The second-generation distannyl-DTPs could not be made as the

acyl groups can undergo nucleophilic attack with BuLi. However, they were able to make the dibromides in good yield. Thus, allowing the synthesis of oligomers **4.7** and **4.8** by Stille and Suzuki coupling in 32–47% yield.

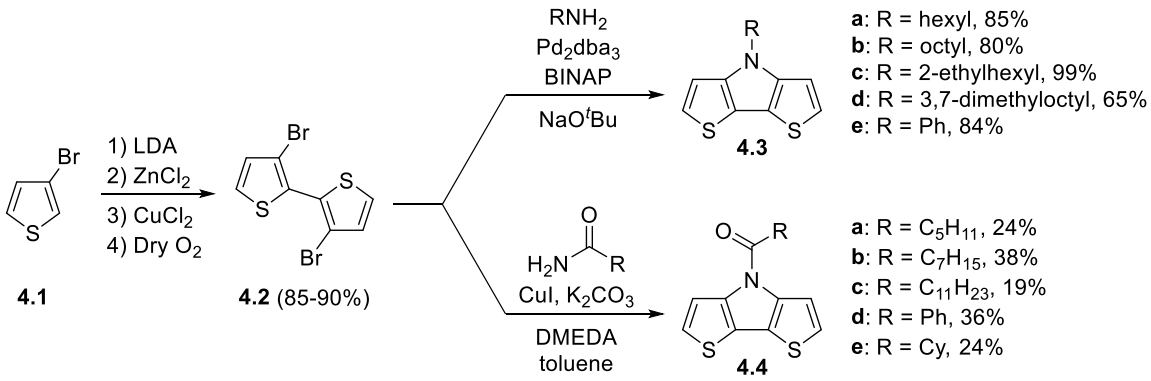

Figure 4.5. Synthesis of first- and second-generation DTPs.

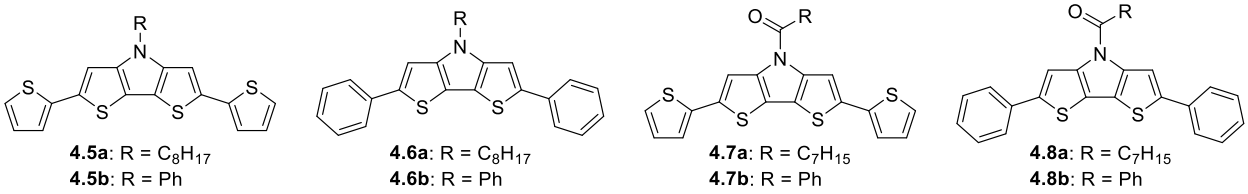

Figure 4.6. DTP-based oligomers synthesized and analyzed by Rasmussen and coworkers.

Table 4.1 shows photophysical data for the parent DTP monomer (**4.3b**) and the DTP oligomers synthesized by Rasmussen and coworkers in 2012 (**4.5**–**4.8**). The DTP monomer exhibits very weak fluorescence, but the DTP oligomers exhibit relatively strong fluorescence. DTP-based oligomers are some of the strongest emitting thiophene-based materials due to their fused-ring nature, which eliminates interannular torsional vibrations (a source of nonradiative deactivation), and their enhanced photochemical stability.[23,26,36] Moreover, the DTP-based oligomers exhibit red-shifted absorption and emission due to the increased conjugation length. The phenyl-capped oligomers have blue-shifted spectra due to the steric interactions between the

phenyl group and DTP core. However, the phenyl-capped oligomers have increased quantum yields due to the reduced number of sulfur atoms, as sulfur atoms usually cause a decrease in quantum yield due to the heavy atom effect. Second-generation DTPs have been found to exhibit increased quantum efficiencies relative to their first-generation counterparts.[30] It has also been found that oligothiophenes functionalized with carbonyl groups exhibit increased fluorescence quantum yields.[26]

Table 4.1. Solution-state photophysical data of DTP and DTP-based oligomers.

Compound	λ_{max}^{abs}(nm)	λ_{max}^{em}(nm)[a]	Φ_F
4.3b[b]	310	324	7.78×10^{-4}
4.5a[c]	400	440,470, (506)	0.32
4.5b[c]	396	444, (464)	0.70
4.6a[c]	381	422, 442, (473)	0.53
4.6b[c]	378	421, 440, (476)	0.87
4.7a[c]	399	446, 468, (504)	0.68
4.7b[c]	398	440, (467)	0.73
4.8a[c]	380	424, 439, (466)	0.62
4.8b[c]	380	424, (443)	0.92

[a] Values in parentheses denote prominent shoulders.
[b] Ref. 29. [c] Ref. 30.

4.1.3. Indium-based Heterocycles

As shown in Figure 4.4 tricyclic-fused bithiophenes that contain group 13 elements have been the least explored with indolo[3,2-*b*:4,5-*b'*]dithiophene yet to be synthesized. However, the indium-based tricyclic-fused biphenyl has been made with the first report in 1995, when Decken et al. prepared indafluorene **4.10** (Figure 4.7).[37] They synthesized **4.10** by lithiating 2,2'-dibromobiphenyl (**4.9**), followed by a reaction with the corresponding arylindium(III) dibromide to give compound **4.10** in low yield (~13%). Not much characterization of **4.10** was reported beyond mass spectroscopy and ^{1}H and ^{13}C NMR data.

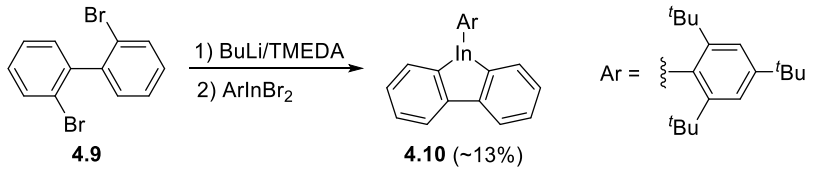

Figure 4.7. Indafluorene synthesized by Decken et al. in 1995.

In 2015, Matsumoto et al. synthesized indafluorene **4.12** via lithiation of 2,2'-diiodobiphenyl (**4.11**) followed by reaction with dichloro[2,4-di-*t*-butyl-6-(*N*,*N*-dimethylaminomethyl)phenyl]dichloroindigane, giving the product in ~27% yield (Figure 4.8).[38] Compound **4.12** was reported to be water sensitive and required purification under an argon atmosphere. Compound **4.12** exhibited an absorption maximum at 282 nm, as well as fluorescence and phosphorescence, with the fluorescence maxima at 309 and 330 nm and the phosphorescence maximum at 487 nm. However, the total quantum yield was low.

4.1.4. Thiazolo[5,4-d]thiazole

In 2017, Woodward et al. reported a series of highly fluorescent thiazolo[5,4-*d*]thiazole (TTz) based oligomers (Figure 4.9).[39] The oligomers were made by double condensation between 4-pyridinecarboxaldehyde and dithiooxamide, followed by dialkylation with methyl tosylate, 1-bromooctane, or benzyl bromide. TTz-based oligomers **4.13**–**4.15** exhibited absorption λ_{max} values between 390–395 nm and peak emission wavelengths ranging from 452–461 nm. They also exhibited high quantum yields ranging from 0.79 to 0.92.

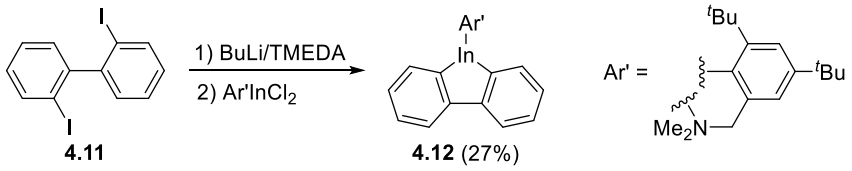

Figure 4.8. Indafluorene synthesized by Matsumoto et al. in 2015.

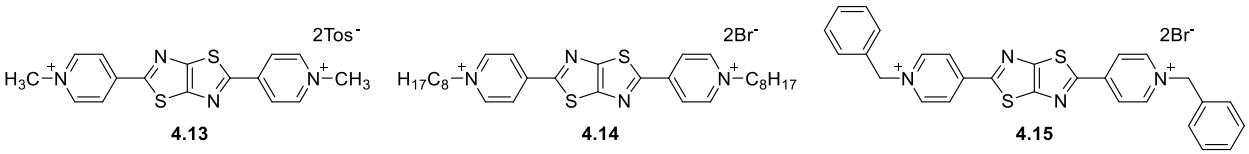

Figure 4.9. Thiazolo[5,4-*d*]thiazole-based oligomers made by Woodward et al.

4.2. Results and Discussion

4.2.1. NIR Emitter Design

Initially, the goal was to synthesize photoluminescent oligomers that emit in the NIR-II region with high quantum yields. The target oligomer had a traditional D-A-D scaffold, but instead of using a traditional acceptor, the ambipolar unit thieno[3,4-*b*]pyrazine (TP) was used as the central unit. The target oligomer had the strong donor unit DTP and was end capped with phenyl groups to protect the α-position of the thiophene ring to increase stability (Figure 4.10). The target compound is expected to exhibit a low-lying LUMO characteristic of TP and a high-lying HOMO due to the strong donor character of DTP and TP. A small HOMO-LUMO gap would lead to a red-shifted absorption onset and emission (if applicable). In addition, the oligomer would exhibit high quantum yields because of the DTP units. Moreover, the oligomer would be functionalized with alkyl side chains, resulting in good solubility in common organic solvents.

4.2.2. Synthesis of N-Alkyldithieno[3,2-b:2',3'-d]pyrrole-based Oligomer

Stannyl-DTP **4.16** was synthesized by modifying a procedure previously reported by Rasmussen and coworkers to make the distannyl analog.[30] This involved treating **4.3b** with BuLi/tetramethylethylenediamine (TMEDA) followed by the addition of Me_3SnCl, letting the reaction warm up to room temperature, and stirring overnight. This mixture was then run through a triethylamine treated silica gel plug to purify stannyl-DTP **4.16**. It has been found that the

distannyl analog undergoes decomposition on silica gel.[40] Therefore, Rasmussen and coworkers found that it could be purified by using a deactivated column followed by rotary evaporation and pumping overnight.[41] Selective production of stannyl-DTP **4.16** was not possible, with some starting material left over along with some distannyl-DTP. Then, Stille coupling was performed with bromobenzene, by modifying a procedure previously reported by Rasmussen and coworkers used to make oligomer **4.6**.[30] This gave *N*-octyl-2-phenyldithieno[3,2-*b*:2',3'-*d*]pyrrole (**4.17**) in 64% yield over two steps.

Stannyl-DTP **4.18** was synthesized by similar methods used to make stannyl-DTP **4.16**. Attempted synthesis of oligomer **4.19** by Stille coupling with 5,7-dibromo-2,3-dihexylthieno[3,4-*b*]pyrazine[42] was unsuccessful (Figure 4.10). UV-vis analysis of the crude sample showed absorbance out to ~900 nm, suggesting that oligomer **4.19** was made. However, the desired product was not obtained upon column chromatography, likely due to its low stability caused by its high-lying HOMO. Alternatively, oligomer **4.19** could be sticking to the silica gel during column chromatography, and other purification methods should be used.

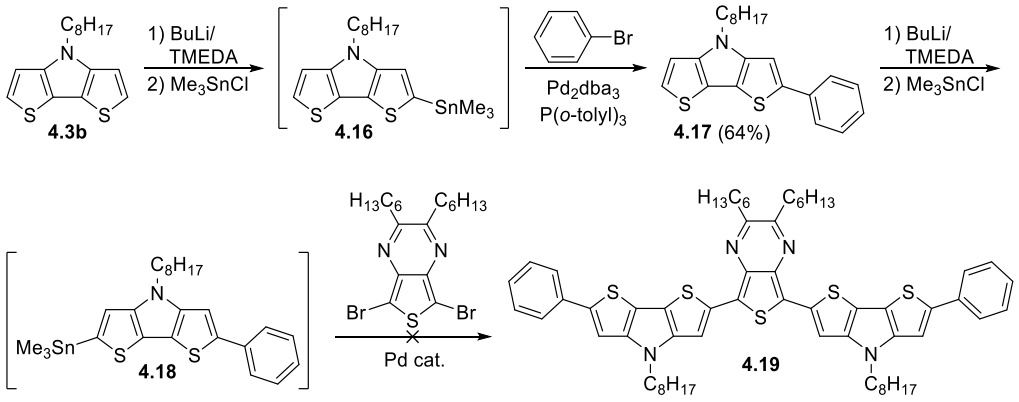

Figure 4.10. Attempted synthesis of oligomer **4.19**.

4.2.3. Synthesis of N-Acyldithieno[3,2-b:2',3'-d]pyrrole-based Oligomer

Due to difficulties in synthesizing oligomer **4.19**, oligomer **4.25** was targeted, which employed *N*-acyl-DTP instead of *N*-alkyl-DTP. The rationale for this was based on previous research that found *N*-acyl-DTPs exhibited a stabilized HOMO and LUMO energy level relative to the *N*-alkyl-DTP, which could potentially help with stability. Additionally, Rasmussen and coworkers found that *N*-acyl-DTP-based oligomers exhibited higher quantum yields than *N*-alkyl-DTP-based oligomers.[30]

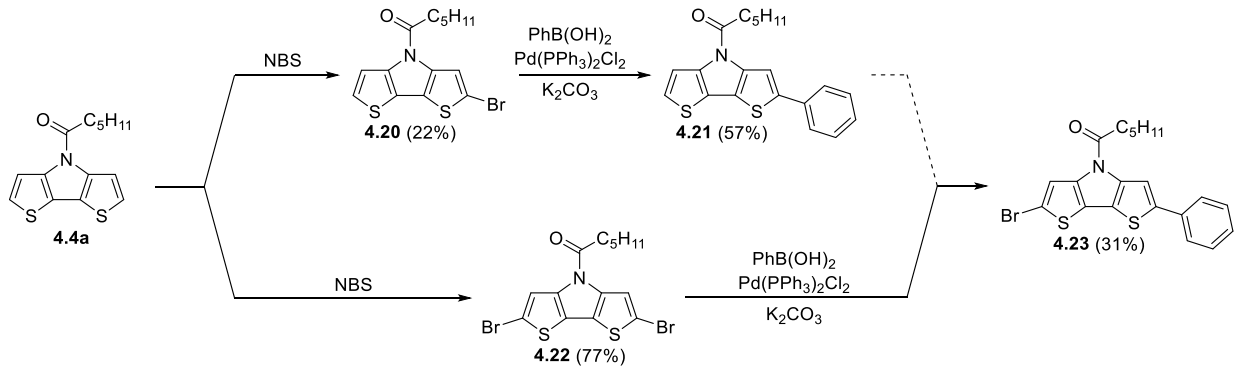

Figure 4.11. Synthesis of *N*-hexanoyl-2-bromo-6-phenyldithieno[3,2-*b*:2',3'-*d*]pyrrole.

N-hexanoyl-2-bromo-6-phenyldithieno[3,2-*b*:2',3'-*d*]pyrrole (**4.23**) was synthesized from DTP **4.4a** by two routes (Figure 4.11). The first route involved making *N*-hexanoyl-2,6-dibromodithieno[3,2-*b*:2',3'-*d*]pyrrole (**4.22**), following a procedure previously reported by Rasmussen and coworkers.[30] This was followed by Suzuki coupling with 1.0 equivalent of phenyl boronic ester to give the monocoupled product in a 31% yield.[30] Attempts were made to increase the yield of this reaction by changing the base and the reaction time, but no significant impact on the yield was observed. In the second route *N*-hexanoyl-2-bromodithieno[3,2-*b*:2',3'-*d*]pyrrole (**4.20**) was made using NBS in 22% yield.[30] Suzuki coupling was carried out with 1.1 equivalents of phenyl boronic ester to give *N*-hexanoyl-2-phenyldithieno[3,2-*b*:2',3'-*d*]pyrrole

(**4.21**) in 57% yield. We deemed the first route to be more efficient for making compound **4.23** due to the low yield of the monobromination step and the need for two separate bromination steps.

Once compound **4.23** was made we attempted to make oligomer **4.25** by two routes. The first route used direct arylation between compound **4.23** and 2,3-dihexylthieno[3,4-*b*]pyrazine (**4.24**)[43] using conditions previously reported by Rasmussen and coworkers to make TP-based alternating copolymers (Figure 4.12).[44,45] UV-vis analysis of the crude sample showed absorbance out to ~900 nm, suggesting that oligomer **4.25** was made. However, no product was isolated upon column chromatography, potentially due to its low stability or that the oligomer is sticking to the silica gel during column chromatography.

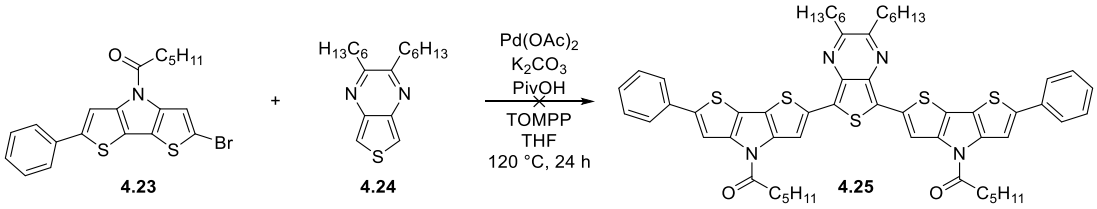

Figure 4.12. Attempted synthesis of oligomer **4.25** by direct arylation.

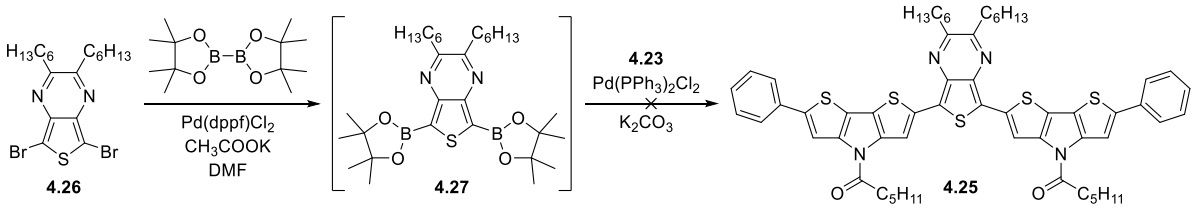

Figure 4.13. Attempted synthesis of oligomer **4.25** by Suzuki coupling.

The second attempt utilized Suzuki coupling to synthesize oligomer **4.25**. This required synthesis of TP boronic ester **4.27**, which was made through cross-coupling between **4.26** and bis(pinacolato)diboron (Figure 4.13), which after purification yielded a mixture of **4.24** and a

second species which we suspected to be compound **4.27**. The crude **4.27** sample was then used for Suzuki coupling with compound **4.23**, which resulted in no product formation.

4.2.4. Synthesis of Indolo[3,2-b:4,5-b']dithiophene

The synthesis of indium-based heterocycle **4.28** was attempted following a common route used to synthesize tricyclic-fused bithiophenes (Figure 4.14).[21] Compound **4.2** was treated with 2.1 equivalents of BuLi to cause metal-halogen exchange. This was followed by the addition of phenylindium(III) dichloride, which was prepared following previously reported procedures.[46] However, the desired product was not obtained, potentially due to its low stability as was observed for indafluorene **4.12**.[38]

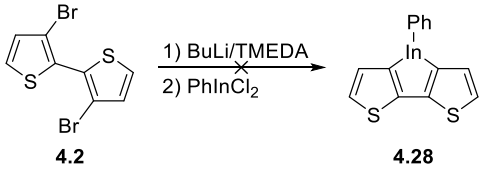

4.2 **4.28**

Figure 4.14. Attempted synthesis of indolo[3,2-*b*:4,5-*b'*]dithiophene.

4.2.5. Synthesis of Thiazolo[5,4-d]thiazole-based Oligomer

Next, oligomer **4.30** was targeted as previous studies report high quantum yields for both DTP- and TTz-based oligomers (Figure 4.15).[30,39] First, formylation of compound **4.17** was carried out by the addition of BuLi at -78 °C, followed by the addition of DMF, warming to room temperature and letting stir for 2 h to give aldehyde **4.29** in 80% yield. Oligomer **4.30** was then made by a double condensation between aldehyde **4.29** and dithiooxamide. It was found that after 5 h a very low yield (< 5%) was recovered. Increasing the reaction time to 12 h led to an increase in the yield to 25% and further increasing the reaction time to 24 h gave the desired oligomer in 65% yield.

Previous work has shown that the addition of an oxidant to make TTz-based compounds results in an increase in yield.[47] More recently, it was found that air could be used in place of a chemical oxidant in some cases.[39] However, conducting the reaction under air at reflux for 12 h gave oligomer **4.30** in very low yield (< 5%).[39]

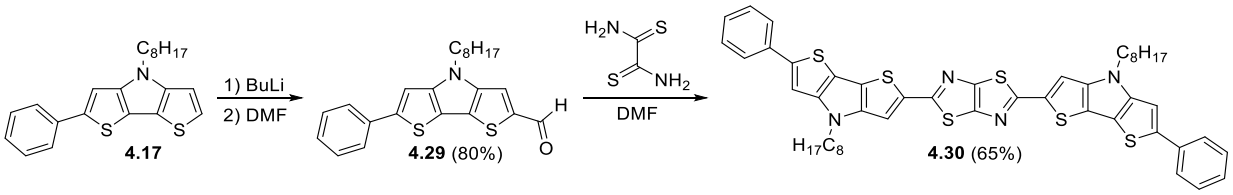

Figure 4.15. Synthesis of oligomer **4.30** from *N*-octyl-2-phenyldithieno[3,2-*b*:2',3'-*d*]pyrrole.

4.2.6. UV-vis Absorption Spectroscopy

Shown in Table 4.2 is the solution-state UV-vis data for the parent first- and second-generation DTP monomers and the corresponding phenyl-capped oligomers. In addition, the solution-state UV-vis spectra of DTPs **4.17** and **4.21** are shown in Figure 4.17. The absorption λ_{max} values of DTPs **4.17** and **4.21** are between that of DTP monomers **4.3b** and **4.4a** and DTP oligomers **4.6a** and **4.8a**, which is due to the increase in conjugation length. Moreover, there is a much larger red shift in the λ_{max} value upon the addition of the first phenyl substituent (43 and 49 nm) compared to the addition of the second phenyl substituent (28 and 26 nm). One difference between the UV-vis spectra for DTPs **4.17** and **4.21** is that DTP **4.21** exhibits a higher energy peak at ~300 nm, whereas DTP **4.17** does not. This trend is also observed for phenyl-capped DTPs **4.6a** and **4.8a**.[30]

Shown in Table 4.3 is the solution-state photophysical data for several TTz- and DTP-based oligomers. Shown in Figure 4.19 is the solution-state UV-vis spectrum for oligomer **4.30**. Oligomer **4.30** exhibits two low energy peaks at 503 and 532 nm. Moreover, the λ_{max} for

oligomer **4.30** is significantly redshifted compared to the λ_{max} for oligomers **4.6a**, **4.13**, and **4.31**. In $CHCl_3$ oligomer **4.30** showed strong emission under 365 nm wavelength light (Figure 4.20).

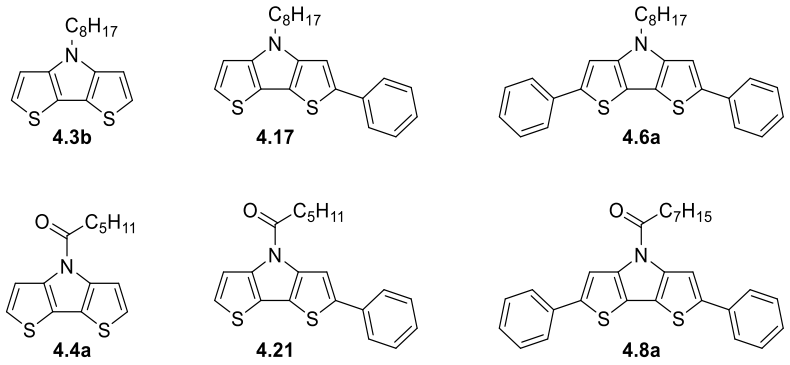

Figure 4.16. *N*-alkyl- and *N*-acyl-DTP monomer and oligomers.

Table 4.2. Solution-state UV-vis data for *N*-alkyl- and *N*-acyl-DTP monomers and oligomers.

Compound	λ_{max} (nm)
4.3b[a]	310
4.17[b]	353
4.6a	381
4.4a	305
4.21[c]	354
4.8a[c]	380

[a] Ref. 29. [b] Ref. 33. [c] Ref. 30.

4.3. Conclusion

The synthesis of oligomers **4.19** and **4.25** were attempted. However, efforts were unsuccessful possibly due to the low stability of the oligomers as a result of their high-lying HOMOs. Nevertheless, novel compounds which could be used to make other oligomers and polymers have been made. In addition, the impact of functionalizing the 2- and 6-positions of *N*-alkyl- and *N*-acyl-DTP was analyzed by UV-vis spectroscopy. It was found that the addition of

the first phenyl substituent resulted in a much larger redshift in λ_{max} than the addition of the second phenyl substituent.

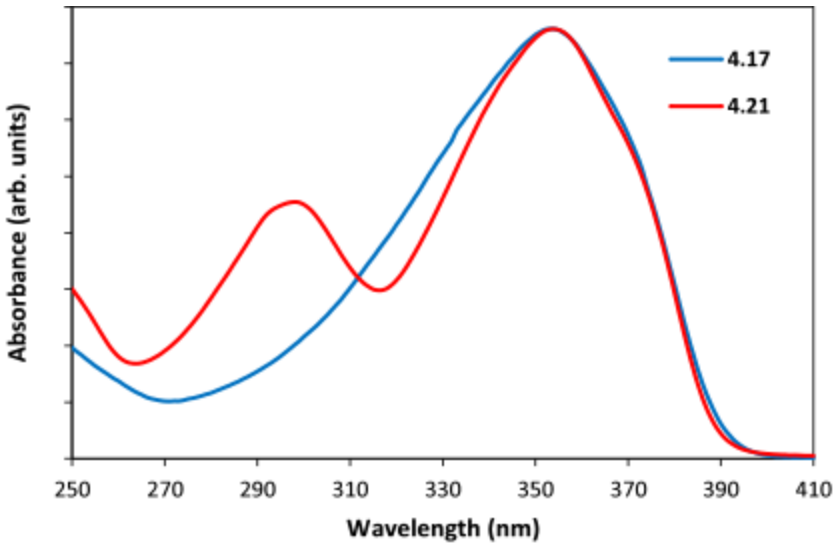

Figure 4.17. Solution-state UV-vis spectra of *N*-alkyl- and *N*-acyl-DTP oligomers.

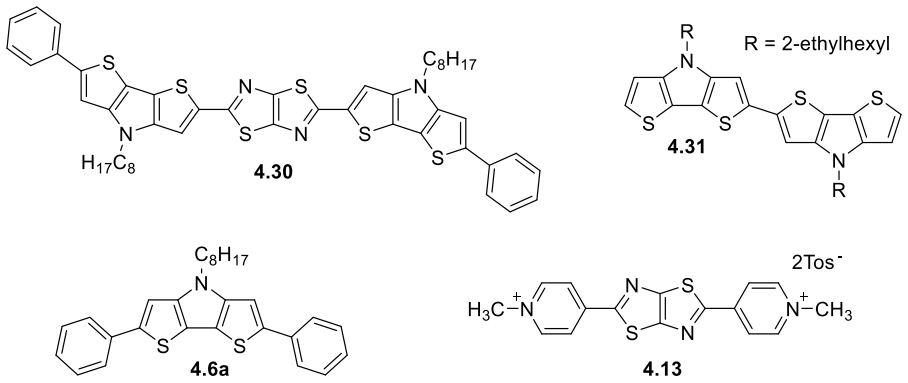

Figure 4.18. TTZ- and DTP-based oligomers.

Oligomer **4.30** was prepared by a double condensation reaction between aldehyde **4.29** and dithiooxamide. It was found that increasing the reaction time led to an increase in the yield giving oligomer **4.30** in 65% yield. Oligomer **4.30** exhibited an absorption λ_{max} at 532 nm, which is significantly red shifted compared to DTP dimer **4.31**, phenyl-capped DTP **4.6a**, and TTz **4.13**,

which is likely due to the extended conjugation of this oligomer. Moreover, oligomer **4.30** exhibited strong emission under 365 nm light illumination.

Table 4.3. TTZ- and DTP-based oligomer photophysical data.

Compound	λ_{max}^{abs}(nm)	λ_{max}^{em}(nm)[a]	Φ_F
4.30	503, 532	-	-
4.31[b]	410	462, 488	0.37
4.6a[c]	381	422, 442, (473)	0.53
4.13[d]	390	~455	0.92

[a] Values in parentheses denote prominent shoulders.
[b] Ref. 48. [c] Ref. 30. [d] Ref. 39.

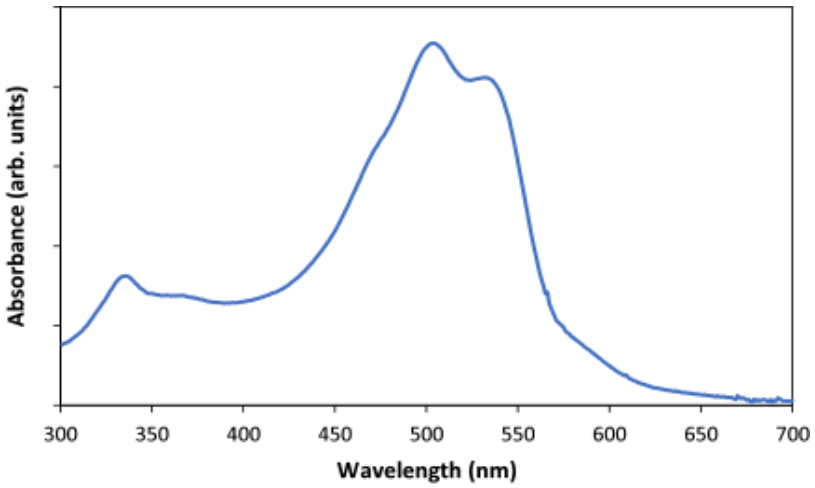

Figure 4.19. Solution-state UV-vis spectrum of oligomer **4.30**.

4.4. Experimental

4.4.1. General

All materials were reagent grade and used without further purification unless noted. DMF was dried by mixing with $MgSO_4$ and flushing through a silica gel plug. $CHCl_3$ was dried by flushing through a silica gel plug. THF, toluene, and hexanes were dried by distillation over sodium/benzophenone. MeCN was dried by distillation over CaH_2 under dry N_2. All dry solvents

were transferred via standard syringe techniques. All reactions were carried out under a dry nitrogen stream unless noted otherwise. Reaction glassware was oven dried before use. ^{1}H and ^{13}C NMR were collected using a 400 MHz spectrometer using $CDCl_3$ as the solvent. NMR peak multiplicity is reported as follows: s = singlet d = double, t = triplet, p = pentet, m = multiplet, and br = broad. A digital thermal couple with a 0.1 °C resolution was used to determine melting points. Previously reported procedures were followed to synthesize *N*-octyldithieno[3,2-*b*:2',3'-*d*]pyrrole[34] and *N*-hexanoyldithieno[3,2-*b*:2',3'-*d*]pyrrole.[33]

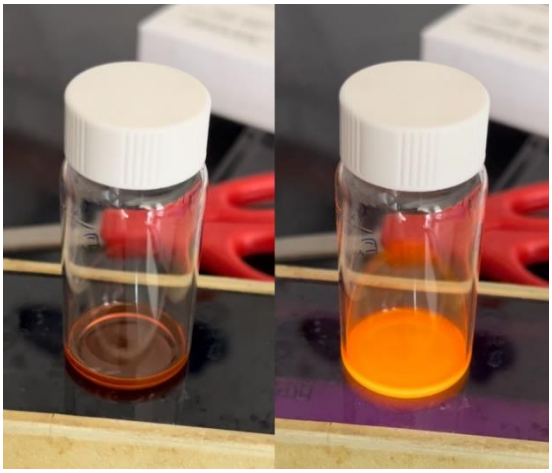

Figure 4.20. Oligomer **4.30** in $CHCl_3$, without and with 365 nm light illumination.

***N*-Octyl-2-phenyldithieno[3,2-*b*:2',3'-*d*]pyrrole (4.17)**. Compound **4.17** was prepared through a modification of a previously reported procedure.[30] To a 50 mL single neck round bottom flask was added, **4.3b** (0.317 g, 1.09 mmol) and dry hexanes (30 mL). The mixture was cooled to 0 °C in an ice bath. TMEDA (0.23 mL, 1.53 mmol) was added. BuLi (2.5 M in hexanes, 0.59 mL, 1.48 mmol) was added dropwise via syringe. The reaction was let stir at 0 °C for 2 h. Me_3SnCl (1.0 M in THF, 1.4 mL, 1.4 mmol) was added dropwise via syringe. The reaction was let warm to room temperature and stirred overnight. The reaction was flushed through a Et_3N-treated silica gel plug using hexanes, concentrated, and pumped overnight to give

a yellow oil (0.423 g). The crude yellow oil, bromobenzene (0.12 mL, 1.14 mmol), Pd_2dba_3 (0.010 g, 0.011 mmol), P(*o*-tolyl)$_3$ (0.013g, 0.043 mmol), and deoxygenated toluene (22 mL) were added to a 50 mL Schlenk tube and heated at 95 °C for 24 h. The reaction was cooled to room temperature. Water was added and the mixture was extracted with $CHCl_3$ three times. The organic layers were combined, dried with Na_2SO_4, filtered and concentrated. The crude product was purified by column chromatography with 95:5 hexanes:DCM to give the product as a pale-yellow oil (0.256 g, 64%). ^{1}H NMR ($(CD_3)_2CO$, 400 MHz): δ 7.73 (d, *J* = 7.6 Hz, 2H), 7.69 (s, 1H), 7.43 (t, *J* = 7.6 Hz, 2H), 7.32 (d, *J* = 5.4 Hz, 1H), 7.29 (t, *J* = 7.6 Hz, 1H), 7.24 (d, *J* = 5.4 Hz, 1H), 4.39 (t, *J* = 7.0 Hz, 2H), 1.94 (p, *J* = 7.0 Hz, 2 H), 1.37–1.26 (m, 10H), 0.86 (t, *J* = 7.0 Hz, 3H). ^{13}C NMR ($CDCl_3$, 400 MHz): δ 145.2, 144.7, 141.5, 135.7, 128.9, 127.1, 125.4, 123.2, 115.0, 114.3, 110.9, 107.1, 47.4, 31.8, 30.4, 29.3, 29.2, 27.1, 22.7, 14.1.

***N*-Hexanoyl-2,6-dibromodithieno[3,2-*b*:2',3'-*d*]pyrrole (4.22)**. Compound **4.22** was prepared through a modification of a previously reported procedure.[30] To a 50 mL three neck round bottom flask equipped with an addition funnel was added, **4.4a** (0.300 g, 1.08 mmol) and dry $CHCl_3$ (9 mL). The flask was wrapped in foil to limit light exposure. In a separate flask was added, NBS (0.421 g, 2.37 mmol) and dry MeCN (9 mL) and cooled to 0 °C in an ice bath. The NBS solution was added dropwise to the **4.4a** solution. The reaction was let stir overnight. Water was added and the mixture was extracted with $CHCl_3$ three times. The organic layers were combined, washed with brine, dried with Na_2SO_4, filtered, and concentrated to give a light-yellow solid. The crude product was purified by column chromatography with 70:30 petroleum ether:DCM to give the product as a white solid (0.442 g, 77%). mp 100.8–102.6 °C; ^{1}H NMR ($CDCl_3$, 400 MHz): δ 7.55 (br, 2H), 2.96 (t, *J* = 7.3 Hz, 2H), 1.89 (p, *J* = 7.3 Hz, 2H), 1.53–1.39

(m, 4H), 0.98 (t, J = 7.3 Hz, 3H). ^{13}C NMR ($CDCl_3$, 400 MHz): δ 169.2, 138.5, 120.7, 119.4, 111.6, 36.2, 31.3, 23.7, 22.5, 14.0.

***N*-Hexanoyl-2-bromodithieno[3,2-*b*:2',3'-*d*]pyrrole (4.20)**. Compound **4.20** was prepared through a modification of a previously reported procedure.[30] To a 50 mL three neck round bottom flask equipped with an addition funnel was added, **4.4a** (0.283 g, 1.02 mmol) and dry $CHCl_3$ (9 mL). The flask was wrapped in foil to limit light exposure. In a separate flask was added, NBS (0.182 g, 1.02 mmol) and dry MeCN (9 mL) and cooled to 0 °C in an ice bath. The NBS solution was added dropwise to the **4.4b** solution. The reaction was let stir overnight. Water was added and the mixture was extracted with $CHCl_3$ three times. The organic layers were combined, dried with Na_2SO_4, filtered, and concentrated to give a yellow solid/oil. The crude product was purified by column chromatography with 65:35 hexanes:DCM to give the product as a white solid (0.0814 g, 22%). ^{1}H NMR ($(CD_3)_2CO$, 400 MHz): δ 7.78 (s, 1H), 7.61 (d, J = 5.4 Hz, 1H), 7.52 (d, J = 5.4 Hz, 1H), 3.19 (t, J = 7.3 Hz, 2H), 1.87 (p, J = 7.3 Hz, 2H), 1.56–1.40 (m, 4H), 0.96 (t, J = 7.3 Hz, 3H). ^{13}C NMR ($CDCl_3$, 400 MHz): δ 169.4, 140.8, 124.8, 121.2, 121.0, 119.8, 116.1, 111.3, 111.2, 36.3, 31.4, 23.8, 22.5, 14.0.

***N*-Hexanoyl-2-phenyldithieno[3,2-*b*:2',3'-*d*]pyrrole (4.21)**. Compound **4.21** was prepared through a modification of a previously reported procedure.[30] To a 50 mL Schlenk tube was added, **4.20** (0.130 g, 0.365 mmol), phenyl boronic acid (0.049 g, 0.402 mmol), and $Pd(PPh_3)_2Cl_2$ (0.0062 g, 0.0088 mmol). Degassed toluene (18 mL) and a degassed solution of K_2CO_3 in water (0.5 mL, 1.6 M) was added and the reaction was heated at 95 °C for 24 h. Water was added, and the mixture was extracted with $CHCl_3$. The organic layers were combined, dried with Na_2SO_4, filtered, and concentrated. The crude product was purified by column chromatography with 60:40 hexanes:DCM to give the product as a yellow oil, which turned to a

solid after a few days in the freezer. (0.074 g, 57%). mp 84.0–87.0 °C; ^{1}H NMR ($(CD_3)_2CO$, 400 MHz): δ 8.00 (s, 1H), 7.77 (d, *J* = 7.6 Hz, 2H), 7.65 (d, *J* = 5.3 Hz, 1H), 7.52 (d, *J* = 5.3 Hz, 1H), 7.47 (t, *J* = 7.6 Hz, 2H), 7.36 (t, *J* = 7.6 Hz, 1H), 3.26 (t, *J* = 7.1 Hz, 2H), 1.91 (p, *J* = 7.1 Hz, 2H), 1.59–1.41 (m, 4H), 0.97 (t, *J* = 7.2 Hz, 3H). ^{13}C NMR ($CDCl_3$, 400 MHz): δ 169.6, 143.4, 141.6, 134.9, 129.0, 127.7, 125.5, 124.5, 121.4, 120.2, 116.2, 112.6, 36.4, 31.5, 23.9, 22.6, 14.0.

***N*-Hexanoyl-2-bromo-6-phenyldithieno[3,2-*b*:2',3'-*d*]pyrrole (4.23)**. Compound **4.23** was prepared through a modification of a previously reported procedure.[30] To a 50 mL Schlenk tube was added, **4.22** (0.179 g, 0.411 mmol), phenyl boronic acid (0.050 g, 0.410 mmol), and $Pd(PPh_3)_2Cl_2$ (0.0064 g, 0.0091 mmol). Degassed toluene (20 mL) and a degassed solution of K_2CO_3 in water (0.5 mL, 1.6 M) was added and the reaction was heated at 95 °C for 48 h. Water was added, and the mixture was extracted with $CHCl_3$ three times. The organic layers were combined, dried with Na_2SO_4, filtered, and concentrated. The crude product was purified by column chromatography with 65:35 hexanes:DCM to give the product as a yellow solid (0.056 g, 31%). ^{1}H NMR ($CDCl_3$, 400 MHz): δ 7.71 (br, 1H), 7.67 (d, *J* = 7.3 Hz, 2H), 7.58 (br, 1H), 7.44 (t, *J* = 7.3 Hz, 2H), 7.34 (t, *J* = 7.3 Hz, 1H), 3.03 (t, *J* = 7.2 Hz, 2H), 1.92 (p, *J* = 7.2 Hz, 2H), 1.54–1.41 (m, 4H), 0.99 (t, *J* = 7.1 Hz, 3H). ^{13}C NMR ($CDCl_3$, 400 MHz): δ 169.4, 143.9, 139.0, 134.6, 129.1, 127.8, 125.5, 121.3, 119.9, 119.5, 112.1, 111.3, 36.3, 31.4, 23.8, 22.6, 14.0.

***N*-Octyl-6-phenyldithieno[3,2-*b*:2',3'-*d*]pyrrole-2-carboxaldehyde (4.29)**. To a 50 mL single neck round bottom flask was added, **4.17** (0.336 g, 0.914 mmol). Dry THF (10 mL) was added and cooled to -78 °C in an acetone/dry ice bath. BuLi (2.5 M in hexanes, 0.44 mL, 1.10 mmol) was added dropwise via syringe. The reaction was let stir at -78 °C for 2 h. Dry DMF (0.15 mL, 1.95 mmol) was added dropwise via syringe. The reaction was let warm to room temperature and stir (2 h total). The reaction was poured over water and the mixture was

extracted with DCM. The organic layers were combined, dried with Na_2SO_4, filtered, and concentrated. The crude product was purified by column chromatography with 70:30 DCM:hexanes to give the product as a yellow solid (0.288 g, 80%). ^{1}H NMR ($CDCl_3$, 400 MHz): δ 9.90 (s, 1H), 7.69 (d, *J* = 7.4 Hz, 2H), 7.66 (s, 1 H), 7.45 (t, *J* = 7.4 Hz, 2H), 7.36 (t, *J* = 7.4 Hz, 1H), 7.27 (s, 1H), 4.27 (t, *J* = 7.1 Hz, 2H), 1.94 (p, *J* = 7.1 Hz, 2H), 1.38–1.27 (m, 10H), 0.89 (t, *J* = 7.0 Hz, 3H).

2,5-Bis(*N*-octyl-2-phenyldithieno[3,2-*b*:2',3'-*d*]pyrrol-6-yl)thiazolo[5,4-*d*]thiazole (4.30). To a 25 mL single neck round bottom flask equipped with a condenser was added, **4.29** (0.318 g, 0.804 mmol) and dithiooxamide (0.048 g, 0.399 mmol). Dry DMF (5 mL) was added and the reaction was heated at reflux for 24 h. Ice was added and stirred until melted. The precipitate was filtered, washed with water, and collected as a black solid. The crude product was purified by column chromatography with 50:50 DCM:hexanes to give the product as a red solid (0.227 g, 65%). ^{1}H NMR ($CDCl_3$, 400 MHz): δ 7.58 (d, *J* = 7.5 Hz, 4H), 7.38 (t, *J* = 7.5 Hz, 4H), 7.29 (t, *J* = 7.5 Hz, 2H), 7.28 (s, 2H), 7.02 (s, 2H), 4.06 (t, *J* = 7.0 Hz, 4H), 1.83 (p, *J* = 7.0 Hz, 4H), 1.33–1.27 (m, 20H), 0.88 (t, *J* = 7.0 Hz, 6H).

4.4.2. Absorption Spectroscopy

Absorption spectroscopy measurements were collected using a Carry 500 dual-beam UV-vis-NIR spectrophotometer. Solution-state spectra were collected with the analyte dissolved in $CHCl_3$.

4.5. References

(1) Su, Y.; Yu, B.; Wang, S.; Cong, H.; Shen, Y. *Biomaterials* **2021**, *271*, 120717.

(2) Tu, L.; Xu, Y.; Ouyang, Q.; Li, X.; Sun, Y. *Chin. Chem. Lett.* **2019**, *30* (10), 1731–1737.

(3) Zhang, N.; Lu, C.; Chen, M.; Xu, X.; Shu, G.; Du, Y.; Ji, J. *J. Nanobiotechnology* **2021**, *19* (1), 132.

(4) Li, L.; Dong, X.; Li, J.; Wei, J. *Dyes Pigments* **2020**, *183*, 108756.

(5) Smith, A. M.; Mancini, M. C.; Nie, S. *Nat. Nanotechnol.* **2009**, *4* (11), 710–711.

(6) Haque, A.; Faizi, Md. S. H.; Rather, J. A.; Khan, M. S. *Bioorg. Med. Chem.* **2017**, *25* (7), 2017–2034.

(7) Nakane, Y.; Tsukasaki, Y.; Sakata, T.; Yasuda, H.; Jin, T. *Chem. Commun.* **2013**, *49* (69), 7584–7586.

(8) Zhang, Y.; Zhang, Y.; Hong, G.; He, W.; Zhou, K.; Yang, K.; Li, F.; Chen, G.; Liu, Z.; Dai, H.; Wang, Q. *Biomaterials* **2013**, *34* (14), 3639–3646.

(9) Welsher, K.; Liu, Z.; Sherlock, S. P.; Robinson, J. T.; Chen, Z.; Daranciang, D.; Dai, H. A *Nat. Nanotechnol.* **2009**, *4* (11), 773–780.

(10) Gong, H.; Peng, R.; Liu, Z. *Adv. Drug Deliv. Rev.* **2013**, *65* (15), 1951–1963.

(11) He, S.; Chen, S.; Li, D.; Wu, Y.; Zhang, X.; Liu, J.; Song, J.; Liu, L.; Qu, J.; Cheng, Z. *Nano Lett.* **2019**, *19* (5), 2985–2992.

(12) Zhang, X.; He, S.; Ding, B.; Qu, C.; Zhang, Q.; Chen, H.; Sun, Y.; Fang, H.; Long, Y.; Zhang, R.; Lan, X.; Cheng, Z. *Chem. Eng. J.* **2020**, *385*, 123959.

(13) Fitzpatrick, J. A. J.; Andreko, S. K.; Ernst, L. A.; Waggoner, A. S.; Ballou, B.; Bruchez, M. P. *Nano Lett.* **2009**, *9* (7), 2736–2741.

(14) Liu, H.-W.; Chen, L.; Xu, C.; Li, Z.; Zhang, H.; Zhang, X.-B.; Tan, W. *Chem. Soc. Rev.* **2018**, *47* (18), 7140–7180.

(15) Antaris, A. L.; Chen, H.; Cheng, K.; Sun, Y.; Hong, G.; Qu, C.; Diao, S.; Deng, Z.; Hu, X.; Zhang, B.; Zhang, X.; Yaghi, O. K.; Alamparambil, Z. R.; Hong, X.; Cheng, Z.; Dai, H. A *Nat. Mater.* **2016**, *15* (2), 235–242.

(16) Dai, H.; Shen, Q.; Shao, J.; Wang, W.; Gao, F.; Dong, X. *The Innovation* **2021**, *2* (1), 100082.

(17) Hong, G.; Antaris, A. L.; Dai, H. *Nat. Biomed. Eng.* **2017**, *1* (1), 0010.

(18) Rasmussen, S. C. Low Bandgap Polymers. In *Encyclopedia of Polymeric Nanomaterials*; Kobayashi, S., Müllen, K., Eds.; Springer: Berlin, 2013; pp 1–13.

(19) Yang, Q.; Ma, Z.; Wang, H.; Zhou, B.; Zhu, S.; Zhong, Y.; Wang, J.; Wan, H.; Antaris, A.; Ma, R.; Zhang, X.; Yang, J.; Zhang, X.; Sun, H.; Liu, W.; Liang, Y.; Dai, H. *Adv. Mater.* **2017**, *29* (12), 1605497.

(20) Yang, Q.; Hu, Z.; Zhu, S.; Ma, R.; Ma, H.; Ma, Z.; Wan, H.; Zhu, T.; Jiang, Z.; Liu, W.; Jiao, L.; Sun, H.; Liang, Y.; Dai, H. *J. Am. Chem. Soc.* **2018**, *140* (5), 1715–1724.

(21) Rasmussen, S. C.; Uzelac, E. J.; Culver, E. W. Tricyclic-Fused Bithiophenes and Related Analogues: Important Building Blocks for Conjugated Materials. In *Advances in Heterocyclic Chemistry*; Scriven, E. F. V.; Ramsden, C. A., Eds.; Elsevier, 2020; Vol. 130, pp 75–144.

(22) Baumgartner, T. *J. Inorg. Organomet. Polym. Mater.* **2005**, *15* (4), 389–409.

(23) Rasmussen, S. C.; Evenson, S. J. *Prog. Polym. Sci.* **2013**, *38* (12), 1773–1804.

(24) Geng, Y.; Tang, A.; Tajima, K.; Zeng, Q.; Zhou, E. *J. Mater. Chem. A* **2019**, *7* (1), 64–96.

(25) Ohshita, J. *Macromol. Chem. Phys.* **2009**, *210* (17), 1360–1370.

(26) Rasmussen, S. C.; Evenson, S. J.; McCausland, C. B. *Chem. Commun.* **2015**, *51* (22), 4528–4543.

(27) Matsumoto, T.; Tanaka, K.; Chujo, Y. *RSC Adv.* **2015**, *5* (68), 55406–55410.

(28) Zanirato, P.; Spagnolo, P.; Zanardi, G. *J. Chem. Soc. Perkin 1* **1983**, 2551–2554.

(29) Ogawa, K.; Rasmussen, S. C. *J. Org. Chem.* **2003**, *68* (7), 2921–2928.

(30) Evenson, S. J.; Pappenfus, T. M.; Delgado, M. C. R.; Radke-Wohlers, K. R.; Navarrete, J. T. L.; Rasmussen, S. C. *Phys. Chem. Chem. Phys.* **2012**, *14* (17), 6101–6111.

(31) Wong, H.-L.; Ko, C.-C.; Lam, W. H.; Zhu, N.; Yam, V. W.-W. *Chem. - Eur. J.* **2009**, *15* (39), 10005–10009.

(32) Balaji, G.; Parameswaran, M.; Jin, T. M.; Vijila, C.; Furong, Z.; Valiyaveettil, S. *J. Phys. Chem. C* **2010**, *114* (10), 4628–4635.

(33) Evenson, S. J.; Rasmussen, S. C. *Org. Lett.* **2010**, *12* (18), 4054–4057.

(34) Koeckelberghs, G.; De Cremer, L.; Vanormelingen, W.; Dehaen, W.; Verbiest, T.; Persoons, A.; Samyn, C. *Tetrahedron* **2005**, *61* (3), 687–691.

(35) Förtsch, S.; Bäuerle, P. *Polym. Chem.* **2017**, *8* (23), 3586–3595.

(36) Mo, H.; Radke, K. R.; Ogawa, K.; Heth, C. L.; Erpelding, B. T.; Rasmussen, S. C. *Phys. Chem. Chem. Phys.* **2010**, *12* (43), 14585–14595.

(37) Decken, A.; Gabbaie, F. P.; Cowley, A. H. *Inorg. Chem.* **1995**, *34* (15), 3853–3854.

(38) Matsumoto, T.; Tanaka, K.; Tanaka, K.; Chujo, Y. *Dalton Trans.* **2015**, *44* (18), 8697–8707.

(39) Woodward, A. N.; Kolesar, J. M.; Hall, S. R.; Saleh, N.-A.; Jones, D. S.; Walter, M. G. *J. Am. Chem. Soc.* **2017**, *139* (25), 8467–8473.

(40) Radke, K. R.; Ogawa, K.; Rasmussen, S. C. *Org. Lett.* **2005**, *7* (23), 5253–5256.

(41) Evenson, S. J.; Mumm, M. J.; Pokhodnya, K. I.; Rasmussen, S. C. *Macromolecules* **2011**, *44* (4), 835–841.

(42) Wen, L.; Duck, B. C.; Dastoor, P. C.; Rasmussen, S. C. *Macromolecules* **2008**, *41* (13), 4576–4578.

43) Kenning, D. D.; Mitchell, K. A.; Calhoun, T. R.; Funfar, M. R.; Sattler, D. J.; Rasmussen, S. C. *J. Org. Chem.* **2002**, *67* (25), 9073–9076.

(44) Culver, E. W.; Anderson, T. E.; López Navarrete, J. T.; Ruiz Delgado, M. C.; Rasmussen, S. C. *ACS Macro Lett.* **2018**, *7* (10), 1215–1219.

45) Anderson, T.; Culver, E.; Almyahi, F.; Dastoor, P.; Rasmussen, S. *Synlett* **2018**, *29* (19), 2542–2546.

(46) Adak, L.; Yoshikai, N. *J. Org. Chem.* **2011**, *76* (18), 7563–7568.

(47) Dessì, A.; Calamante, M.; Mordini, A.; Zani, L.; Taddei, M.; Reginato, G. *RSC Adv* **2014**, *4* (3), 1322–1328.

(48) Yassin, A.; Leriche, P.; Roncali, J. *Macromol. Rapid Commun.* **2010**, *31*, 1467–1472.

CHAPTER 5. CONCLUSION AND FUTURE WORK

5.1. Introduction

Conjugated organic materials have gained interest as they combine the optical and electrical properties of inorganic semiconductors with the mechanical properties of organic plastics, allowing them to be used in various applications such as organic photovoltaics (OPVs), near-infrared (NIR) photodetectors, and fluorescence bioimaging. For OPVs, due to the Shockley-Queisser limit, a material with a bandgap of 1.34 eV is ideal to maximize solar cell power conversion efficiency.[1,2] For NIR photodetectors, low bandgap materials are required to generate photoresponse in the NIR region. For bioimaging, a material that absorbs and emits light of wavelengths of 700–900 nm and 1000–1700 nm are ideal due to reduced absorption, autofluorescence, and scattering in these regions.[3] For all of these applications tuning of the bandgap or HOMO-LUMO gap is crucial. As mentioned in chapter 1 there are several factors that can impact the bandgap or HOMO-LUMO gap of or a conjugated organic material such as planarity, substituents, and intermolecular interactions. Moreover, two common design approaches used to make low bandgap conjugated materials are increasing quinoidal character of the compounds backbone and donor-acceptor frameworks.[4] The fused-ring unit thieno[3,4-*b*]pyrazine (TP) was targeted as it can be used to make materials with low bandgaps due to a combination of its proquinoidal and ambipolar nature. However, the fused-ring nature of the TP unit generally result in materials of low solubility, which is problematic as devices such as OPVs are commonly processed from solution. However, the solubility of conjugated organic materials can be tuned through molecular design with branched alkyl side chains used to improve solubility in common organic solvents and polar side chains (e.g., oligoether side chains) used to improve solubility in aqueous environment for applications such as bioimaging.[5–7]

5.2. Conclusion

5.2.1. Grignard Metathesis Polymerization of Poly(2,3-dialkylthieno[3,4-b]pyrazine)s

Previously reported poly(thieno[3,4-*b*]pyrazine)s (PTPs) made by Grignard metathesis (GRIM) polymerization by Rasmussen and Koeckelberghs were of relatively low molecular weights.[8–10] Both researchers had different explanations for the low molecular weights. Rasmussen proposed that the low solubility of PTPs resulted in low solubility induced precipitation of the growing polymer chain during synthesis. However, Koeckelberghs suggested that the low molecular weight is due to catalyst dissociation caused by the electron-deficient nature of the polymer, which leads to a weak association between the active catalyst and the growing polymer chain. However, this seems unlikely as the TP unit exhibits properties of both a strong donor and a strong acceptor with polymerization occurring at the electron rich portion of the TP unit. Thus, the low solubility was targeted.

Several PTPs functionalized with branched alkyl side chains were synthesized by GRIM polymerization. Interestingly, the PTPs functionalized with branched side chains were of similar molecular weight to poly(2,3-dihexylthieno[3,4-*b*]pyrazine) (PHTP). Furthermore, the polymers functionalized with 2-ethylhexyl and 2-octyldodecyl side chains were completely soluble in $CHCl_3$, whereas the synthesis of PHTP resulted in some insoluble material. These results suggest that the low molecular weight of these PTPs made by GRIM polymerization is not a result of their low solubility and due to some other factor.

It was found that the UV-vis-NIR spectra of the PTPs could be tuned significantly by changing the branched side chain with 2-ethylhexyl side chains leading the most red-shifted absorption λ_{max} value and the 2-octyldodecyl side chains leading to the most blue-shifted λ_{max} value. One interesting finding was that both the hexyl functionalized polymer and 2-octyldodecyl

functionalized polymer exhibited a broad spectral profile, whereas the 2-ethylhexyl and 3,7-dimethyloctyl functionalized polymers exhibited narrow spectral profiles. Moreover, all polymers exhibited similar bandgaps ranging from 1.06 to 1.10 eV.

5.2.2. Photonic Devices Made from Poly(2,3-bis(2-ethylhexyl)thieno[3,4-b]pyrazine)

Photonic devices were prepared from poly(2,3-bis(2-ethylhexyl)thieno[3,4-*b*]pyrazine) (PEHTP) and [6,6]-phenyl-C_{61}-butyric acid methyl ester (PCBM). The highest power conversion efficiency (PCE) determined from these devices was ~0.27%, which was significantly higher than the previously reported maximum PCE for photonic devices prepared from PHTP of 0.13%.[11] The improvement in PCE is likely due to the improved processability of PEHTP compared to PHTP, which results in better interfaces in the active layer and better interfaces between the active layer and the transport layers. However, the open circuit voltage (V_{OC}) of PTP devices are low, which is thought to be because the LUMO of PTPs and PCBM is similar, which does not create a large enough driving force for good charge separation to occur.[12] Nonetheless, the PEHTP devices exhibited an external quantum efficiency (EQE) and specific detectivity (D^*) of 3.78% and 8.0 x 10^9 Jones at 1110 nm, respectively. Determining the specific detectivity using only the dark current (as is commonly reported through the literature)[13] gave a specific detectivity value of 2.98 x 10^{12} Jones. In addition, PEHTP is one of only about 20 polymers that show photoresponse below 1000 nm, and of these polymers PEHTP is one of the least synthetically complex.[13]

5.2.3. Acenaphtho[1,2-b]thieno[3,4-e]pyrazine-based Solution Processable Conjugated Polymers with Bandgaps Below 0.7 eV

Researchers have focused on making zero or very low bandgap polymers to make materials with enhanced electrical conduction, and as bandgap is decreased the absorption is

shifted to the NIR portion of the spectrum, potentially resulting in a colorless transparent conducting material.[14] Extended TPs are popular monomeric units used to make low bandgap polymers.[15] For example, in 2008 Rasmussen and coworkers synthesized poly(acenaphtho[1,2-*b*]thieno[3,4-*e*]pyrazine) (PATP) via electropolymerization and although PATP exhibits one of the lowest bandgaps for a conjugated polymer (0.50 eV), the polymer was insoluble in common organic solvents, and thus was not useful for devices.[16]

Thus, it was hypothesized that pairing the acenaphtho[1,2-*b*]thieno[3,4-*e*]pyrazine (ATP) unit with the very soluble TP analog, 2,3-bis(2-octyldodexyl)thieno[3,4-*b*]pyrazine, would result in a material with good solubility and a low bandgap. The low bandgap solution-processible polymers poly(acenaphtho[1,2-*b*]thieno[3,4-*e*]pyrazine-*ran*-2,3-bis(2-octyldodecyl)thieno[3,4-*b*]pyrazine) (ATP-*ran*-ODTP) and poly(acenaphtho[1,2-*b*]thieno[3,4-*e*]pyrazine-*alt*-2,3-bis(2-octyldodecyl)thieno[3,4-*b*]pyrazine) (ATP-*alt*-ODTP) were prepared via GRIM polymerization and direct arylation polymerization (DArP), respectively, in moderate yields (52 and 60%, respectively). Both polymers exhibited bandgaps of less than 0.7 eV and good solubility in chloroform (> 20 mg/mL). In particular, ATP-*ran*-ODTP exhibited a bandgap of 0.64 eV, which is one of the lowest bandgaps reported for a solution-processable polymer.[13,17–19] However, both polymers were of low molecular weight potentially due to the low solubility of this polymer or the poor compatibility of the monomers with GRIM polymerization and DArP. The average degree of polymerization for ATP-*ran*-ODTP was about 12 (if we assume a 1-to-1 ratio of monomeric units) and for ATP-*alt*-ODTP was about seven, which are far below the effective conjugation length of polythiophenes (ca. 20 to 30 thiophene rings).[20,21] Thus, increasing the molecular weight of ATP-*ran*-ODTP and ATP-*alt*-ODTP may lead to a decrease in the bandgap.

5.2.4. Small Molecule Fluorophores

Fluorescence bioimaging has gained interest due to its affordability, high sensitivity, and fast feedback relative to other imaging methods.[3,22,23] Light wavelengths of 700–900 nm and 1000–1700 nm are ideal for bioimaging due to the reduced absorption, autofluorescence, and scattering in these regions.[3] A common design of small molecule NIR emitters is the donor-acceptor-donor (D-A-D) framework, which results in species with red-shifted absorption due to the donor-acceptor interactions that were discussed in chapter 1. Thus, we theorized that a D-A-D small molecule where D = dithieno[3,2-*b*:2',3'-*d*]pyrrole (DTP) and A = TP would exhibit absorption and emission in the wavelength regions ideal for bioimaging. Moreover, a previous report by Rasmussen and coworkers found that DTP-based oligomers exhibited high fluorescence quantum yields.[24] The synthesis of two DTP and TP-based oligomers was attempted with little success possibly due to their low stability caused by their high-lying HOMO. Nonetheless, several novel compounds were synthesized that could be used to make other conjugated materials.

Work by Woodward et al. showed that that thiazolo[5,4-*d*]thiazole (TTz)-based oligomers exhibit high quantum yields.[25] In addition, the synthesis of TTz-based oligomers is straightforward as they are made by a double condensation reaction between an aldehyde and dithiooxamide. Thus, it was hypothesized that the small molecule 2,5-bis(*N*-octyl-2-phenyldithieno[3,2-*b*:2',3'-*d*]pyrrol-6-yl)thiazolo[5,4-*d*]thiazole (DTP_2-TTz) could be synthesized easily and the oligomer would exhibit high quantum yields. DTP_2-TTz was synthesized in 65% yield as a red solid. The oligomer exhibited solution-state absorption in the visible portion of the spectrum with absorption maxima at 503 and 532 nm. These absorption values are red-shifted relative to the DTP trimer, which exhibits a maximum absorption at 464

nm.[26] In addition, while irradiated with 365 nm light the oligomer exhibited bright orange emission.

5.3. Future Work

5.3.1. Grignard Metathesis Polymerization of Poly(2,3-dialkylthieno[3,4-b]pyrazine)s

Future work should investigate what is inhibiting the GRIM polymerization of PTPs. A catalyst transfer polymerization mechanism (CTP) should be targeted to make PTPs as CTP has been used to produce materials with controlled molecular weight and low polydispersity.[27,28]

One potential issue with the GRIM polymerization of PTPs could be that the polymerization is inhibited by the interaction between the Ni catalyst and the TP unit N atoms. Interactions between transition metals and the TP unit N atoms have been previously proposed by Rasmussen and coworkers in the polymerization of TP using $FeCl_3$.[29] Thus, future work should repeat the polymerization of PEHTP. However, at the end of the reaction more catalyst should be added, followed by reflux for another hour to see if further chain growth occurs. A Ni(0) source should be added instead of a Ni(II) source as the latter would need to undergo two transmetalation steps to be converted to the active catalyst.

Another potential issue with the GRIM polymerization of PTPs could be that the 5-bromo-7-bromomagnesio-2,3-dialkylthieno[3,4-*b*]pyrazines (**5.2**) are not selectively produced upon treating the 5,7-dibromo-2,3-dialkylthieno[3,4-*b*]pyrazines (**5.1**) with methylmagnesium bromide and instead some 5,7-dibromomagnesio-2,3-dialkylthieno[3,4-*b*]pyrazine (**5.3**) is produced. To test this hypothesis, H^+ quenching experiments could be carried out (Figure 5.1).[30] This has previously been found to be an issue for Grignard metathesis of 4,7-dibromo-2-(2-octyldodecyl)-2H-benzo[*d*][1,2,3]triazole (Br_2BTz), and it was found that making the activated

monomer by treating Br_2BTz with BuLi followed by $MgBr_2$ led to selective production of 4-bromo-7-chloromagnesio-2-(2-octyldodecyl)-2H-benzo[*d*][1,2,3]triazole.[30]

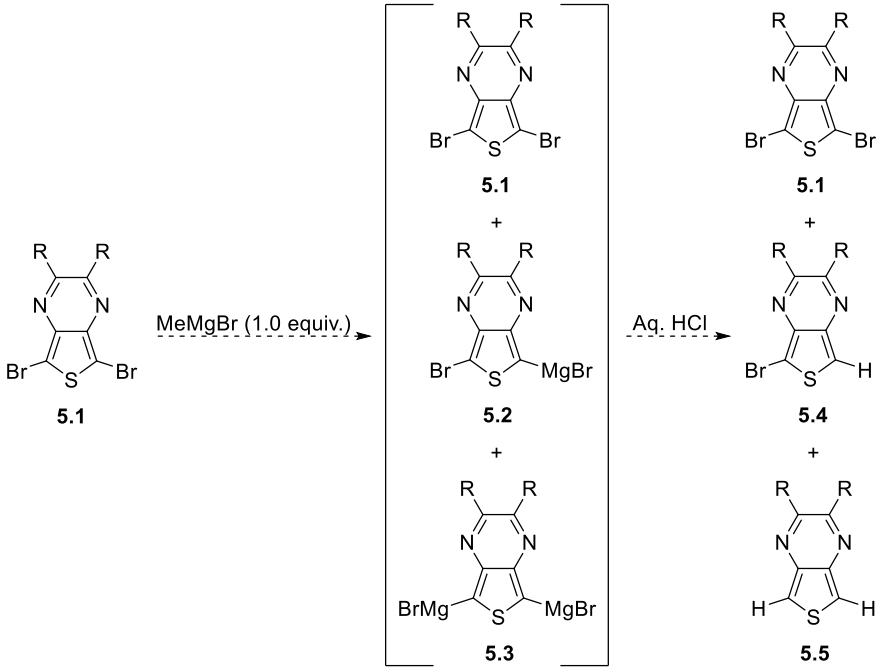

Figure 5.1. Proposed H^+ quenching experiment of the Grignard metathesis step.

5.3.2. Photonic Devices Made from Poly(2,3-bis(2-ethylhexyl)thieno[3,4-b]pyrazine)

As previously mentioned, the V_{OC} of both PHTP and PEHTP devices are low, which is thought to be because the LUMO of the PTPs and PCBM is similar, which does not create a large enough driving force for good charge separation to occur.[31] The low V_{OC} of PTP devices could be targeted by pairing PEHTP with a different acceptor material that has a lower LUMO than PCBM, such as IT-4F or Y6 (Figure 5.2). Their low LUMOs could create enough of a driving force to allow for good charge separation in the resulting photonic device, leading to improved performance.

5.3.3. Low Bandgap Solution-Processable Polymers

As both ATP-*ran*-ODTP and ATP-*alt*-ODTP exhibit very low bandgaps, NIR photodetector devices should be fabricated from these polymers as they could be used to make devices with one of the widest spectral regions of a conjugated polymer.[13] As discussed in chapter 3 these polymers exhibit a LUMO energy level of -3.9 eV, which may be too low for pairing with PCBM, thus they may work well if paired with a different acceptor material like IT-4F or Y6 (Figure 5.2). In addition, determining photodetector figures of merit such as EQE and D^* would be useful to collect.

This work has resulted in very low bandgap solution-processable conjugated polymers using the ATP unit. Thus, future studies should investigate other ways to solubilize the ATP unit while retaining a low bandgap. One possibility is PATPs functionalized with branched side chains (Figure 5.3). ATP analog **5.6** could be synthesized by modifying a previously reported procedure by Rasmussen and coworkers.[33] GRIM polymerization would be an effective way to make polymer **5.7** as previous work by Rasmussen and coworkers has shown that PTPs made by GRIM polymerization exhibit enhanced solubility compared to PTPs produced by other methods.[8] In addition, it would be interesting to see how this polymer would compare to ATP-*ran*-ODTP and ATP-*alt*-ODTP in terms of bandgap, solubility, and synthetic complexity.

Other potential future work is changing the ratio of monomers added to the reaction flask when making ATP-*ran*-ODTP by GRIM polymerization. By increasing the ratio of ATP-to-ODTP the resulting material could potentially have a smaller bandgap than the 1-to-1 copolymer. In addition, it would be interesting to see how much ODTP is required to retain good solubility (~10 mg/mL) of the polymer.

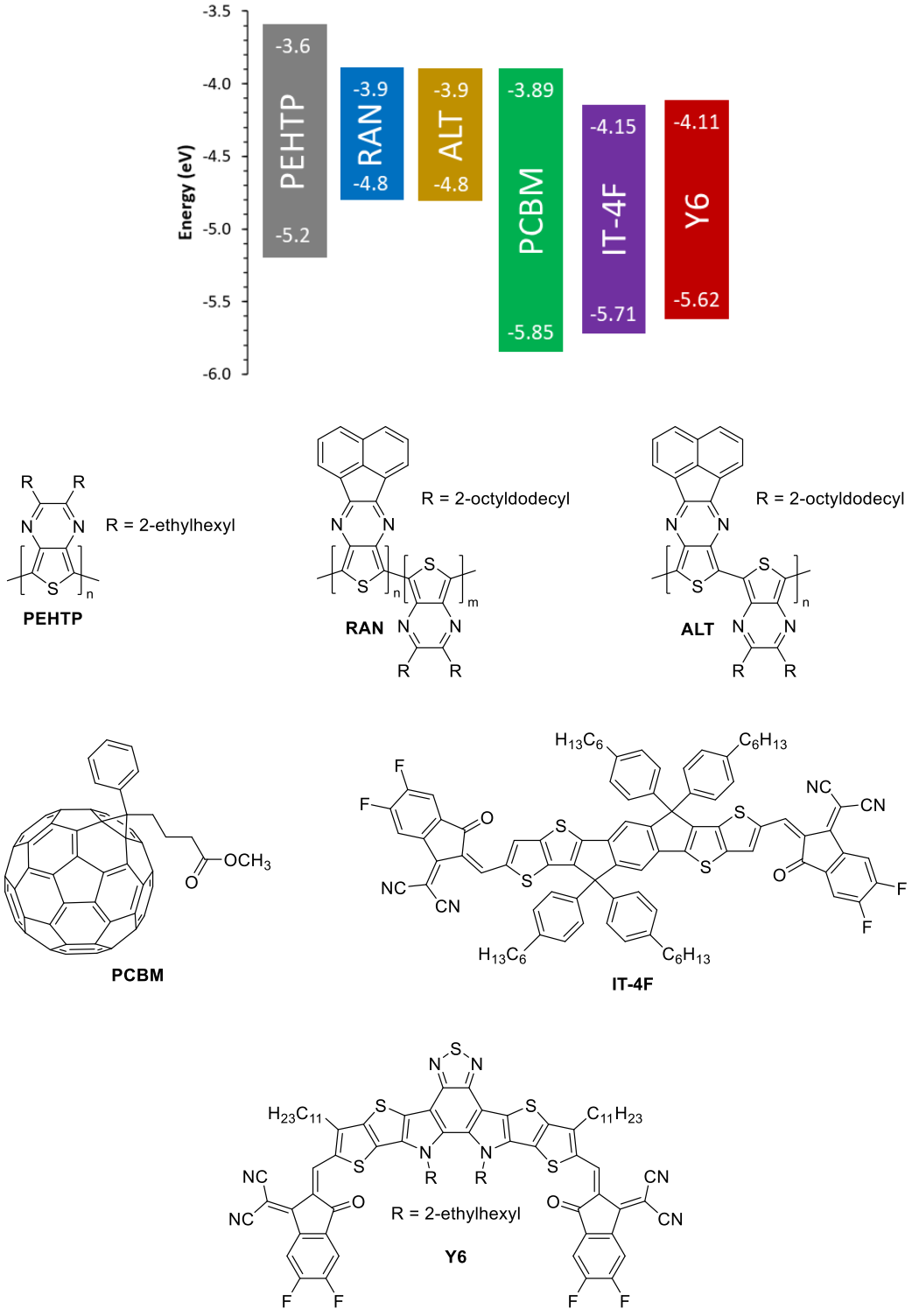

Figure 5.2. Energy levels of PEHTP, ATP-*ran*-ODTP (RAN), ATP-*alt*-ODTP (ALT), and common acceptor materials.[32]

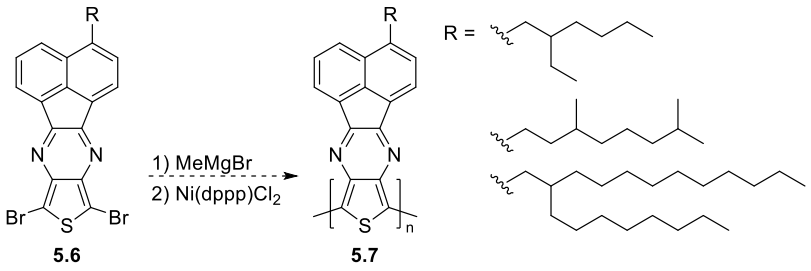

Figure 5.3. Synthesis of branched side chain functionalized PATPs by GRIM polymerization.

5.3.4. Small Molecule Fluorophores

Future work should first involve collecting an emission spectrum for the DTP_2-TTz oligomer. If results are promising this creates the opportunity to synthesize a variety of other small molecule emitters that incorporate the TTz unit, such as oligomers **5.8** and **5.9** shown in Figure 5.4. The proposed oligomer **5.8** is end capped with fluorene instead of a phenyl ring. Fluorene-based oligomers and polymers have been found to exhibit high quantum yields.[34,35] Thus, this could cause the corresponding oligomer to also exhibit high quantum yields. In addition, the increase in conjugation length could potentially result in a redshift in both absorption and emission. Proposed oligomer **5.9** is end capped with quinoxaline units instead of phenyl rings. Due to the acceptor character of the quinoxaline unit this could introduce donor-acceptor interactions, which could redshift absorption and emission. In addition, this oligomer has a longer conjugation length than the phenyl capped analog, which could further contribute to a redshift in absorption and emission.

The successful synthesis of DTP_2-TTz opens future possibility of making a dithieno[3,2-*b*:2',3'-*d*]pyrrole (DTP)-TTz alternating copolymer as shown in Figure 5.5. *N*-octyldithieno[3,2-*b*:2',3'-*d*]pyrrole-2,6-dicarboxaldehyde (**5.10**) can be made by modifying the formylation procedure detailed in chapter 4. Polymer **5.12** can then be made by a condensation reaction

between **5.10** and the dithiooxamide (**5.11**) (Figure 5.5). Polymer **5.12** is likely to exhibit strong emission.[12,25,36]

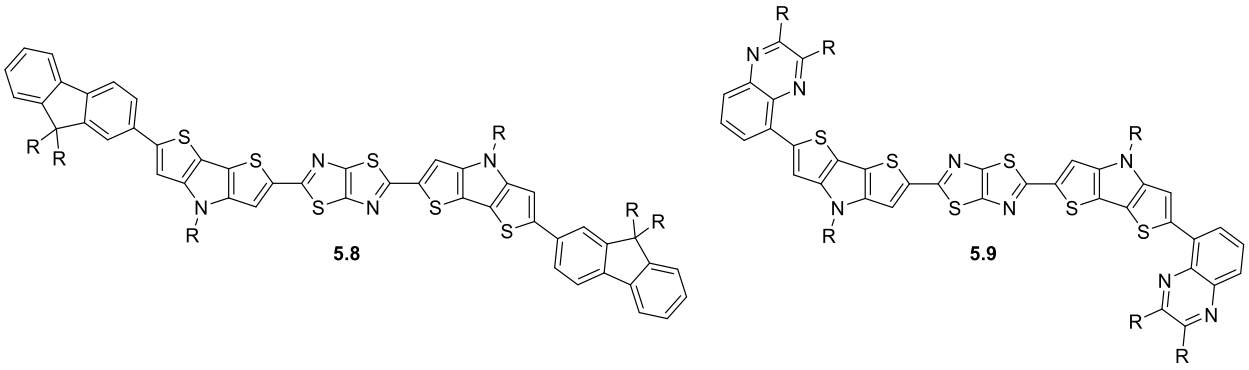

Figure 5.4. Proposed TTz- and DTP-based oligomers.

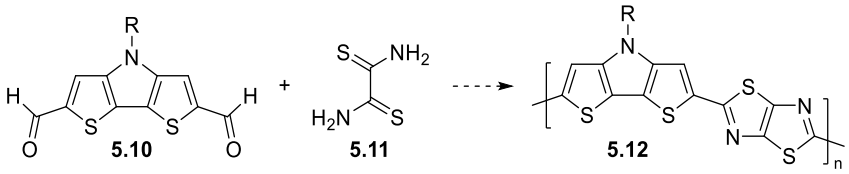

Figure 5.5. Proposed synthesis of a DTP-TTz alternating copolymer.

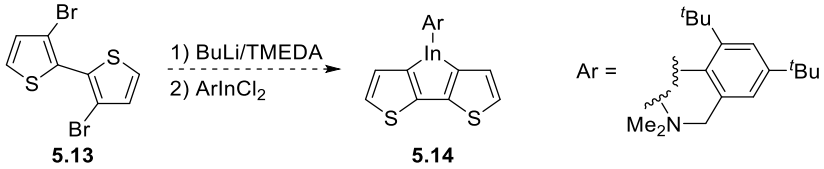

Figure 5.6. Proposed synthesis of InDT functionalized with the Mamx ligand.

As discussed in chapter 4, attempts at synthesizing the indolo[3,2-*b*:4,5-*b'*]dithiophene (InDT) were unsuccessful, potentially due to its low stability. Previous reports have shown that bulky aryl groups can be used to improve the stability of indafluorenes,[37,38] with Matsumoto et al. using the 2,4-di-*tert*-butyl-6-[(dimethylamino)methyl]phenyl (Mamx) ligand. Future work

should include functionalizing InDT with the Mamx ligand as this could potentially increase the stability of the compound (Figure 5.6).

5.4. References

(1) Rühle, S. *Sol. Energy* **2016**, *130*, 139–147.

(2) Shockley, W.; Queisser, H. J. **1961**, *32* (3), 510–519.

(3) Su, Y.; Yu, B.; Wang, S.; Cong, H.; Shen, Y. *Biomaterials* **2021**, *271*, 120717.

(4) Rasmussen, S. C.; Gilman, S. J.; Wilcox, W. D. *Conjugated Polymers – Synthesis and Design*; ACS In Focus, American Chemical Society: Washington, D.C., 2023, *Submitted*.

(5) Lei, T.; Wang, J.-Y.; Pei, J. *Chem. Mater.* **2014**, *26* (1), 594–603.

(6) Mei, J.; Bao, Z. *Chem. Mater.* **2014**, *26* (1), 604–615.

(7) Meng, B.; Liu, J.; Wang, L. *Polym. Chem.* **2020**, *11* (7), 1261–1270.

(8) Wen, L.; Duck, B. C.; Dastoor, P. C.; Rasmussen, S. C. *Macromolecules* **2008**, *41* (13), 4576–4578.

(9) Willot, P.; Moerman, D.; Leclère, P.; Lazzaroni, R.; Baeten, Y.; Van Der Auweraer, M.; Koeckelberghs, G. *Macromolecules* **2014**, *47* (19), 6671–6678.

(10) Mulholland, M. E.; Wen, L.; Rasmussen, S. C. *Topol. Supramol. Polym. Sci.* **2015**, *2* (1) 18–29.

(11) Duck, B. C.; Vaughan, B.; Wen, L.; Heth, C. L.; Rasmussen, S. C.; Zhou, X.; Belcher, W. J.; Dastoor, P. C. *Sol. Energy Mater. Sol. Cells* **2013**, *110*, 8–14.

(12) Rasmussen, S. C.; Evenson, S. J. *Prog. Polym. Sci.* **2013**, *38* (12), 1773–1804.

(13) Rasmussen, S. C.; Gilman, S. J.; Culver, E. W.; Wilcox, W. D. *Gen. Chem.* **2021**, *7* (2), 200019.

(14) Rasmussen, S. C.; Pomerantz, M. In *Handbook of Conducting Polymers: Theory, Synthesis, Properties, and Characterization*, 3rd ed.; Skotheim, T. A.; Reynolds, J. R., Eds.; CRC Press: Boca Raton, FL, 2007, Chapter 12.

(15) Rasmussen, S. C.; Schwiderski, R. L.; Mulholland, M. E. *Chem. Commun.* **2011**, *47* (41), 11394–11410.

(16) Nietfeld, J. P.; Heth, C. L.; Rasmussen, S. C. *Chem. Commun.* **2008**, 981–983.

(17) Rasmussen, S. C.; Gilman, S. J.; Wilcox, W. D. *Gen. Chem.* **2023**, *9*, 220010.

(18) Mikie, T.; Osaka, I. *J. Mater. Chem. C* **2020**, *8* (41), 14262–14288.

(19) Ji, X.; Fang, L. *Polym. Chem.* **2021**, *12* (10), 1347–1361.

(20) Izumi, T.; Kobashi, S.; Takimiya, K.; Aso, Y.; Otsubo, T. *J. Am. Chem. Soc.* **2003**, *125* (18), 5286–5287.

(21) Ma, J.; Li, S.; Jiang, Y. *Macromolecules* **2002**, *35* (3), 1109–1115.

(22) Tu, L.; Xu, Y.; Ouyang, Q.; Li, X.; Sun, Y. *Chin. Chem. Lett.* **2019**, *30* (10), 1731–1737.

(23) Zhang, N.; Lu, C.; Chen, M.; Xu, X.; Shu, G.; Du, Y.; Ji, J. *J. Nanobiotechnology* **2021**, *19* (1), 132.

(24) Evenson, S. J.; Pappenfus, T. M.; Delgado, M. C. R.; Radke-Wohlers, K. R.; Navarrete, J. T. L.; Rasmussen, S. C. *Phys. Chem. Chem. Phys.* **2012**, *14* (17), 6101–6111.

(25) Woodward, A. N.; Kolesar, J. M.; Hall, S. R.; Saleh, N.-A.; Jones, D. S.; Walter, M. G. *J. Am. Chem. Soc.* **2017**, *139* (25), 8467–8473.

(26) Yassin, A.; Leriche, P.; Roncali, J. *Macromol. Rapid Commun.* **2010**, *31* (16), 1467–1472.

(27) Sheina, E. E.; Liu, J.; Iovu, M. C.; Laird, D. W.; McCullough, R. D. *Macromolecules* **2004**, *37* (10), 3526–3528.

(28) Yokoyama, A.; Miyakoshi, R.; Yokozawa, T. *Macromolecules* **2004**, *37* (4), 1169–1171.

(29) Kenning, D. D.; Rasmussen, S. C. *Macromolecules* **2003**, *36* (17), 6298–6299.

(30) Bridges, C. R.; McCormick, T. M.; Gibson, G. L.; Hollinger, J.; Seferos, D. S. *J. Am. Chem. Soc.* **2013**, *135* (35), 13212–13219.

(31) Duck, B. C.; Vaughan, B.; Cooling, N.; Zhou, X.; Holdsworth, J. L.; Wen, L. L.; Rasmussen, S. C.; Dastoor, P. C.; Belcher, W. J. *Sol. Energy Mater. Sol. Cells* **2013**, *114*, 65–70.

(32) Pan, M.-A.; Lau, T.-K.; Tang, Y.; Wu, Y.-C.; Liu, T.; Li, K.; Chen, M.-C.; Lu, X.; Ma, W.; Zhan, C. *J. Mater. Chem. A* **2019**, *7* (36), 20713–20722.

(33) Nietfeld, J. P.; Schwiderski, R. L.; Gonnella, T. P.; Rasmussen, S. C. *J. Org. Chem.* **2011**, *76* (15), 6383–6388.

(34) Feng, L.; Zhang, C.; Bie, H.; Chen, Z. *Dyes Pigm.* **2005**, *64* (1), 31–34.

(35) Chen, Z.; Bouffard, J.; Kooi, S. E.; Swager, T. M. *Macromolecules* **2008**, *41* (18), 6672–6676.

(36) Rasmussen, S. C.; Evenson, S. J.; McCausland, C. B. *Chem. Commun.* **2015**, *51* (22), 4528–4543.

(37) Matsumoto, T.; Tanaka, K.; Tanaka, K.; Chujo, Y. *Dalton Trans.* **2015**, *44* (18), 8697–8707.

(38) Decken, A.; Gabbaie, F. P.; Cowley, A. H. *Inorg. Chem.* **1995**, *34* (15), 3853–3854.